1-1-2006

One dimensional model and pulse generation of a supercharger

Martin Hardis
Iowa State University

One dimensional model and pulse generation of a supercharger

by

Martin Hardis

A thesis submitted to the graduate faculty
in partial fulfillment of the requirements for the degree of
MASTER OF SCIENCE

Major: Mechanical Engineering

Program of Study Committee:
J. Adin Mann III, Major Professor
Michael G. Olsen
Thomas J. Rudolphi

Iowa State University
Ames, Iowa
2006

Graduate College
Iowa State University

This is to certify that the master's thesis of

Martin Hardis

has met the requirements of Iowa State University

Signatures have been redacted for privacy

Table of Contents

Acknowledgements

I would like to thank several individuals who have greatly helped me in completing my thesis. Firstly, I would like to thank my parents for their support and guidance throughout my entire life. They have always been there for me in so many ways. Secondly, to Dr. J. Adin Mann, my major professor, who has been an excellent teacher for me. He has taught me valuable knowledge that will never be taught in classes to become a good engineer as well as a good individual. Finally, I would like to thank Eaton Corporation for supporting this research project and giving students the chance to build their career in engineering.

Abstract

A reduced order model that captures the key aspects of a roots type supercharger has been developed. The goal of this reduced order model is to obtain the greatest computation speed for an acceptable accuracy. Key phenomena that dominate the response in the supercharger were identified first, and then implemented in the reduced order model.

The reduced order model was developed based on one dimensional supercharger model from Sorenson. This model was then improved by adding backflow slot features (previously done by Carroll), a carryback slot, and finally a pressure pulse generated by the carryback slot. The output of this model, supercharger performance (volumetric and J1723 isentropic efficiency), was then compared with measured data from Eaton Corporation. The results agree after a supercharger wall temperature is increased with respect to the pressure ratio and rotor speed. This suggests that there is another heat generation source in the supercharger that has not been accounted for in the model, such as mechanical loss due to friction. A further investigation on the supercharger wall temperature needs to be conducted to verify this hypothesis. If the investigation results do not support this hypothesis, other source of heat generation in the supercharger should be investigated.

Chapter 1
Introduction

A supercharger, a positive displacement compressor, is one type of forced induction system that is used in an internal combustion engine. It increases air pressure and density in the intake manifold by pumping more air into the engine than the engine would use without a supercharger. This high pressurized air provided by the supercharger causes more fuel to be burnt during combustion process, which results in a greater combustion explosion. This greater combustion explosion creates more downward force on the piston, in turn creating more horsepower and improving performance over non-supercharged vehicles. The supercharger is matched to the engine based on its displacement and belt ratio.

The key to the increased horsepower is associated to the amount of air that can be compressed into the cylinder; hence, compressing air is an important function of a supercharger. Typical boost of a supercharger is between 6 and 8 psi and atmospheric pressure on sea level is 14.7 psi. This means by using supercharger about 50% more of air can get into the engine, resulting in an increase in horsepower of about 40 to 50% (Harris 2006).

There are three types of superchargers: centrifugal, roots, and screw type. The main difference between all three types is how the air inside the supercharger is moved to the intake manifold of the engine. Screw type and roots type use different types of intermeshing lobes and a centrifugal compressor uses an impeller (Harris 2006). Examples of these superchargers are shown in Figure 1.1, 1.2, and 1.3 (Howstuffworks.com).

Centrifugal superchargers, Figure 1.1, use an impeller spun by a drive pulley. Air is drawn into the centrifugal supercharger; then gets compressed by an internal rotating impeller and forced out through the scroll of the supercharger. One advantage of centrifugal superchargers is a lower discharge temperature compared to other superchargers, which leads to a higher reliability and performance. However, they do not produce as much boost in the lower range of motor rotation rates (Harris 2006).

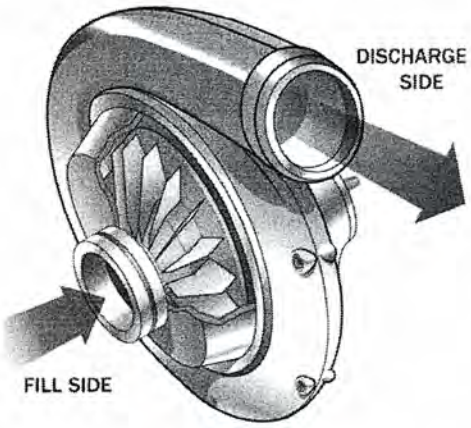

Figure 1.1 Centrifugal supercharger (Harris 2006).

Roots type superchargers, Figure 1.2, are the oldest type of supercharger. Unlike the use of an impeller in centrifugal superchargers, they use two intermeshing rotors to compress air to the manifold and thus create boost. Typically, root superchargers have rotors with two or three lobes depending on the size of the supercharger. Air gets in from the fill side and then gets carried through the system to the discharged side. The advantage of roots type superchargers is that they deliver boost through the entire range of motor rotation rates. They, however, produce hotter discharge temperatures than other superchargers and add more weight to the vehicle (Harris 2006).

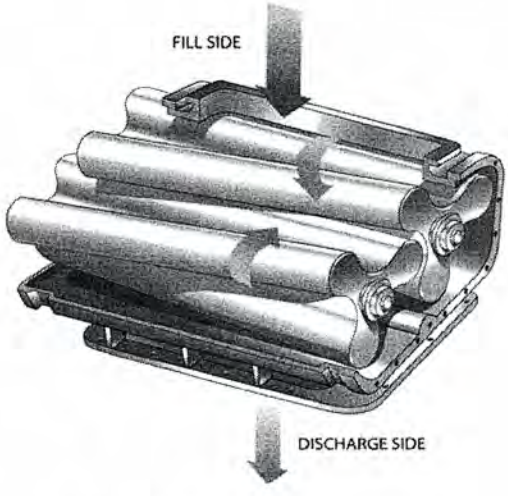

Figure 1.2 Roots type supercharger (Harris 2006).

Screw type superchargers, Figure 1.3, are the predecessor of roots type superchargers. Even though the internal design of the screw type supercharger is similar to the roots type, screw type superchargers exhibit internal compression. Like a roots type compressor, as the air is passed through the supercharger, it gets trapped into pockets created by rotor lobes. However, these pockets of air between the internal screws decrease in size towards the outlet since the rotors have conical taper. This makes a screw type compressors have higher thermal efficiency than roots type superchargers. Two main advantages of screw type superchargers are that they produce high boost levels in the lower range of motor rotation rates and they run cooler than roots type superchargers (Harris 2006).

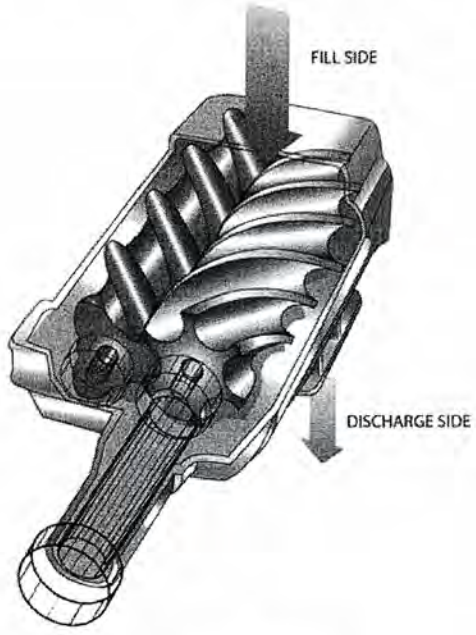

Figure 1.3 Screw type supercharger (Harris 2006).

The other type of force induction system is a turbocharger. The main difference between a supercharger and a turbocharger is in their power supply. A turbocharger uses exhaust gas from the engine, while a supercharger is driven by a belt that is directly connected to the engine. In turbochargers, exhaust gas from the engine flows through a turbine, which in turn spins the compressor. Turbochargers are more efficient than superchargers in terms of power consumption since they use "waste energy" to be their

source of power (Harris 2006). On the other hand, the main drawback of a turbocharger is what is called turbocharger lag. This is the time delay that a turbocharger spends waiting for the engine to produce enough exhaust to spin the supercharger and deliver boost. At lower motor speeds, a turbocharger will not function because exhaust gas velocities are not high enough to move the turbine. Therefore, superchargers have an advantage because they are driven continuously while the motor runs.

1.1 Previous Work

Although there have been some amount of work done on superchargers, only few studies are documents in the open literature. Most of the work was done by companies and therefore, the findings are kept confidential.

In a general sense, some approaches to model a supercharger range from using computational fluids dynamics (CFD) as the most general approach and then using a reduced one dimensional model as the simplest approach. In all cases, using experimental work to direct and verify the model is an important part of developing an accurate modeling methodology.

Modeling a supercharger using a one dimensional model was done previously by S.C. Sorenson. He developed a one dimensional model using thermodynamic relationships to analyze a supercharger. There were two students from Iowa State University that have done some work on superchargers as well; Nathanael Meyer and Curtis Carroll. Nathanael Meyer developed tools to understand and predict noise phenomena in a supercharger (Meyer 2003, pg. 64). Curtis Carroll focused on the backflow slots on a supercharger. He developed a model that was able to generate a pressure rise profile that is caused by the backflow slots (Carroll 2004, pg. 80). There is also an experimental work on a supercharger being done at Iowa State University that focuses on the air velocity and related fluid properties using particle image velocimetry (PIV).

The approach taken in this thesis is to follow the previous one dimensional modeling work by Sorenson and Carroll which emphasized using experimental data analysis tools

developed by Meyer to focus the modeling on phenomena that dominate the supercharger response.

1.2 Reduced Order Model

The goal of the reduced order model is to use the lowest order model to get the key aspects of the supercharger performance. While a general model, such as a three dimensional time-based computational fluid dynamics (CFD) model can eventually be made for the supercharger, the goal of the reduced order model is to get the greatest computation speed for an acceptable accuracy. Such a model can then be used for the iterative process of design.

A key step in the development of a reduced order model is to identify and understand the phenomena in the supercharger that dominate the response, be it efficiency or noise. Once identified, the work then proceeds to use the simplified model of those phenomena that provides adequate accuracy.

The process of identifying the phenomena can be through experiments or computational work. In the case of the current supercharger, the advanced computational tools (such as CFD) are not available, so the focus was on the experimental results. In the future, as the CFD process is improved, it may prove possible to use the time consuming CFD work to further identify phenomena to be used in the reduced order model.

The reduced order model takes into account the basic key features of the supercharger, such as the flow effects, heat transfer effects, and also the variation in the volumes and areas inside the supercharger as the rotor turn.

1.3 Research Overview

The goal of this research was to develop a computational tool for supercharger design. The computational tool is based on a simplified one dimensional model of the supercharger following previous work done by Sorenson. The model is augmented with the response of the backflow slots and the acoustic pulses generated by the carryback slot.

The input to the computational tool is the geometry of the supercharger as a function of rotor angle. The geometry is quantified in terms of volumes and surface areas. The surface areas include surface areas for heat transfer and areas for flow, including leakage flow between the rotor and the wall. Additional input is the rotor speed and pressure ratio. The program requires an initial estimate of the flow rate, but then varies the flow rate to attain the desired pressure ratio.

The computational tool predicts the air performance of the supercharger and the pressure signals in the supercharger. From the signals, a prediction of the noise generated by the supercharger can be developed in the future. The air performance is quantified by the volumetric efficiency and the J1723 isentropic efficiency. Comparisons of the predictions and measured values show that the computational tool is capable of showing the trends of the efficiency as a function of motor speed (RPM) and pressure ratio between the supercharger outlet and inlet.

1.4 Thesis Outline

This thesis will discuss previous work on modeling a roots type supercharger done by S.C. Sorenson. The theory on modeling the supercharger using one dimensional thermodynamic relationships will be discussed first, followed by improvements made to the computational tool, such as including the backflow slots. Finally, a carryback slot pulse model will be presented. Detailed algorithms of the computational tool will then be discussed, including the thorough explanation of inputs, the main program, and outputs. The results on backflow slot improvements will be presented in graph form displaying pressure and temperature signals over 120 degrees of rotor motion. Efficiencies as the output of the computational tool will then be compared to measured data. The process of matching the efficiency results between the computational model and measured data will also be discussed. Carryback slot pulse results will be analyzed and compared to measured data. Finally, the summary and conclusion of the work in this thesis will be presented, followed by some suggestions for future work.

Chapter 2
Theory

S.C. Sorenson did significant work to model a three lobe roots type supercharger. The model was able to capture some critical aspects of the supercharger using one dimensional thermodynamic relationships. It divides the three lobe roots type supercharger into three to five separate control volumes depending on the angle of rotation and thermodynamic conditions of the control volumes (Sorenson 1984, pg. 115). Each control volume is connected to the adjacent control volumes through small leakage flow areas. In Figure 2.1, supercharger cross sectional view for Sorenson's model, the supercharger is divided into 4 separate control volumes: inlet (I), low pressure receiver 1 (R1), outlet (R3), and trapped volume 2 (T2). The leakage flow areas and their directions for this particular angle position are circled: $\dot{m}_{LI1}, \dot{m}_{LI2}, \dot{m}_{RPT1}$, and $\dot{m}_{T2}$.

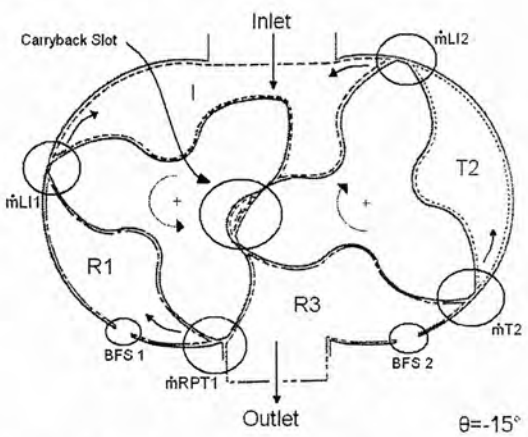

Figure 2.1 Sorenson's model supercharger cross sectional view showing control volumes, backflow slots, flow areas, and their directions (Sorenson 1984, pg. 116).

In Figure 2.1 and other similar supercharger cross sectional views the inlet is on the top; the outlet is on the bottom; the left rotor turns counterclockwise; and the right rotor turns clockwise. The rotor speeds (in RPM) and pressure ratio serve as input values in Sorenson's model. Then, thermodynamic relationships are assigned to each control volume and solved

for temperature and pressure values on every angle increment. After all the temperature and pressure values in those control volumes are solved, the supercharger efficiency is calculated to obtain the performance index of the supercharger. A more detailed discussion of Sorenson's model will be presented later in this chapter.

Overall, Sorenson's model was able to predict the performance (supercharger efficiency) trends accurately. A much closer agreement with the measured data was found more in lower rotors speeds than it was in high rotors speed (Sorenson 1984, pg.126). It was also concluded that the leakage flow was found to be an important factor influencing the volumetric efficiency with the inlet area and the heat transfer effects having a much smaller influence (Sorenson 1984, pg. 127). In short, the strength of Sorenson's model is that it takes into account the leakage flows and heat transfer effects in a supercharger. It does not, however, model other features of the supercharger that have effect on the supercharger performance, such as backflow slots (Carroll 2004, pg. 81).

Backflow slots, BFS1 and BFS2, (circled in Figure 2.1) are flow areas located near the outlet. Their purpose is to reduce the noise due to the sudden pressure change created by the trapped volume as it opens to the outlet. The work to model backflow slots was previously done by Curtis Carroll from Iowa State University. As Carroll suggested in his thesis, the work that he has done can be expanded further by combining Sorenson's model and his backflow slot model. The anticipated result was that the new model would give a more accurate prediction on the pressure and temperature profiles as well as the supercharger efficiency, especially at low rotor speeds. Another important finding by Carroll was that the pressure pulse seen in the measured data is not caused by backflow slots (Carroll 2004, 65). He suggested that the carryback slot, which is located on the inlet side of the rotors, be investigated as the source of pulses (See Figure 2.1). The goal for this pressure pulse investigation is to better match the pressure profile prediction to the measured data.

Discussion on the development of a simplified model that incorporates all these effects will be presented. Background information of Sorenson's work will first be discussed; followed by some improvements made to the model such as backflow slots, the carryback slot, and pressure pulse generation.

2.1 Sorenson's Model

The roots type supercharger studied has two three lobe rotors (Figure 2.1); therefore, the cycle repeats every 120 degrees. Furthermore, since the supercharger is symmetric with respect to the two rotors, the first 60 degrees of the 120 degrees cycle is the mirror of the second 60 degrees. Hence, the base equations for the first 60 degrees are the same as the second 60 degrees; the difference between the two will be just on the left and right side orientation of the supercharger. Therefore, only 120 degrees of the full 360 degrees shaft rotations needs to be modeled. In reality, the supercharger is not exactly symmetric, but the non-symmetry can be included in the model parameter rather than in the base equations. Before developing the equations, different control volumes have to be defined for a single 120 degree cycle.

2.1.1 Supercharger Subsystem

Sorenson's model divides a three lobe rotors supercharger into between three and five separate control volumes, depending on the geometric and/or thermodynamic conditions of the supercharger (Sorenson 1984, pg. 115). These volumes change as the shaft rotates. Figure 2.1 shows an example of the supercharger's control volumes at one particular shaft angle, -15 degree. At this angle, there are four types of control volumes; inlet volume (I), trapped volume (T2), low pressure receiver volume (R1), and outlet volume (R3).

The inlet control volume is bounded by the inlet port, housing, and the two rotors (denoted as I in Figure 2.1). Fresh air comes into the inlet control volume. As the shaft rotates this volume gets trapped, and is finally delivered to the outlet. The inlet volume is connected to the trapped volumes by flow through the clearance between the rotor tips and the housing.

The trapped control volume is a constant volume system bounded between the rotor lobes, housing, inlet, and outlet control volume (denoted as T2 in Figure 2.1). The control volume remains closed until the leading rotor tip passes the outlet port at which point the trapped air gets mixed with high pressure air from the outlet control volume. Depending on

the rotation angle and the location of the inlet and outlet ports, either one or two trapped volumes exist. There are leakage flows that enter and leave this control volume depending on the pressure in this and the adjacent control volume.

The remaining portion of the supercharger system is an outlet control volume. It may consist of one or two parts; a high pressure receiver only or both a low pressure receiver (denoted as R1 in Figure 2.1) and a high pressure receiver (denoted as R3 in Figure 2.1). When the trapped volume first opens to the outlet, it becomes a low pressure receiver. Air from the high pressure receiver is assumed to flow to the low pressure receiver system and mix. During the mixing process, the low and high pressure receivers are considered to be two separate control volumes. The low pressure receiver then ceases to exist after both pressures are equal or an arbitrary angle of rotation is reached.

As previously discussed, since these control volumes change as the shaft turns, a step by step control volume definition will be presented for 15 degree increments. Since the second 60 degrees mirrors the first 60 degrees of angle rotation, only the first 60 degrees of angle rotation of a 120 degrees cycle will be discussed in this chapter. All diagrams of the supercharger cross sectional view were taken from Sorenson's technical paper (Sorenson 1984, pg 116-117).

Figure 2.2 shows the supercharger at the beginning of the cycle. The low pressure receiver (R1) is just created as the leading tip of the left hand rotor passes the outlet port. The high pressure receiver (R3) flows through the clearance between the tip and the housing to the low pressure receiver (R1). This clearance gets larger as the rotors turn. On the right hand side, the trapped volume (T2) moves toward the outlet.

Figure 2.3 shows the supercharger configuration at 0 degree. This particular supercharger configuration, where the tips of the two rotors pointing to the left hand side of the supercharger, is considered very important since this position is used as the standard 0 degree position for modeling other types of three blade roots type superchargers. This 0 degree position will also be used later for modeling the M-45 supercharger from Eaton Corporation. It can be seen that the flow area between R3 and R1 has increased. It is possible that the pressures have already equalized. If the pressures are the same, the R1 and

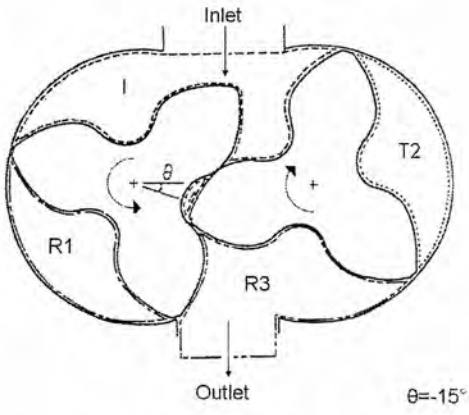

Figure 2.2 Supercharger configuration at the start of the cycle, -15 degree (Sorenson 1984, pg. 116).

R3 will be merged into one control volume (R3) with a volume equal to their sum. In this case the minimum number of three systems exists. The trapped volume, T2, is getting closer to the outlet port. The left hand side of the supercharger is almost forming a new trapped volume (T1).

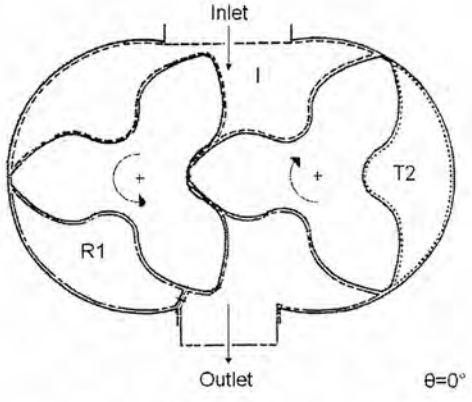

Figure 2.3 Supercharger configuration at 0 degree (Sorenson 1984, pg. 116).

Figure 2.4 shows the supercharger configuration at 15 degree. The left hand side trapped volume (T1) is just created. If the pressure at R1 is still below the pressure at R3, then the maximum number of five systems exists. The volume T2 continues its rotation toward the

outlet port and the inlet volume has decreased dramatically due to the creation of the trapped volume.

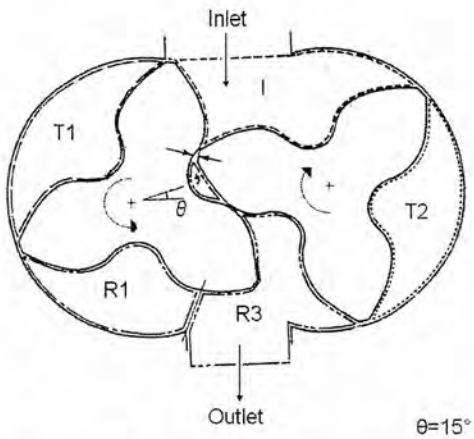

Figure 2.4 Supercharger configuration at 15 degree (Sorenson 1984, pg. 117).

Figure 2.5 shows the supercharger configuration at 30 degree. The volume T2 is getting closer to the outlet. The right hand portion of the inlet is being moved towards becoming another trapped volume.

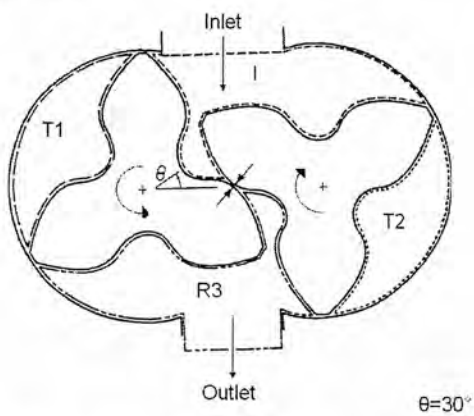

Figure 2.5 Supercharger configuration at 30 degree (Sorenson 1984, pg. 117).

Figure 2.6 shows the supercharger configuration at 45 degree. It is symmetric to the supercharger configuration at -15 degree in Figure 2.2. The volume T2 is finally opened to the outlet (R3); thus becoming the low pressure receiver (R2). The volume T1 on the left hand side is moving towards the outlet as the rotors turn.

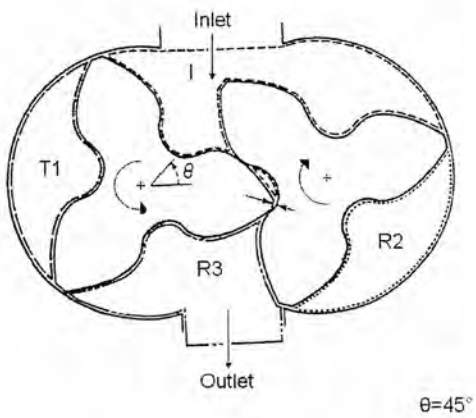

Figure 2.6 Supercharger configuration at 45 degree (Sorenson 1984, pg. 117).

Heat transfer areas, flow areas, and volume areas for each control volumes are determined at this 15 degree increment. To achieve a better accuracy in the pressure and temperature results, a linear interpolation from those five angular positions is taken to obtain those geometric values at a smaller angle increment, for example a 1degree increment.

2.1.2 Flows

Air flows have to exist within a supercharger due to the fact that there is a pressure difference between each control volume. The flow can be coming into the supercharger, out of the supercharger, or it can be within the supercharger itself.

In this model, there are two types of air flows that are considered. One is the flow that is inherent and essential for the operation of supercharger. This type of flow includes inlet flow ($\dot{m}_{in}$), which is a flow of fresh air that comes into a supercharger system, outlet flow ($\dot{m}_{out}$), which is a flow of compressed air that leaves the supercharger system, and finally the flow from a high pressure region to a low pressure region ($\dot{m}_{RPT}$). The last flow usually occurs at the time when the trapped volume just opens up to the outlet. That is when two volumes with different pressure mix with each other. This flow is more complicated to analyze than the inlet and outlet flows because there is no finite location to determine the flow area. More detailed discussion of this flow area can be seen in subsection 2.1.3.

The second type of the flow is leakage flow. This type of flow is not essential in the operation of supercharger and does not have good effects on its performance; however, they always occur due to the need of finite clearances. In general these flows represent parasitic losses in the system. The leakage flows that are considered in this model are the leakage between two rotor tips ($\dot{m}_{tip}$), the leakage from the trapped volume to the inlet ($\dot{m}_{LI}$), the leakage from the outlet to the trapped volume ($\dot{m}_{T}$), and the leakage from the low pressure receiver to the trapped volume ($\dot{m}_{T}$). Only the flow area for leakage between two rotors tip is determined by the clearance between the tips of the two rotors, the flow areas for the rest of the leakages are determined by the clearance between the tip and the supercharger housing. The controlling pressures for $\dot{m}_{tip}$ are the inlet pressure (P_I) and the outlet pressure (P_{R3}). The controlling pressures for $\dot{m}_{LI}$ are the inlet pressure (P_I) and the trapped volume pressure (P_T). The controlling pressures for $\dot{m}_{T}$ can be the trapped pressure (P_T) and the outlet pressure (P_{R3}) or the trapped pressure (P_T) and the low pressure receiver pressure (P_{R1}), depending on which control volume the flow is from.

All flows are assumed to be quasi-steady and isentropic. The adjustment for non-ideal flow effects are made through the flow coefficient. The two possibilities for the mass flow is that it is either choked or non-choked for a compressible fluid. In the case of a choked flow, the mass flow rate is

$$\dot{m} = \left\{ K \cdot \left(\frac{2}{\gamma+1} \right)^{\left(\frac{\gamma+1}{2\gamma-2} \right)} \right\} \cdot \frac{1}{6 \cdot N} \qquad \textbf{2.1}$$

and for a non-choked flow, the mass flow rate is

$$\dot{m} = \left\{ K \cdot \left(\frac{2}{\gamma-1} \right) \cdot \left[\left(\frac{P}{P_o} \right)^{\left(\frac{2}{\gamma} \right)} - \left(\frac{P}{P_o} \right)^{\left(\frac{\gamma+1}{\gamma} \right)} \right] \right\}^{1/2} \cdot \frac{1}{6 \cdot N} \qquad \textbf{2.2}$$

where

$$K \equiv \frac{C_f \cdot A \cdot P_o}{R \cdot T_o} \left(\gamma \cdot R \cdot T_o\right)^{1/2} \qquad \textbf{2.3}$$

γ : specific heat ratio (dimensionless)
N : rotor speed (RPM)
P : downstream air pressure (Pa)
P_o : upstream air pressure (Pa)
T_o : upstream air temperature (K)
C_f : flow coefficient (dimensionless)
A : flow area (m^2)
R : gas constant for air (kJ/kg K)

Since flows occur from high pressure to low, the upstream pressure (P_o) is always higher than downstream pressure (P).

2.1.3 Flow Areas

A key set of parameters in the supercharger model are the flow areas. These areas are both critical to the supercharger operation and exist because of the expected manufacturing tolerances between parts. There are four flow areas that need to be considered in this model; inlet area, receiver filling area, tip clearance area between rotors, and clearance area between the rotor tip and supercharger housing.

The inlet area is an area through which fresh air first enters the supercharger system. This area does not change as the shaft turns. For this model, the inlet area is measured at the edge of the supercharger inlet.

The receiver filling area (Figure 2.7) is the most complicated flow area in this model. It is defined by the minimum distance between the outlet port and the rotor lobe that has just passed the port. This area starts with the size of the clearance between the rotor tip and housing and increases as the rotors turn. In an actual supercharger, this flow area does not

exist; hence, this area serves an imaginary boundary to separate the low pressure receiver (R1 or R2) and the outlet volume (R3) when there is a pressure difference between the two control volumes.

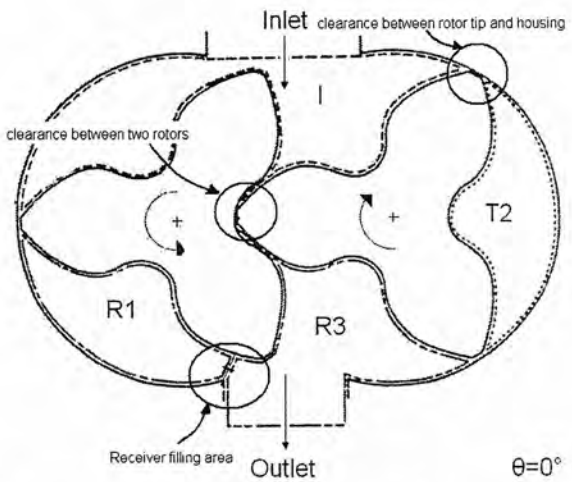

Figure 2.7 Supercharger cross sectional view showing multiple flow areas (Sorenson 1984, pg. 116).

To obtain this receiver filling area, two end values of the receiver filling area were measured; one at the time when the trapped volume starts to open to the outlet and one after the rotors turn 15 degrees. Considering that these superchargers operate at 4000 RPM at the lowest speed for the data measurement and these control volumes are small (approximately 120 cm^3 for R1 and 280 cm^3 for R3 at -15 degree), then 15 degree is justified to be a sufficient amount of time for those pressures to mix. A linear interpolation was then taken from those values in order to get this receiver filling area at a smaller angle increment. The model also takes into account that this area will not exists after the two pressures equalize. Hence, there are two conditions that are applied to the receiver filling area in this model. First, when there is a pressure difference, the receiver filling area will be used and $\dot{m}_{RPT}$ will be calculated. Second, when the pressures equalize (even when the rotors have not rotated for 15 degrees), the receiver filling area will be ignored and $\dot{m}_{RPT}$ will not be calculated.

The next flow area is the tip clearance area between two rotors, Figure 2.7. There are two possibilities of tip clearance area depending on angle position; one is along the line of

contact for the curve profile of the rotors (tip flow 1 in Figure 2.8) and the other is the clearance between the rotor tip and rotor lobe (tip flow 2 in Figure 2.8). This model, however, assumes that the leakage area between the two rotors to be constant regardless of which part of the rotors creates the flow boundary.

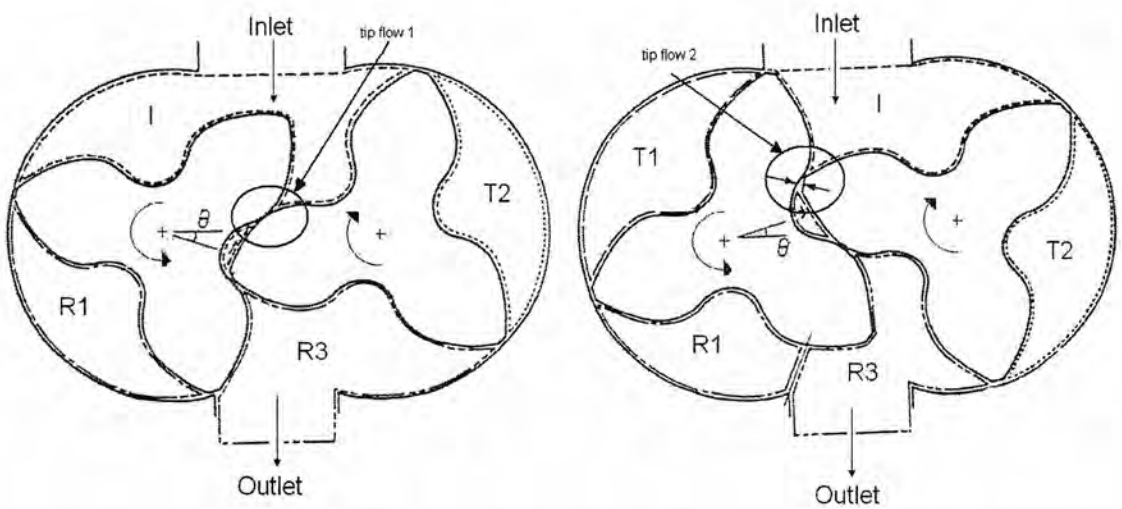

Figure 2.8 Supercharger configuration showing two different tip flows (Sorenson 1984, pg. 116-117).

The last flow that is considered in this model is the clearance area between the rotor tip and housing, Figure 2.7. This area is the leakage path around the side of the supercharger. It is the minimum distance between the rotor tip and supercharger housing. This distance stays constant in magnitude throughout the rotation of the blades.

2.1.4 Equations

For each control volumes, the following equations are applied:

1. Equation of state

$$P_i \cdot V_i = m_i \cdot R \cdot T_i \qquad \textbf{2.4}$$

2. Conservation of mass

$$\frac{dm_i}{d\theta} = \sum_{in} \dot{m}_j - \sum_{out} \dot{m}_j \qquad \textbf{2.5}$$

3. Conservation of energy

$$\dot{Q}_i - \dot{W}_i = \frac{d(m_i \cdot u_i)}{d\theta} - \sum_{in} \dot{m}_j \cdot h_j + \sum_{out} \dot{m}_j \cdot h_j \qquad \textbf{2.6}$$

$$\dot{Q}_i = h_i \cdot A_i \cdot (T_{wall} - T_i) \qquad \textbf{2.7}$$

where:

P_i : air pressure at control volume i (Pa)

V_i : volume of air at control volume i (m^3)

m_i : mass of air at control volume i (kg)

T_i : air temperature at control volume i (K)

$\frac{dm_i}{d\theta}$: angular rate of change of mass at control volume i (kg/deg.)

$\dot{m}_j$: mass flow rate (kg/deg.)

$\dot{Q}_i$: convection heat transfer rate at control volume i (J/deg.)

$\dot{W}_i$: work done within control volume i – due to volume change (J/deg.)

u_i : internal energy at control volume i (J/kg)

h_j : enthalpy (J/kg)

The variables that must be solved from these equations are the mass (m_i), the temperature (T_i), and the pressure (P_i).

Sorenson suggested in his model to assume that convection occurs between the supercharger wall and the air inside the supercharger, equation 2.7. A wall temperature of 320K was arbitrarily chosen for all surfaces at all conditions (Sorenson 1984, pg. 120). Hence, the direction of the heat transfer varies between each control volume depending on the temperature of the air inside the control volume. If the air is hotter than the wall temperature, then the convection process occurs from the air to the supercharger wall. If the wall temperature is hotter than the air, then the convection process occurs from the supercharger wall to the air.

2.1.5 Analysis of Sorenson's Model Supercharger Subsystem

In this section, the equations discussed in section 2.1.2 and 2.1.4 will be applied to one particular angle position (-15 degree). Each control volume and its mass flows will be analyzed and finally temperature and pressure from each control volume will be solved for. Detailed information on the unit conversion in the following formulas can be seen in Appendix A.

As seen in Figure 2.9, the mass flows in and out of the control volume R1 are $\dot{m}_{RPT1}$ and $\dot{m}_{LI1}$, respectively. Since the angle that is being analyzed is the beginning of the cycle, temperature and pressure at each control volume are unknown. Hence, these values need to be guessed as an initial condition. For the next angle step, the mass flows are calculated from the pressure differences across each area, that were calculated in the previous angle step.

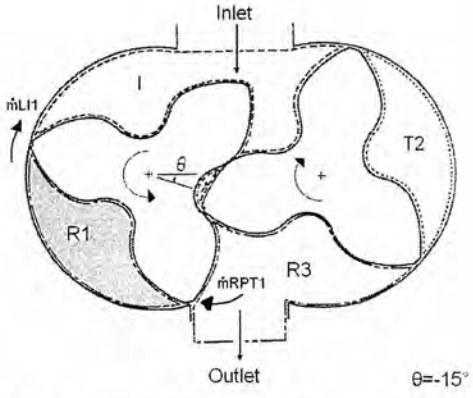

Figure 2.9 Analyzing the R1 control volume (Sorenson 1984, pg.116).

First the Mach number for the $\dot{m}_{RPT1}$ flow is calculated to see if the flow is choked,

$$M_{RPT1} = \left\{ \frac{2}{\gamma - 1} \left[\left(\frac{P_{R3}}{P_{R1}} \right)^{\frac{\gamma - 1}{\gamma}} - 1 \right] \right\}^{1/2} \qquad \textbf{2.8}$$

The controlling pressures for $\dot{m}_{RPT1}$ are P_{R3} and P_{R1}. Since flow is coming in from the outlet, R3, into R1, the upstream and downstream pressures are P_{R3} and P_{R1}, respectively. If $M_{RPT1} \geq 1$, then $\dot{m}_{RPT1}$ is a choked flow and is calculated as:

$$\dot{m}_{RPT1} = \left\{ K \cdot \left(\frac{2}{\gamma+1} \right)^{\frac{\gamma+1}{2\gamma-2}} \right\} \cdot \frac{1}{6 \cdot N} \qquad \textbf{2.9}$$

If $M_{RPT1} < 1$, then $\dot{m}_{RPT1}$ is a non-choked flow and is calculated as:

$$\dot{m}_{RPT1} = \left\{ K_{RPT1} \cdot \left(\frac{2}{\gamma-1} \right) \left[\left(\frac{P_{R1}}{P_{R3}} \right)^{\frac{2}{\gamma}} - \left(\frac{P_{R1}}{P_{R3}} \right)^{\frac{\gamma+1}{\gamma}} \right] \right\}^{1/2} \cdot \frac{1}{6 \cdot N} \qquad \textbf{2.10}$$

The same Mach number and flow calculations are done for $\dot{m}_{LI1}$. The upstream and downstream pressures are PR1 and PI, respectively. After all flows in the control volume are calculated, the continuity equation, equation 2.5, is applied,

$$\frac{dm_{R1}}{d\theta} = \dot{m}_{RPT1} - \dot{m}_{LI1} \qquad \textbf{2.11}$$

The temperature at R1 for the new angle, T_{R1_new}, is then solved for using the conservation of energy equation, equation 2.6, that has been modified algebraically,

$$T_{R1\_new} = T_{R1} + \left(\frac{\theta \cdot \left(\dot{Q}_{R1} - P_{R1} \cdot \frac{dV_{R1}}{d\theta} - C_v \cdot T_{R1} \cdot \frac{dm_{R1}}{d\theta} - Cp \cdot \left(\dot{m}_{LI1} \cdot T_{R1} - \dot{m}_{RPT1} \cdot T_{R3} \right) \right)}{m_{R1} \cdot C_v} \right) \qquad \textbf{2.12}$$

where all temperatures, pressures, volumes, areas, and flow areas are from the previous time step. For this case, the temperature and pressures are obtained from the guessed initial conditions. The detailed algebraic manipulation for the energy equation is presented in Appendix B.

The same analysis is applied to control volume T2, Figure 2.10. The flow rates are calculated as for the control volume R1, but with the upstream and downstream pressure for the $\dot{m}_{T2}$ flow being P_{R3} and P_{T2}, respectively and for the $\dot{m}_{LI2}$ flow being P_{T2} and P_{in}, respectively.

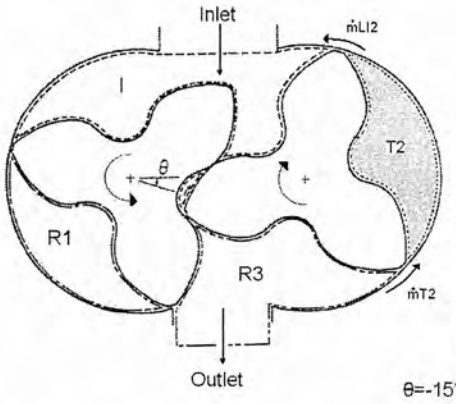

Figure 2.10 Analyzing the T2 control volume (Sorenson 1984, pg. 116).

The continuity and conservation of energy equations for T2 are:

$$\frac{dm_{T2}}{d\theta} = \dot{m}_{T2} - \dot{m}_{LI2} \qquad \textbf{2.13}$$

and

$$T_{T2\_new} = T_{T2} + \left(\frac{\theta \cdot \left(\dot{Q}_{T2} - P_{T2} \cdot \frac{dV_{T2}}{d\theta} - C_v \cdot T_{T2} \cdot \frac{dm_{T2}}{d\theta} - Cp \cdot \left(\dot{m}_{LI2} \cdot T_{T2} - \dot{m}_{T2} \cdot T_{R3} \right) \right)}{m_{T2} \cdot C_v} \right) \qquad \textbf{2.14}$$

The analysis continues to the inlet control volume, Figure 2.11. The upstream and downstream pressure for $\dot{m}_{tip}$ flow is P_{R3} and P_I, respectively. The continuity equation and conservation of energy for the inlet volume are

$$\frac{dm_I}{d\theta} = \dot{m}_{LI2} + \dot{m}_{LI1} + \dot{m}_{in} + \dot{m}_{tip} \qquad \textbf{2.15}$$

$$T_{I\_new} = T_I + \left(\frac{\theta \cdot \left(\dot{Q}_I - P_I \cdot \frac{dV_I}{d\theta} - C_v \cdot T_I \cdot \frac{dm_I}{d\theta} - Cp \cdot \left(-\dot{m}_{LI2} \cdot T_{T2} - \dot{m}_{LI1} \cdot T_{R1} - \dot{m}_{tip} \cdot T_{R3} - \dot{m}_{in} \cdot T_{up} \right) \right)}{m_I \cdot C_v} \right) \qquad \textbf{2.16}$$

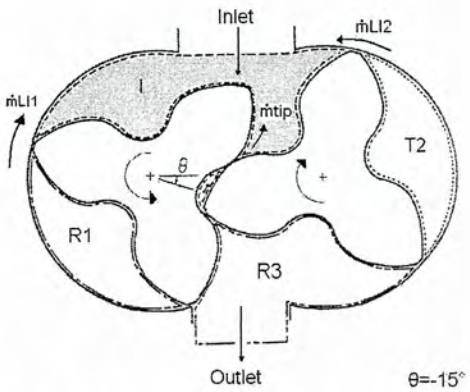

Figure 2.11 Analyzing the inlet control volume (Sorenson 1984, pg. 116).

where $\dot{m}_{LI1}$ and $\dot{m}_{LI2}$ have already been calculated and $\dot{m}_{in}$ is the density of air at the inlet multiplied by the volumetric rate of change for the inlet (See Appendix B for details).

The final control volume, the outlet control volume (R3), is likewise analyzed. The continuity equation and conservation of energy for outlet volume are:

$$\frac{dm_{R3}}{d\theta} = -\dot{m}_{RPT1} - \dot{m}_{T2} - \dot{m}_{out} - \dot{m}_{tip} \qquad \textbf{2.17}$$

$$T_{R3\_new} = T_{R3} + \left(\frac{\theta \cdot \left(\dot{Q}_{R3} - P_{R3} \cdot \frac{dV_{R3}}{d\theta} - C_v \cdot T_{R3} \cdot \frac{dm_{R3}}{d\theta} - Cp \cdot \left(\dot{m}_{RPT1} \cdot T_{R3} + \dot{m}_{T2} \cdot T_{R3} + \dot{m}_{tip} \cdot T_{R3} + \dot{m}_{out} \cdot T_{R3} \right) \right)}{m_{R3} \cdot C_v} \right) \quad \textbf{2.18}$$

where the mass flows $\dot{m}_{RPT1}$, $\dot{m}_{T2}$, and $\dot{m}_{tip}$ are already known from other control volumes and the outlet mass flow ($\dot{m}_{out}$) is from the assigned outlet volume flow rate multiplied by the density of air at the outlet volume (See Appendix B for details).

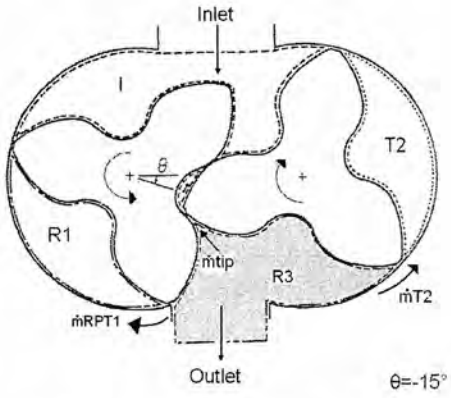

Figure 2.12 Analyzing the outlet control volume (Sorenson 1984, pg. 116).

The same analysis is done for the next incremental angle for the whole cycle, a total of 120 degrees.

2.1.6 Conversion from Temperature to Pressure

The energy equations presented above only solve for the temperature at each incremental angle; hence, a method of converting these calculated temperatures to pressures is needed. Sorenson in his technical papers did not specifically mention how to obtain these pressures, but he made two assumptions to his model that would lead to two ways for doing the temperature to pressure conversion. The assumptions are that all mass flows in the supercharger are considered to be isentropic and the working air inside the supercharger

behaves as an ideal gas. The analysis on each technique will be presented in this subsection and the results from each technique will be presented in chapter 4.

For the isentropic flow approach, pressure values are calculated using:

$$P = \frac{P_o}{\left(\frac{T_o}{T}\right)^{\gamma/\gamma-1}} \qquad \textbf{2.19}$$

where:

P : pressure at the next angle increment (Pa)

P_o : pressure at the previous angle increment (Pa)

T : temperature at the next angle increment (K)

T_o : temperature at the previous angle increment (K)

γ : specific heat ratio (dimensionless)

This formula is applied to every control volume to obtain the pressure at every angle increment. In this approach, the pressure for the next increment is obtained using the next incremental temperature and also the temperature and pressure from the previous increment.

For the ideal gas approach, pressure values are calculated using:

$$P_i = \frac{\left(m_i + \frac{dm_i}{d\theta}\cdot\theta\right)\cdot R\cdot T_i}{V_i} \qquad \textbf{2.20}$$

where

P_i : air pressure in control volume i at the next angle increment (Pa)

T_i : air temperature in control volume i at the next angle increment (K)

m_i : mass of air in control volume at the previous angle increment (kg)

$\frac{dm_i}{d\theta}$: rate of change of mass with respect to angle for control volume i (kg/deg.)

θ : angle increment (deg.)

R : gas constant for standard air (kJ/kg K)

V_i : volume at control volume i at the next angle increment (m^3)

In this approach the next incremental pressure is obtained from the mass, temperature and volume for the next increment. The mass for the next increment is obtained by adding the mass increase for one angle increment ($\frac{dm_i}{d\theta} \cdot \theta$) to the total mass from the previous angle increment m_i.

Both the isentropic flow and ideal gas approaches will be integrated to the model one at a time and the efficiency result from the two will be compared to determine which method should be used. The comparison of the efficiency result using these two approaches is presented in chapter 4.

2.2 Model Improvements

In addition to implementing the model from Sorenson, some improvements were added. The addition focused on phenomena that measured data showed were important. This includes some adjustments to Sorenson's model on the supercharger outlet area, the addition of backflow slots, the addition of a carryback slot, and the pulse generation due to the carryback flow. First the actual M-45 supercharger will be compared to Sorenson's supercharger, and then adjustments to Sorenson's model will be discussed. The information on the backflow slot is then presented; followed by different options in modeling the backflow slot. Then test data from Eaton Corporation which leads to a hypothesis of carryback slot as a source of pulse variation will be presented. Finally, the pressure pulse model will be discussed.

2.2.1 Adjustments to Sorenson's Model

In order to appropriately model the M-45 supercharger, Sorenson's model needs to be adjusted. The key adjustment is focused on shifting the angle position and also on the size and shape of the inlet and outlet flow areas. In this section, the key differences between the supercharger in Sorenson's model and the M-45 supercharger will first be discussed, followed by the analysis of the M-45 supercharger for a 120 degrees cycle. Finally, the

adjustments that were made to Sorenson's model for modeling the M-45 supercharger will be presented.

There are some discrepancies between the supercharger assumed in Sorenson's model and the actual M-45 supercharger. First the supercharger's outlet shape assumed in Sorenson's model is different from the one in the M-45 supercharger. The outlet assumed in Sorenson's model has a rectangular shape, whereas the outlet in the M-45 supercharger has a triangle shape. Figure 2.13 shows the M-45 supercharger picture with and without the casing when it is viewed perpendicularly to the outlet. The left picture shows the triangle shaped outlet flow area of the supercharger casing. The right picture shows the inside view (60 degree twisted rotors) of the supercharger without the casing while the rotors are positioned at 29 degree. On the right picture and other similar pictures, the supercharger orientation stays the same. The left rotor turns counterclockwise, the right rotor turns clockwise.

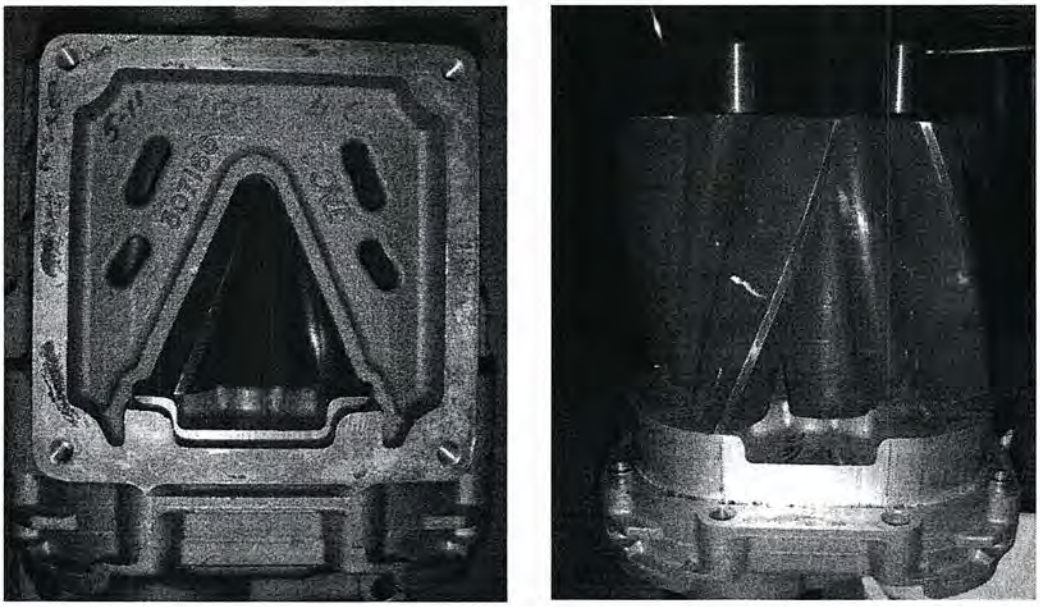

Figure 2.13 M-45 supercharger outlet view with and without casing.

Even though Sorenson did not mention any specific details on the shape or size of the outlet flow area, the shape of the outlet flow area is implicitly stated when the supercharger control volumes was discussed at every 15 degree increment. Figure 2.14 shows a comparison of the supercharger diagram at 30 degree from Sorenson's technical paper and

the actual M-45 supercharger at 29 degree with an imaginary rectangular shaped outlet flow area. In Sorenson's supercharger diagram (left picture), it is clearly seen that trapped volume (T1) has opened to the outlet for quite a while since the leading tip of the trapped volume (circled area) has far passed the outlet port. Hence, on the right picture, for it to agree with Sorenson's diagram on the left, the shape of the outlet flow area has to be rectangular (as drawn), instead of triangular like on the one from Figure 2.13. The circled area in these two pictures shows the same trailing tip.

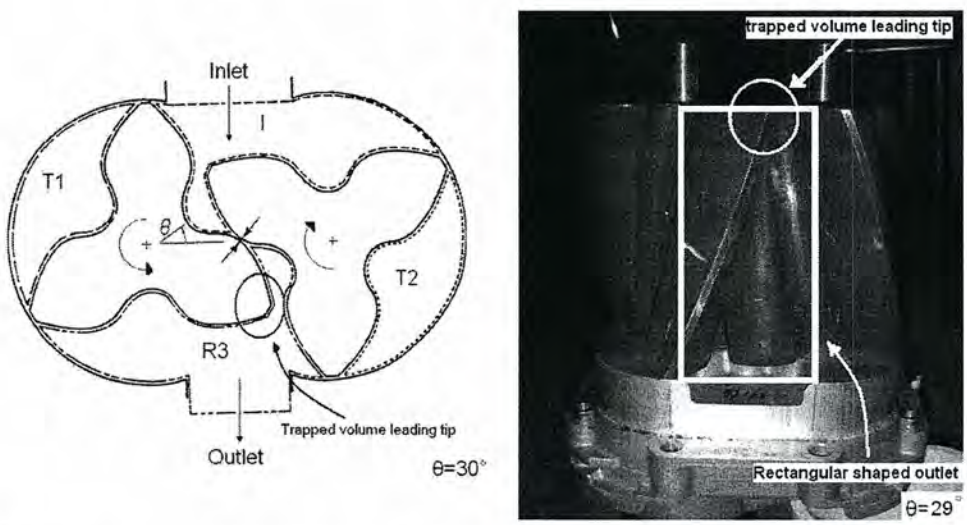

Figure 2.14 Cross sectional view of Sorenson's supercharger (Sorenson 1984, pg. 117) and outlet view of the supercharger with rectangular shaped outlet flow area.

It can be seen on the right picture that having a rectangular shaped outlet results in the leading tip of the trapped volume already passed the outlet at 29 degree. Therefore, it is concluded that the outlet flow area in Sorenson's model has a rectangular shape.

This outlet flow area shape difference causes the discrepancies in the angle position when the trapped volume opens to the outlet. Taking the same picture as in Figure 2.14 and adding in a triangle shaped outlet flow area (instead of rectangular shape) shows that at this position (29 degree) the trapped volume has just opened to the outlet, Figure 2.15. The other discrepancy is that the length of the actual outlet area is about half of the length of the M-45

supercharger, which is different from the length of the rectangular outlet in Figure 2.14. The longer the outlet area, the more mass flow that comes in to the low pressure receivers. Hence, the mixing process gets even faster. Based on this comparison on the shape and size of the outlet flow area, the M-45 supercharger is analyzed to determine which control volumes exist at each angle. The results conclude that over 120 degree cycle, the M-45 supercharger can be distinguished into 4 different configurations.

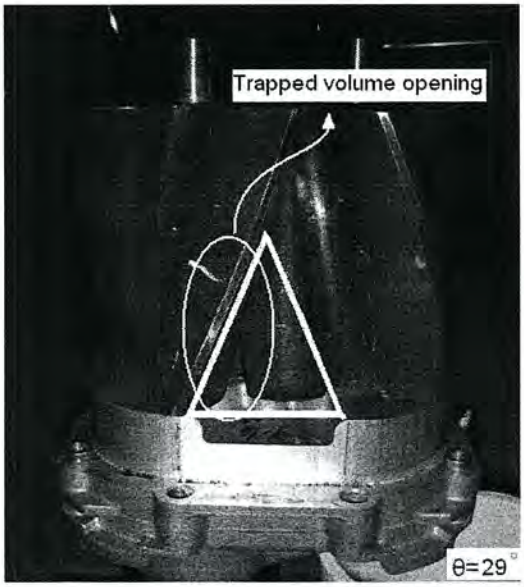

Figure 2.15 M-45 supercharger inside view with imaginary triangular outlet at 29 degree.

Figure 2.16 shows the M-45 supercharger at the start of the cycle, -15 degree (the first configuration). The control volumes are T1, outlet (R3), T2, and inlet. Note that the trapped volume (T1) has not open to the outlet until 29 degree.

The second configuration of the M-45 supercharger is shown in Figure 2.17. The low pressure receiver R1 has just been created, although it is not clearly shown here that the leading tip of the trapped volume (T1) has just passed the outlet. Refer back to Figure 2.15 for a better representation of what is really happening. One other adjustment to Sorenson's supercharger model is that at this angle the new trapped volume (T1) is created, Figure 2.17. This is caused by the inlet area of the M-45 supercharger being bigger than the one from the

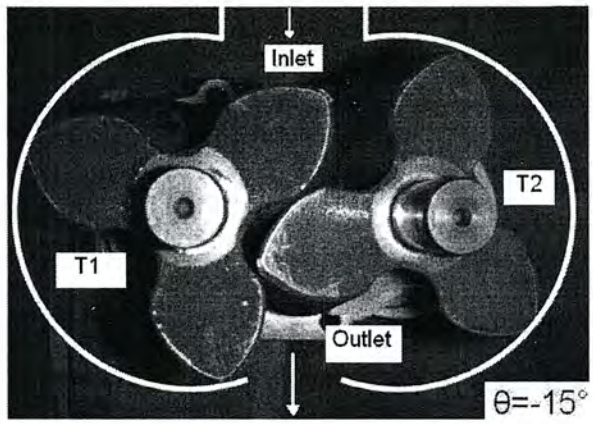

Figure 2.16 M-45 supercharger configuration at -15 degree.

supercharger in Sorenson's model. Hence, the maximum numbers of control volumes exist at this angle; the volumes are the inlet, T1, R1, outlet (R3), and T2.

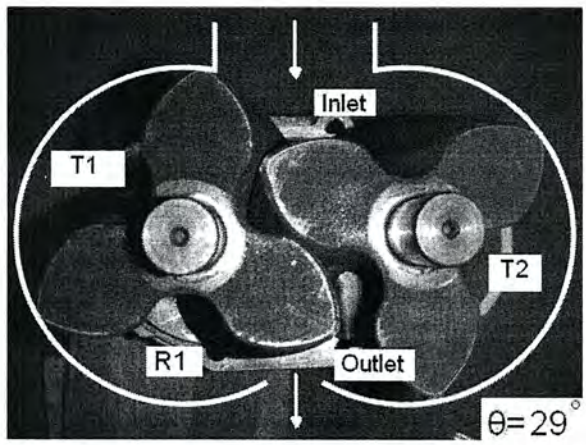

Figure 2.17 M-45 supercharger configuration at 29 degree.

The third configuration of the M-45 supercharger starts at 45 degree, Figure 2.18. This angle position exists due to the symmetry of the supercharger – the configuration at 45 degree is symmetric to the one at -15 degree. At this point, pressure at R1 is considered to have been mixed with the outlet pressure; therefore, the control volumes that exist at this point are the inlet, T1, outlet (R3), and T2.

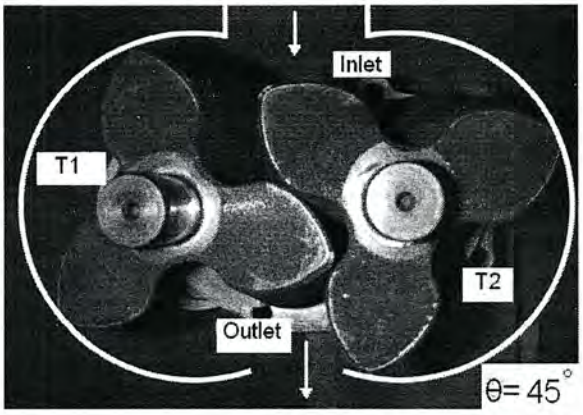

Figure 2.18 M-45 supercharger configuration at 45 degree.

The last configuration, the fourth, of the M-45 supercharger starts at 89 degree (Figure 2.19). Again, this configuration is symmetric to the second configuration (at 29 degree). Here the right low pressure receiver (R2) has just been created and started to mix with the outlet. The control volumes that exist at this point are the inlet, T1, outlet (R3), R2, and T2. Note that the new trapped volume (T2) is created at the time the leading T2 opens to the outlet.

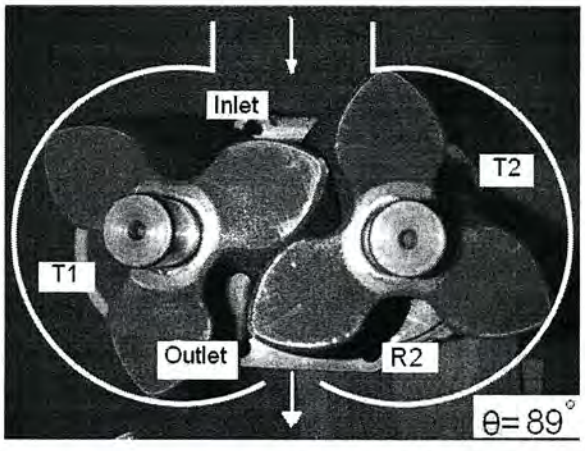

Figure 2.19 M-45 supercharger configuration at 89 degree.

To sum up, configuration 1 (when the inlet, T1, outlet, and T2 exist) occurs from -15 degree to 29 degree. Configuration 2 (when the inlet, T1, R1, outlet, and T2 exist) occurs from 30 degree to 44 degree. Configuration 3 (when the inlet, T1, outlet, and T2 exist)

occurs from 45 degree to 88 degree. Lastly, configuration 4 (when the inlet, T1, outlet, R2, and T2 exist) occurs from 89 degree to 105 degree. Furthermore, the symmetry between configuration 1 and 3 and between configuration 2 and 4 has an angle difference of 60 degree. This is inherently caused by the geometric aspect of the supercharger; the supercharger has two intermeshing rotors and each rotor has three lobes.

The flow, continuity and energy equations discussed in section 2.1.2 and 2.1.5 and the angle shift have to be adjusted accordingly to accommodate all control volumes that exists in the M-45 supercharger. For example, a new control volume T1 has to be added when the leading T1 opens to the outlet, at 29 degree, since previously in Sorenson's model, the new T1 has not been created yet when the leading T1 opens to the outlet, at -15 degree (Figure 2.20).

The following is one example of the adjustments made. Figure 2.20 shows Sorenson's model at -15 degree on the left and the M-45 supercharger at 29 degree on the right. These two different angle positions are picked since both have one thing in common; the trapped volume (T1) just opens to the outlet. As seen in Figure 2.20, at this configuration, the actual M-45 supercharger has one more leakage flow due to the new formation of the trapped volume (T1).

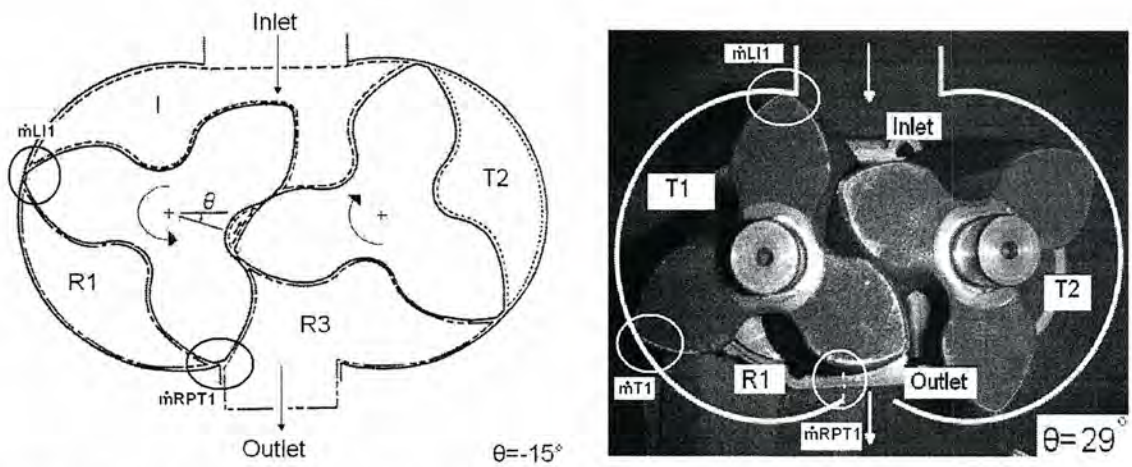

Figure 2.20 Comparison between Sorenson's supercharger model (Sorenson 1984, pg. 116) and M-45 supercharger at the time when trapped volume (T1) just opens to the outlet.

Table 2.1 shows how the continuity and energy equations compare between the two models, all the differences between the two are circled. All the adjustments made to the model are to accommodate the new trapped volume (T1) that is created. Most of the changes made are rather minor, by switching around the mass flow terms and the temperature terms, although one big change made to the model is done by adding in a brand new continuity and energy equations for the control volume T1.

Adjustments to the mass flow rate need to be done when analyzing control volume R1. Since the M-45 has created a new trapped volume at this point, the flow rate coming out from R1 is now $\dot{m}_{T1}$. The same adjustment is also made to the energy equation. A new control volume T1 is created, therefore a new set of continuity and energy equations needs to be added. The inlet and outlet flow rate for this control volume are $\dot{m}_{T1}$ and $\dot{m}_{LI1}$, respectively. For the inlet control volume, only the energy equation needs to be changed. All the flows stay the same; $\dot{m}_{LI1}$, $\dot{m}_{LI2}$, $\dot{m}_{lip}$, and $\dot{m}_{in}$. The temperature term needs to be changed in the energy equation, since $\dot{m}_{LI1}$ now comes from the control volume T1, the $\dot{m}_{LI1}$ term is then multiplied by T_{T1}.

After all these adjustments are made to all four configurations for the 120 degree cycle, the next step of the model improvement, which is adding the backflow slot feature, can be made.

2.2.2 Backflow Slots Feature Addition

The purpose of backflow slots is to reduce noise that is created by the supercharger due to a sudden pressure change in the outlet region when the trapped volume opens to the outlet. At the time when the trapped volume opens to the outlet volume, two different pressures, the trapped volume with low pressure and the outlet volume with high pressure, are exposed to each other. The noise is quite loud especially at high pressure ratios, such as 1.4, 1.6, and 1.8. Backflow slots increase the trapped volume pressure before it fully opens to the outlet by flowing air from the outlet region into the trapped volume at a slower

Table 2.1 Equation comparison between Sorenson supercharger and M-45 supercharger.

Control Volume Analyzed	Equation	Supercharger	
R1	Continuity	Sorenson	$\frac{dm_{R1}}{d\theta} = \dot{m}_{RPT1} - \dot{m}_{LI1}$
		M-45	$\frac{dm_{R1}}{d\theta} = \dot{m}_{RPT1} - \dot{m}_{T1}$
	Energy	Sorenson	$T_{R1\_new} = T_{R1} + \left(\frac{\theta \cdot \left(\dot{Q}_{R1} - P_{R1} \cdot \frac{dV_{R1}}{d\theta} - C_v \cdot T_{R1} \cdot \frac{dm_{R1}}{d\theta} - Cp \cdot \left(\dot{m}_{LI1} \cdot T_{R1} - \dot{m}_{RPT1} \cdot T_{R3} \right) \right)}{m_{R1} \cdot C_v} \right)$
		M-45	$T_{R1\_new} = T_{R1} + \left(\frac{\theta \cdot \left(\dot{Q}_{R1} - P_{R1} \cdot \frac{dV_{R1}}{d\theta} - C_v \cdot T_{R1} \cdot \frac{dm_{R1}}{d\theta} - Cp \cdot \left(\dot{m}_{T1} \cdot T_{R1} - \dot{m}_{RPT1} \cdot T_{R3} \right) \right)}{m_{R1} \cdot C_v} \right)$
T1	Continuity	Sorenson	N/A
		M-45	$\frac{dm_{T1}}{d\theta} = \dot{m}_{T1} - \dot{m}_{LI1}$
	Energy	Sorenson	N/A
		M-45	$T_{T1\_new} = T_{T1} + \left(\frac{\theta \cdot \left(\dot{Q}_{T1} - P_{T1} \cdot \frac{dV_{T1}}{d\theta} - C_v \cdot T_{T1} \cdot \frac{dm_{T1}}{d\theta} - Cp \cdot \left(\dot{m}_{LI1} \cdot T_{T1} - \dot{m}_{T1} \cdot T_{R1} \right) \right)}{m_{T1} \cdot C_v} \right)$
Inlet	Continuity	Sorenson	$\frac{dm_I}{d\theta} = \dot{m}_{LI2} + \dot{m}_{LI1} + \dot{m}_{in} + \dot{m}_{tip}$
		M-45	$\frac{dm_I}{d\theta} = \dot{m}_{LI2} + \dot{m}_{LI1} + \dot{m}_{in} + \dot{m}_{tip}$
	Energy	Sorenson	$T_{I\_new} = T_I + \left(\frac{\theta \cdot \left(\dot{Q}_I - P_I \cdot \frac{dV_I}{d\theta} - C_v \cdot T_I \cdot \frac{dm_I}{d\theta} - Cp \cdot \left(-\dot{m}_{LI2} \cdot T_{T2} - \dot{m}_{LI1} \cdot T_{R1} - \dot{m}_{tip} \cdot T_{R3} - \dot{m}_{in} \cdot T_{up} \right) \right)}{m_I \cdot C_v} \right)$
		M-45	$T_{I\_new} = T_I + \left(\frac{\theta \cdot \left(\dot{Q}_I - P_I \cdot \frac{dV_I}{d\theta} - C_v \cdot T_I \cdot \frac{dm_I}{d\theta} - Cp \cdot \left(-\dot{m}_{LI2} \cdot T_{T2} - \dot{m}_{LI1} \cdot T_{T1} - \dot{m}_{tip} \cdot T_{R3} - \dot{m}_{in} \cdot T_{up} \right) \right)}{m_I \cdot C_v} \right)$

rate than when the rotor passes the outlet opening. At low rotors speed, the test data shows that the backflow slots manage to equalize the trapped volume pressure with the outlet

pressure before the trapped volume opens to the outlet (Meyer 2003, 32). In this case, there will not be a strong pulsation noise generated within the supercharger when the trapped volume is fully opened to the outlet.

Figure 2.21 shows where the backflow slots (BFS) are located in the M-45 supercharger from the cross sectional view. Figure 2.22 shows the picture of M-45 supercharger with the backflow slots viewed perpendicularly to the outlet region. While there are two backflow slots for each rotor in the picture shown in Figure 2.22, they are considered as one in the model. The number of backflow slots, their orientation, and shape will be included in the characteristics of one backflow slot. The backflow slots BFS1 and BFS2 (in Figure 2.21) denote a backflow slot on the left and right side of the supercharger. Air in the outlet volume starts flowing into the trapped volume as the leading rotor tip of the trapped volume passes the backflow slots.

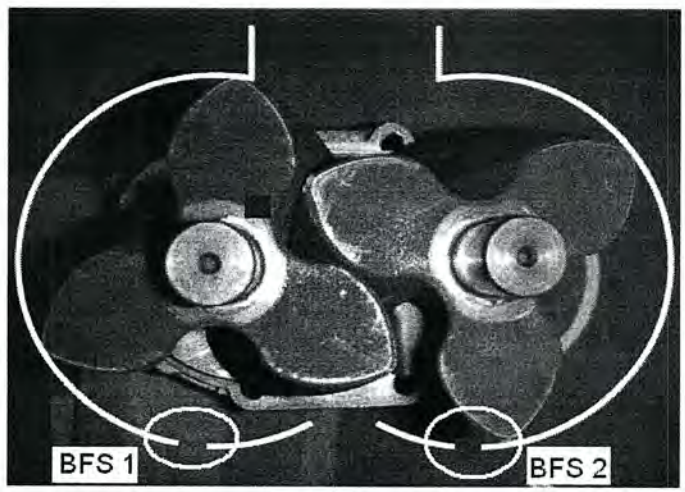

Figure 2.21 Supercharger configuration with backflow slots.

There are two methods to model the backflow slots; one is by using Carroll's backflow slot model and the other is by expanding Sorenson's formulation. These two methods will be presented and analyzed; the method that models the M-45 supercharger the best will be used. Carroll's method will be discussed first, followed by Sorenson's method. Finally, both methods will be compared and the best one will be chosen. The results of adding the backflow slots model will be presented in chapter 4.

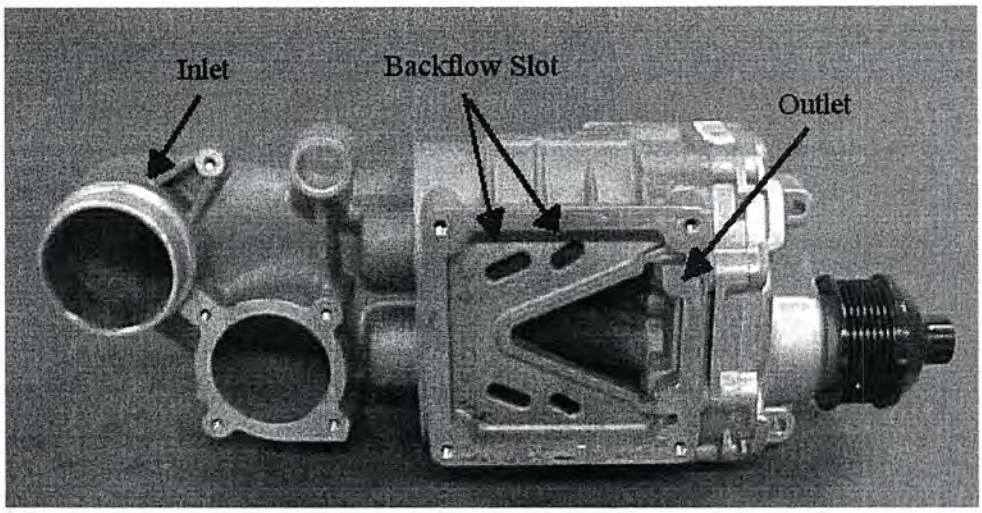

Figure 2.22 Eaton's M-45 supercharger viewed perpendicularly to the outlet region.

Curtis Carroll, in his thesis, suggested to model the backflow slot using fundamental thermodynamic relations. To begin, the flow through the backflow slot is assumed to be isentropic, that is, the temperatures in the trapped volume and outlet are equivalent. Also, air will be treated as an ideal gas with k= 1.4 (Carroll 2004, 56). The specific heat ratio (k) in Carroll's thesis is the same as γ in this thesis. The basic idea of Carroll's improved flow model is to obtain the mass of air in the trapped volume using the ideal gas equation.

$$m = \left(\frac{P_o}{R \cdot T_o} \right) \cdot V \qquad \textbf{2.21}$$

The flow is then checked whether it is choked or not. The mass flow rate term is the same for both choked and non-choked flow,

$$\dot{m} = \frac{P}{R \cdot T} \cdot A_{BFS} \cdot v \qquad \textbf{2.22}$$

The difference between the two is in the velocity term (v). For choked flow,

$$v = \sqrt{k \cdot R \cdot T} \qquad \textbf{2.23}$$

and for non-choked flow,

$$v = M \cdot \sqrt{k \cdot R \cdot T} \qquad \textbf{2.24}$$

where:

$$M = \left\{ \frac{2}{k-1} \left[\left(\frac{P_{outlet}}{P_{ev}} \right)^{\frac{k-1}{k}} - 1 \right] \right\}^{1/2} \qquad \textbf{2.25}$$

The amount of mass that has moved into the trapped volume is finally calculated by multiplying the mass flow rate by the time increment (Carroll 2004, pg. 56 and 57).

$$m_{added} = \left(\frac{P_{ev}}{R \cdot T_o} \cdot A_{BFS} \cdot v_{actual} \right) \cdot \Delta t \qquad \textbf{2.26}$$

The second method to model the backflow slots is to expand Sorenson's formulation. Since backflow slots operate similarly as leakage flows in Sorenson's model, they then could be added to the simplified model as another "leakage" flow that goes into the trapped volume. Both Carroll's method and the expansion of Sorenson's method check whether the flow is choked or not. In addition, both methods assume isentropic flow. To sum up, this second method (the expansion of Sorenson's formulation) is similar to the method that Carroll developed.

However, since Carroll only analyzed the backflow slots part of the supercharger, there is one assumption that he had to make to his model that is not applicable when the trapped volume temperature is calculated as a separate control volume, the assumption of constant temperature between the trapped and the outlet volume. This assumption is not true in the actual supercharger. In addition, using the second method to model the backflow slots is much simpler due to the uniformity of the equations used. Hence, Sorenson's method is used to model the backflow slots.

When analyzing the M-45 supercharger model in the previous section, it was observed that backflow slots open to the outlet at 5 degree for the left hand side part and at 65 degree for the right hand side part. Some more adjustments to the continuity and energy equations need to be made to accommodate backflow slots. Since the backflow slots only come into the trapped volume and low pressure receiver, the changes are only made to the continuity and energy equations for trapped volumes (T1 and T2) and low pressure receiver volumes (R1 and R2).

For the M-45 supercharger, the left side backflow slots start to open to the outlet at 5 degree and completely open to the outlet at 27 degree. The equations used for trapped volume T1 is in Table 2.2. Changes made to the M-45 supercharger model are circled. When the two pressures, P_{T1} and P_{R3}, equalize, there will not be any mass flow through the backflow slots and the new outlet volume is the trapped volume and the old outlet volume combined. If the trapped volume pressure is lower than the outlet pressure after the backflow slots area fully opens, the flow will still go through the maximum area of the backflow slots. The trapped volume T1 then opens to the outlet at 29 degree. At this point, if the pressure at T1 is still lower than the outlet pressure (P_{R3}), then the equation for the low pressure receiver (R1) with the backflow slot term is used. Notice that there is mass flow through the backflow slots due to the pressure difference between control volumes R1 and R3.

The M-45 supercharger model uses values for the backflow slot area that Carroll developed, the linearly increasing area assumption. As seen in Figure 2.22, there are two backflow slots at each side, one opens first and the second one opens at a later time (Carroll 2004, pg. 47). Figure 2.23 is the backflow slot area opening as a function of rotor angle that Carroll used and was used here.

2.2.3 Carryback Slot

The next improvement made to the M-45 supercharger model is the addition of the carryback slot feature. Carroll in his acoustics model concluded that the backflow slots are not a significant source of pressure pulsations, which provides further evidence that the fluctuations in the measured data are likely from a source other than the backflow slots

Table 2.2 Equation comparison for M-45 supercharger with and without backflow slots.

Control Volume Analyzed	Equation	Backflow Slots	
T1	Continuity	No	$\frac{dm_{T1}}{d\theta} = \dot{m}_{T1} - \dot{m}_{LI1}$
		Yes	$\frac{dm_{T1}}{d\theta} = \dot{m}_{T1} + \dot{m}_{BFS1} - \dot{m}_{LI1}$
	Energy	No	$T_{T1\_new} = T_{T1} + \left(\frac{\theta \cdot \left(\dot{Q}_{T1} - P_{T1} \cdot \frac{dV_{T1}}{d\theta} - C_v \cdot T_{T1} \cdot \frac{dm_{T1}}{d\theta} - Cp \cdot \left(\dot{m}_{LI1} \cdot T_{T1} - \dot{m}_{T1} \cdot T_{R3} \right) \right)}{m_{T1} \cdot C_v} \right)$
		Yes	$T_{T1\_new} = T_{T1} + \left(\frac{\theta \cdot \left(\dot{Q}_{T1} - P_{T1} \cdot \frac{dV_{T1}}{d\theta} - C_v \cdot T_{T1} \cdot \frac{dm_{T1}}{d\theta} - Cp \cdot \left(\dot{m}_{LI1} \cdot T_{T1} - \dot{m}_{T1} \cdot T_{R3} + \dot{m}_{BFS1} \cdot T_{R3} \right) \right)}{m_{T1} \cdot C_v} \right)$
When trapped volume has not opened to outlet			
R1	Continuity	No	$\frac{dm_{R1}}{d\theta} = \dot{m}_{RPT1} - \dot{m}_{T1}$
		Yes	$\frac{dm_{R1}}{d\theta} = \dot{m}_{RPT1} + \dot{m}_{BFS1} - \dot{m}_{T1}$
	Energy	No	$T_{R1\_new} = T_{R1} + \left(\frac{\theta \cdot \left(\dot{Q}_{R1} - P_{R1} \cdot \frac{dV_{R1}}{d\theta} - C_v \cdot T_{R1} \cdot \frac{dm_{R1}}{d\theta} - Cp \cdot \left(\dot{m}_{LI1} \cdot T_{R1} - \dot{m}_{RPT1} \cdot T_{R3} \right) \right)}{m_{R1} \cdot C_v} \right)$
		Yes	$T_{R1\_new} = T_{R1} + \left(\frac{\theta \cdot \left(\dot{Q}_{R1} - P_{R1} \cdot \frac{dV_{R1}}{d\theta} - C_v \cdot T_{R1} \cdot \frac{dm_{R1}}{d\theta} - Cp \cdot \left(\dot{m}_{LI1} \cdot T_{R1} - \dot{m}_{RPT1} \cdot T_{R3} + \dot{m}_{BFS1} \cdot T_{R3} \right) \right)}{m_{R1} \cdot C_v} \right)$
When trapped volume has opened to outlet			

(Carroll 2004, 82). As Carroll proposed, another possible source of pressure pulsation, the carryback slot, will be investigated further. The carryback slot is located on the inlet side of the rotor. This control volume is created due to the 60 degree twisted and intermeshing rotors (Figure 2.24). The size of the carryback slot volume is rather small compared to other volumes such as the trapped, inlet and outlet volumes. For the M-45 supercharger, it was

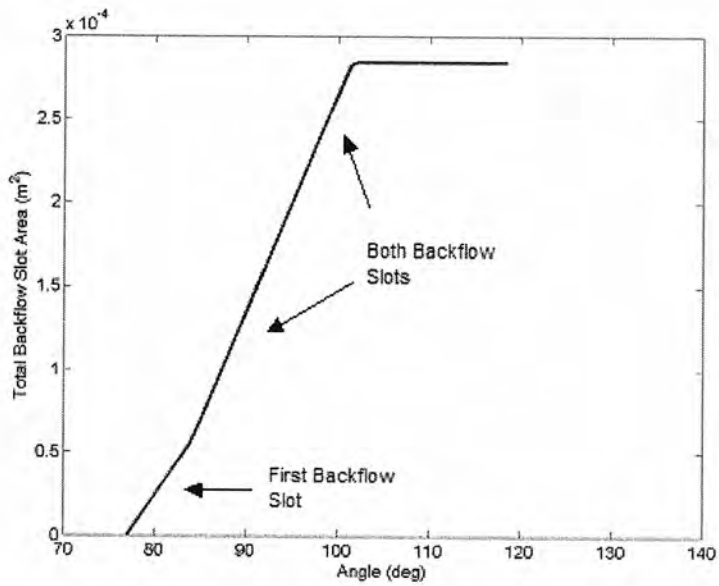

Figure 2.23 Backflow slots area as a function of angle (Carroll 2004, pg. 48).

observed that this control volume only exists on a small angle (12 degrees); then it opens to the inlet control volume. For each 120 degrees, the carryback slot volume is created twice, at -15 degree and at 45 degree. This section covers the data showing evidence of the carryback pulse, the changes made to the energy and continuity equations due to the carryback slot addition, and the siren noise model that is used to model the carryback pulses.

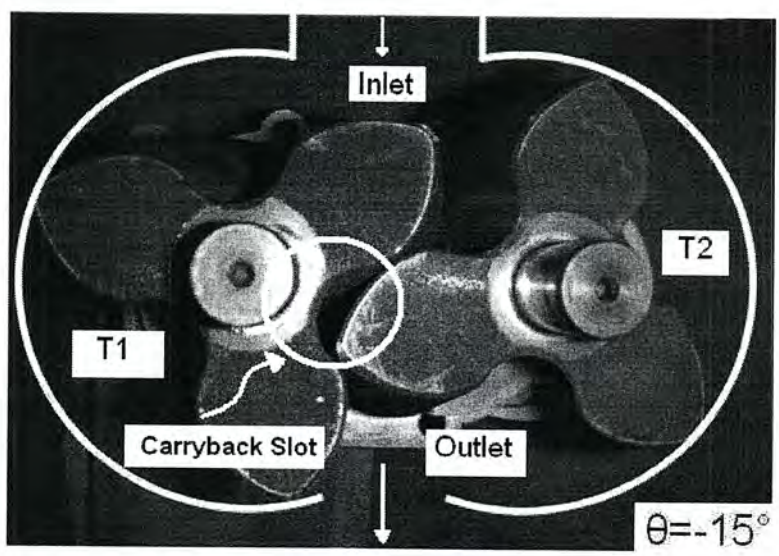

Figure 2.24 Carryback slot volume.

2.2.3.1 Carryback Pulse Evidence Data

Figures 2.25 and 2.26 show measured data (provided by Eaton Corporation) from a transducer placed in the carryback slot of the supercharger. Figure 2.25 shows the signal in the carryback slot for a pressure ratio of 1.4 and changing rotor speeds. Figure 2.26 shows the signal in the carryback slot at a rotor speed of 16000 RPM and different pressure ratios.

As seen in Figure 2.25, for all speeds the pulses at 15 degrees and 135 degrees and the pulses at 75 and 195 degrees are correlated between different rotor speeds. This suggests that these events are caused by the same event that occurs at that angle. The other pulses occur at different angles, suggesting that they are related to a time dependent phenomena, such as sound propagation. It is worth noting, that pulses A1 and A2 being 120 degrees apart are generated by one rotor and the pulses B1 and B2 being 120 degrees apart and 60 degrees shifted from A1 and A2 are from the other rotor. Figure 2.26 shows that the amplitude of the pulse depends on the pressure ratio, with the amplitude increasing with increased pressure ratio.

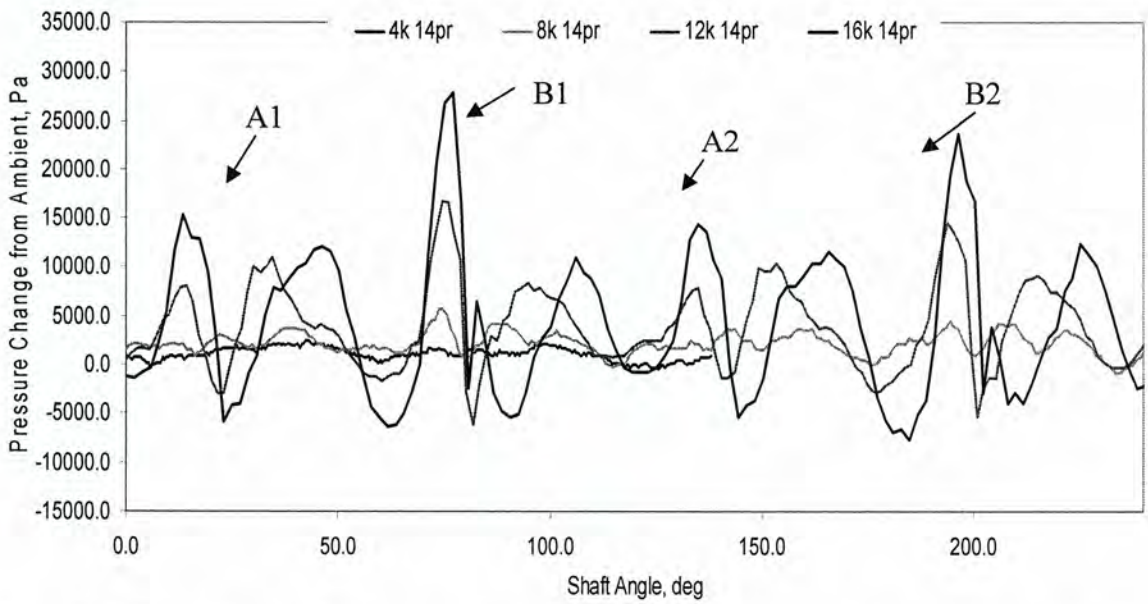

Figure 2.25 Measured pressure signals in the carryback slot at 1.4 pressure ratio and different rotor speeds.

Following the conclusions from Figure 2.25 that there are pulses generated at the carryback slot, the time signals from Figure 2.25 were plotted as a function of time, where the time at 75 degrees was set a zero time, Figure 2.27. By plotting as a function of time, then time dependent phenomena should be identified. The results in Figure 2.27 show that the second pulse, labeled "reflected pulse", now lines up, suggesting that this pulse arrives at the carryback slot after it has propagated from its original source. It was hypothesized that the source was the carryback slot. Following this hypothesis, Figure 2.28 shows a schematic of the supercharger with the carryback slot generating a pulse and then propagating through the supercharger.

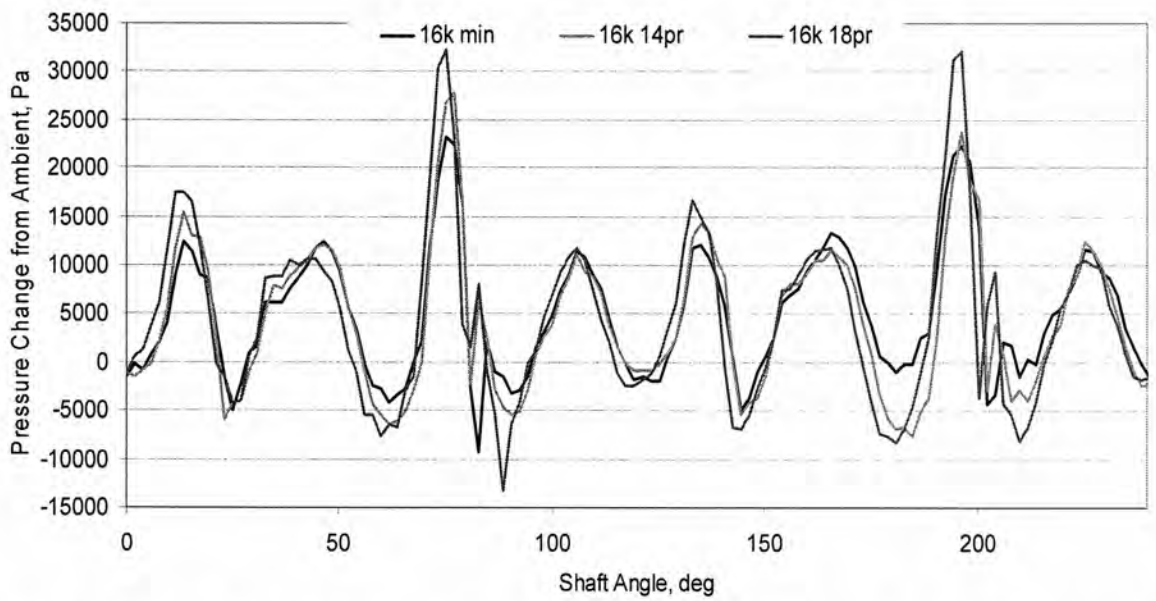

Figure 2.26 Measured pressure signals in the carryback slot at 16000 RPM and different pressure ratios.

Figure 2.29 shows a signal measured at several points in a supercharger with the supercharger operating at a pressure ratio of 1.4 and a rotor speed of 16000 RPM. However, the signals were adjusted in angle by the distance from the angle of the rotor rotation during the time that it would take to propagate from the carryback slot to the transducer location. There is a clear correlation of the pulse at sensor 3, which is along the body of the housing

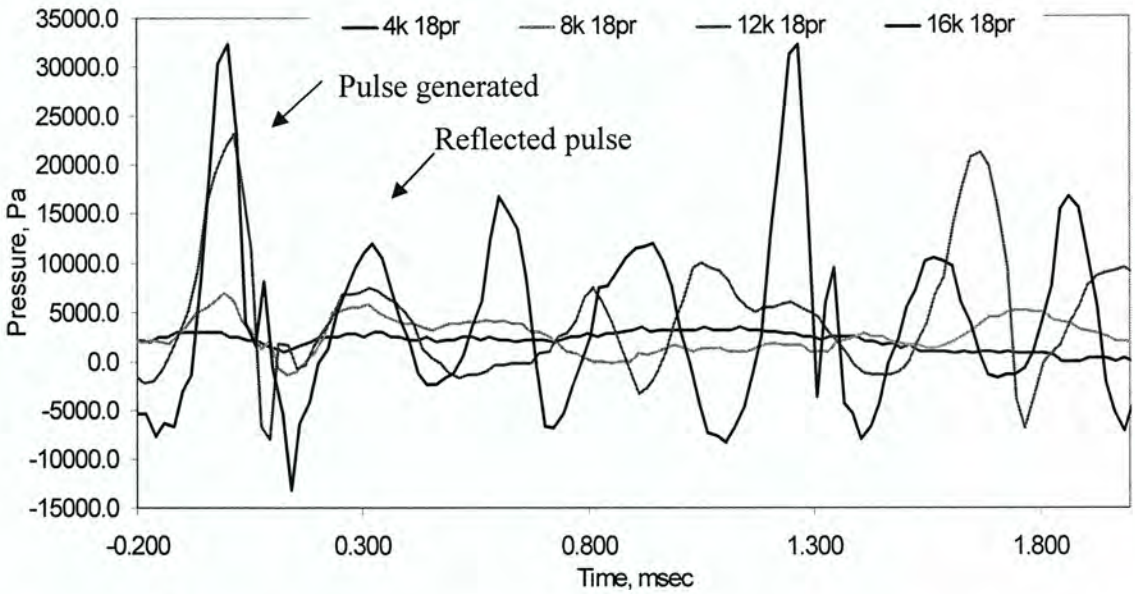

Figure 2.27 Measured pressure signals in the carryback slot at 1.8 pressure ratio and different rotor speeds. Data is plotted with respect to time with the time of the pulse generation at 75 degree set as zero time.

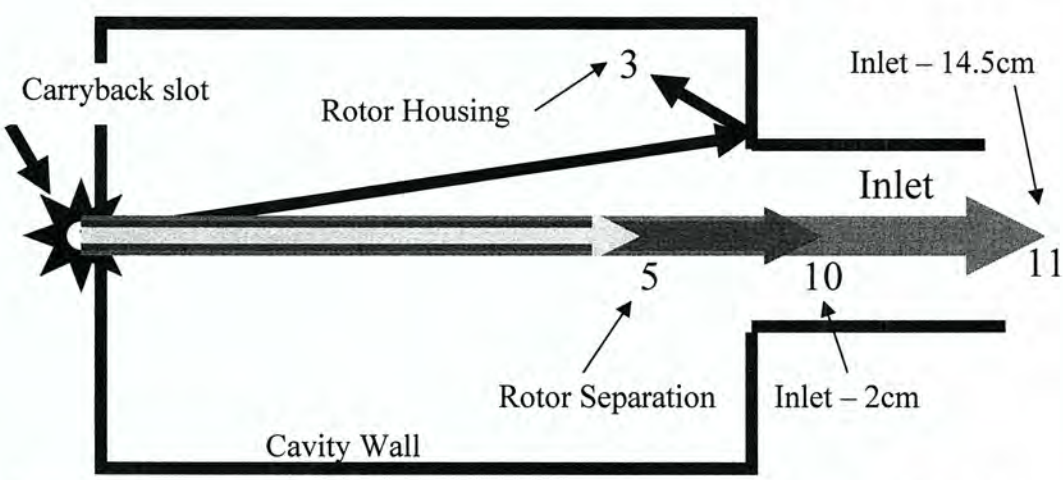

Figure 2.28 Schematic of the pulse generated in the carryback slot propagating in the supercharger. The numbers indicate the points where data is shown in Figure 2.29.

and the inlet transducers (see the circled areas in Figure 2.29). In the other transducers, the pulse is less strong, but nonetheless present.

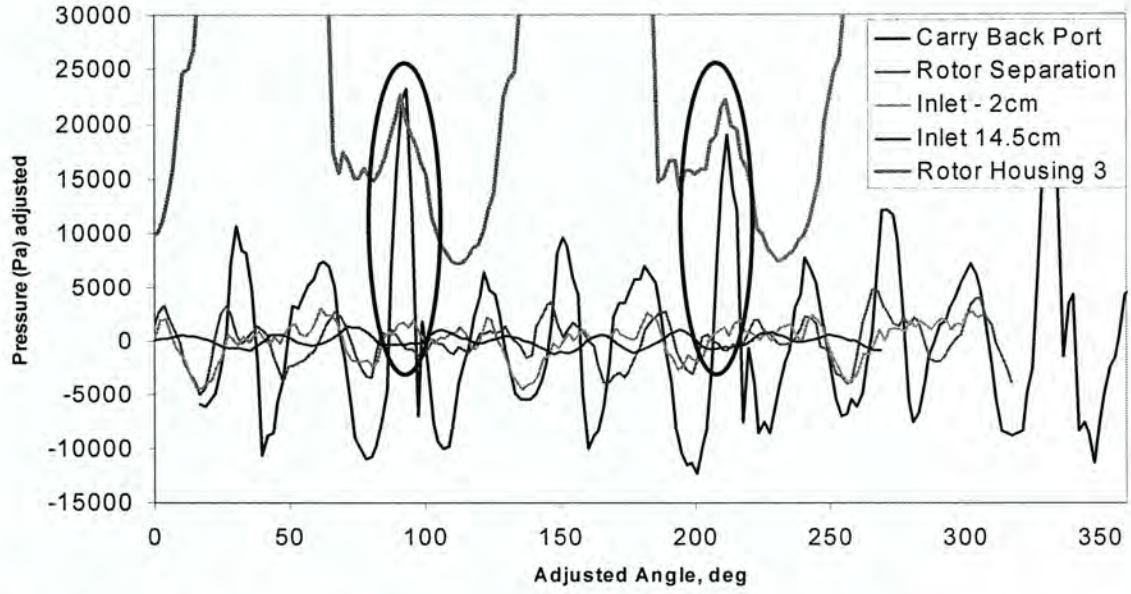

Figure 2.29 Signals at different points in the supercharger. The signals were shifted in angle relative to the time of propagation from the carryback slot to the transducer locations.

Based on these results it was decided to model a noise pulse generated at the carryback slot and then propagate it within the supercharger using a plane wave propagation model. In such a case, multiple reflections will need to be tracked.

2.2.3.2 Equations for Carryback Volume

A new set of continuity and energy equations is needed to add a carryback volume into the supercharger model. The carryback volume is in between the inlet and outlet control volumes; therefore, leakage flows will flow through these control volumes. Due to the rotation orientation of the rotors (left rotor turns counterclockwise and right rotor turns clockwise), the carryback volume initially takes some part of the outlet to create a new control volume, and after 12 degree it opens to the inlet side. Hence, to start, the carryback volume has the outlet pressure and temperature. It is assumed that for the M-45 supercharger that after 12 degree all mass in the carryback volume transfers instantaneously to the inlet

since the size of the carryback volume is very small compared to the inlet control volume. During the 12 degree period, the carryback control volume exists in the supercharger system, and there are two leakage flows due to the tip clearance from each rotor, one to the inlet and one to the outlet. The carryback slot control volume is assumed to have the highest pressure and temperature in the supercharger system since it takes the air from the outlet at the start of formation and the air is compressed as the rotors turn. See Table 2.3 for the equations for the carryback volume. The changes made to the M-45 supercharger model are circled.

As seen, adding the carryback slot control volume affects the inlet and outlet control volumes since they are connected to the carryback volume though leakage flows. For the inlet control volumes, mass flow from the carryback slot to the inlet volume, $\dot{m}_{cbI}$, needs to be added in the continuity and energy equations. The same is true for the outlet control volume; mass flow from the carryback slot to outlet volume, $\dot{m}_{cbR3}$, needs to be added in.

2.2.3.3 Carryback Slot Pulse Model

A model for the shape and amplitude of the carryback slot pulse was needed. The approach was to model the amplitude of the pulse using a siren noise model and to model the shape of the pulse using experimental data.

The output from the one dimensional model (the M-45 supercharger model) is a carryback mass flow rate to the inlet ($\dot{m}_{cbI}$) at -3 degree. However, because of the simplicity of the model, and a suggestion by Sorenson, the mass flow from the carryback slot takes place over one step in the calculation. Thus, the shape of the pulse is not captured in the flow model; however, the mass flow rate is.

Using the mass flow rate, a model of the pulse amplitude, p(t), can be implemented using theories developed for a siren (Pla 1987),

$$p(t) = \frac{\left(\dot{m}_{cbI}(t)\right)^2}{4\rho\kappa^2\left(S(t)\right)^2} \qquad \textbf{2.27}$$

Table 2.3 Equation comparison for M-45 supercharger with and without carryback slot.

Control Volume Analyzed	Equation	Carryback Slot	
Inlet	Continuity	No	$\frac{dm_I}{d\theta} = \dot{m}_{LI2} + \dot{m}_{LI1} + \dot{m}_{in} + \dot{m}_{tip}$
		Yes	$\frac{dm_I}{d\theta} = \dot{m}_{LI2} + \dot{m}_{LI1} + \dot{m}_{in} + \dot{m}_{tip} + \dot{m}_{cbI}$
	Energy	No	$T_{I\_new} = T_I + \left(\frac{\theta \cdot \left(\dot{Q}_I - P_I \cdot \frac{dV_I}{d\theta} - C_v \cdot T_I \cdot \frac{dm_I}{d\theta} - Cp \cdot \left(-\dot{m}_{LI2} \cdot T_{T2} - \dot{m}_{LI1} \cdot T_{T1} - \dot{m}_{tip} \cdot T_{R3} - \dot{m}_{in} \cdot T_{up} \right) \right)}{m_I \cdot C_v} \right)$
		Yes	$T_{I\_new} = T_I + \left(\frac{\theta \cdot \left(\dot{Q}_I - P_I \cdot \frac{dV_I}{d\theta} - C_v \cdot T_I \cdot \frac{dm_I}{d\theta} - Cp \cdot \left(-\dot{m}_{LI2} \cdot T_{T2} - \dot{m}_{LI1} \cdot T_{T1} - \dot{m}_{tip} \cdot T_{R3} - \dot{m}_{in} \cdot T_{up} - \dot{m}_{cbI} \cdot T_{cb} \right) \right)}{m_I \cdot C_v} \right)$
Carry back Slot	Continuity	No	N/A
		Yes	$\frac{dm_I}{d\theta} = -\dot{m}_{cbR3} - \dot{m}_{cbI}$
	Energy	No	N/A
		Yes	$T_{cb\_new} = T_I + \left(\frac{\theta \cdot \left(\dot{Q}_{cb} - P_{cb} \cdot \frac{dV_{cb}}{d\theta} - C_v \cdot T_{cb} \cdot \frac{dm_{cb}}{d\theta} - Cp \cdot \left(\dot{m}_{cbI} \cdot T_{cb} + \dot{m}_{cbR3} \cdot T_{R3} \right) \right)}{m_{cb} \cdot C_v} \right)$
Outlet	Continuity	No	$\frac{dm_{R3}}{d\theta} = -\dot{m}_{RPT1} - \dot{m}_{T2} - \dot{m}_{out} - \dot{m}_{tip}$
		Yes	$\frac{dm_{R3}}{d\theta} = -\dot{m}_{RPT1} - \dot{m}_{T2} - \dot{m}_{out} - \dot{m}_{tip} + \dot{m}_{cbR3}$
	Energy	No	$T_{R3\_new} = T_{R3} + \left(\frac{\theta \cdot \left(\dot{Q}_{R3} - P_{R3} \cdot \frac{dV_{R3}}{d\theta} - C_v \cdot T_{R3} \cdot \frac{dm_{R3}}{d\theta} - Cp \cdot \left(\dot{m}_{RPT1} \cdot T_{R3} + \dot{m}_{T2} \cdot T_{R3} + \dot{m}_{tip} \cdot T_{R3} + \dot{m}_{out} \cdot T_{R3} \right) \right)}{m_{R3} \cdot C_v} \right)$
		Yes	$T_{R3\_new} = T_{R3} + \left(\frac{\theta \cdot \left(\dot{Q}_{R3} - P_{R3} \cdot \frac{dV_{R3}}{d\theta} - C_v \cdot T_{R3} \cdot \frac{dm_{R3}}{d\theta} - Cp \cdot \left(\dot{m}_{RPT1} \cdot T_{R3} + \dot{m}_{T2} \cdot T_{R3} + \dot{m}_{tip} \cdot T_{R3} + \dot{m}_{out} \cdot T_{R3} - \dot{m}_{cbR3} \cdot T_{cb} \right) \right)}{m_{R3} \cdot C_v} \right)$

where:

$\dot{m}_{cbl}(t)$: mass flow from carryback slot (kg/deg)

ρ : density of air (kg/m^3)

κ : flow coefficient

S : surface area (m^2)

The data provided by the simplified flow model is $\dot{m}_{cbl}(\theta)$, but it is modeled as a single event, while the data indicates a time variation in the resulting sound pressure. The actual pressure signals measured in the carryback slot were evaluated to identify an equation that could be used to predict the pulse time signal.

The analysis began by isolating the pulse in the carryback slot, Figure 2.30. The signal depends on the pressure ratio and rotor speed. All the data was normalized relative to the rotor rotation rate and the amplitude of integral of the pressure signal over positive values. The resulting normalized pressure pulses are shown in Figure 2.31. The normalized curves reveal a base shape that can be parameterized.

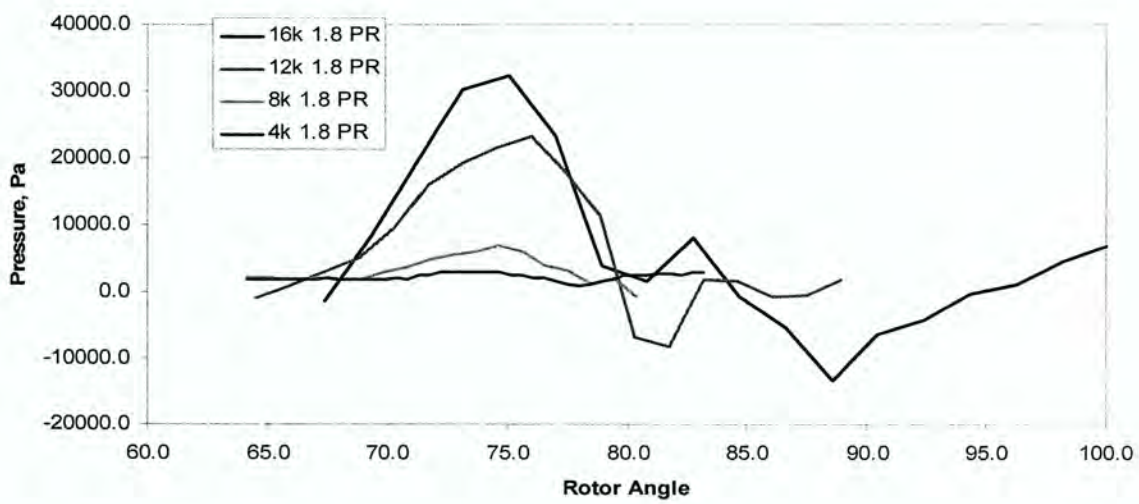

Figure 2.30 Examples of the carryback pressure pulse at 1.8 pressure ratio and varying speeds.

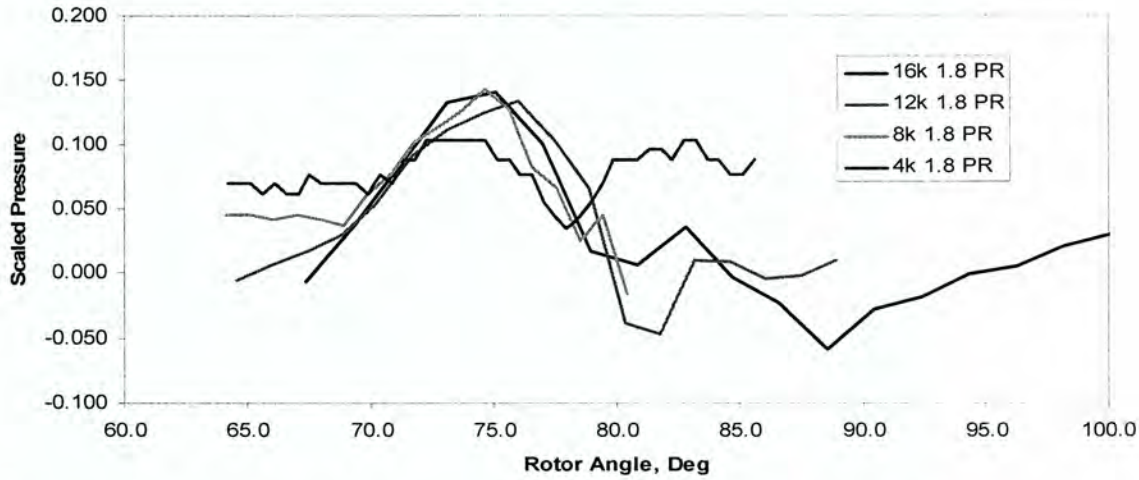

Figure 2.31 Examples of the normalized carryback pressure pulse at 1.8 pressure ratio and varying speeds.

The normalized curves were then curve fitted to a cosine function and multiplied by a decaying exponential. Examples of the curve fit are shown in Figure 2.32

The normalized model was then multiplied by the amplitude predicted in equation 2.27 using the results from the M-45 supercharger model. The final equation for the direct path pulse is

$$\text{direct path pulse} = p(t) \cdot e^{-\tau(\theta-\theta_o)} \cdot \sin\left(\frac{2\pi(\theta-\theta_o)}{T}\right) \qquad \textbf{2.28}$$

where:

p(t) : pressure pulse amplitude (Pascal) from equation 2.27

τ : decay

θ : angle (degree)

θ_o : angle delay (degree)

T : period (s)

The values τ, T, and θ_o are varied to fit the measured data.

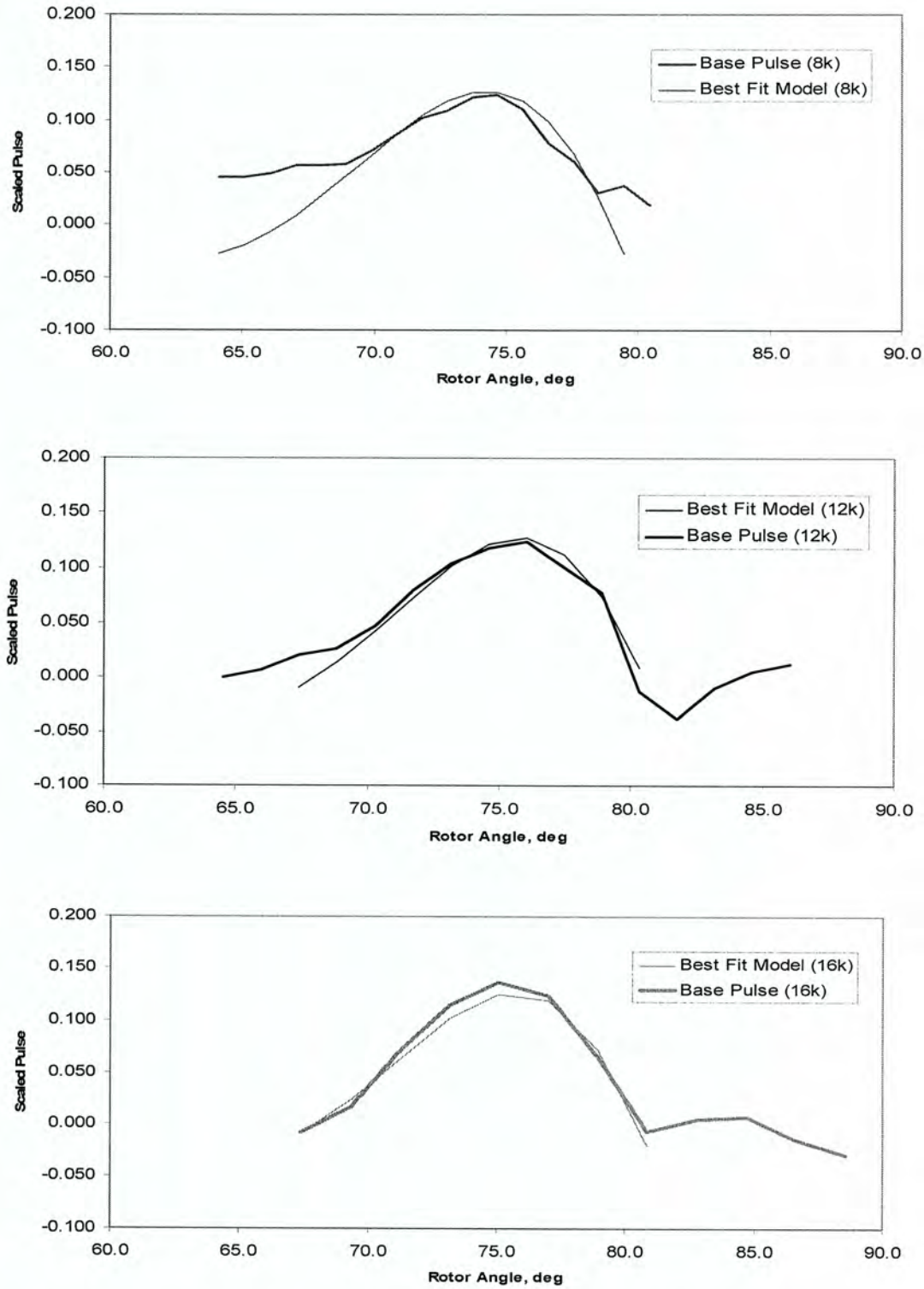

Figure 2.32 Examples of the curve-fitted normalized carryback pressure pulse at 1.8 pressure ratio and varying speeds.

The reflection path pulse equation is the direct path pulse equation multiplied by the reflection coefficient. The reflection coefficient, whose value is between 0 and 1, is added to simulate the effect of the reduction in the pulse magnitude after a reflection. It was determined from trial and error that reflection coefficient of 0.5 gives the closest result to the measured data. The model calculates up to a third reflection. Thus the second reflection coefficient is 0.5^2 times the original signal and the third reflection coefficient is 0.5^3 times the original signal. It is also assumed that the pulse generated by the carryback slot propagates in two directions, into the inlet side and also into the outlet side.

The pressure signal at one transducer location (Meyer 2004, 36) is analyzed in this thesis (labeled as "x" in Figure 2.33). Due to its location, the transducer reads the outlet pressure from -15 degree to -9 degree, the trapped 2 pressure from -8 degree to 45 degree, and finally the outlet pressure again from 46 degree to 105 degree. The model assumes that this transducer reads the control volume pressure, the direct path, the 1st reflection, the 2nd reflection, and the 3rd reflection pressure pulses from the inlet side of supercharger, and also the direct path, the 1st reflection, the 2nd reflection, the 3rd reflection pressure pulses from the outlet side of the supercharger.

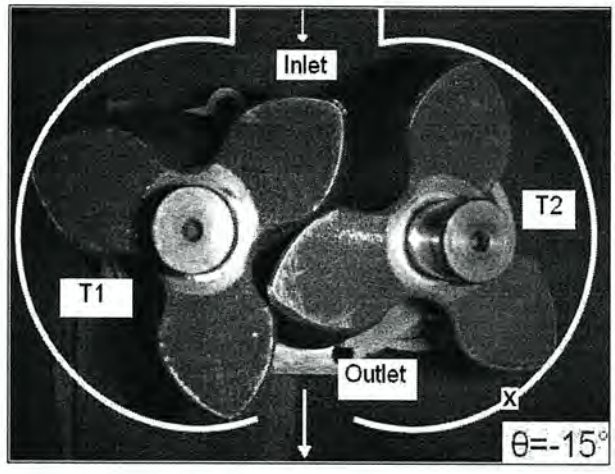

Figure 2.33 Pressure transducer location.

The control volume pressure at the transducer location is output from the M-45 supercharger model. The direct path and all the reflection pressure pulses are then calculated and superimposed to the pressure signal generated by the M-45 supercharger model.

2.3 Supercharger Efficiency

Supercharger efficiency is one of the outputs of the M-45 supercharger model that was compared with the measured data provided by Eaton Corporation for the model validation. The two supercharger efficiencies that will be discussed here are the volumetric efficiency and the J1723 isentropic efficiency.

The volumetric efficiency is:

$$\text{volumetric efficiency} = \frac{\dot{V}_{inlet}}{V_{displaced}} \times 100 \qquad \textbf{2.29}$$

It is defined as the ratio of the actual inlet volume flow rate to the total trapped volume capacity per one revolution, called the volume displaced. For one revolution, the volume displaced in a supercharger is equal to 6 trapped volumes; hence,

$$V_{displaced/rev} = 6 \cdot V_{trapped} / rev \qquad \textbf{2.30}$$

The J1723 isentropic efficiency (SAE J1723 supercharger testing standard) is calculated as follows:

$$J1723 \text{ efficiency} = \frac{T_{inlet}\left(PR^{0.286} - 1\right)}{T_{outlet} - T_{inlet}} \times 100 \qquad \textbf{2.31}$$

where:

T_{inlet} : average inlet temperature for the cycle (K)

T_{outlet} : average outlet temperature for the cycle (K)

PR : calculated pressure ratio of the supercharger (dimensionless)

Chapter 3
Computation Process

There are two models that will be discussed in this chapter; the M-45 supercharger model and the carryback pulse model. The major discussion in this chapter will focus more on the computational process of the supercharger model since the carryback pulse model has a rather straight forward computation process. One thing to emphasize in the supercharger model is that it consists of two iteration processes; temperature iteration and pressure ratio iteration. Some of the outputs of the supercharger model are the inputs to the carryback pulse model. Hence, for future work, these two models can be combined.

3.1 M-45 Supercharger Model

The M-45 supercharger model, developed in MatLab, is used to predict the performance of a supercharger (supercharger efficiency) as well as temperature and pressure profiles. An iterative procedure was incorporated in order to obtain a final solution. The algorithm consists of two iteration processes, the first iterates on a given input condition (outlet volumetric flow rate) until the temperature would converge. Then this outlet volumetric flow rate is varied until the converged temperature is achieved and the calculated pressure ratio is predicted as the requested value.

The main program in the M-45 supercharger model, supercharger_model.m, includes a total of 8 different sub-programs for each different geometric and thermodynamic condition of the supercharger. These sub-programs are categorized by which control volume exists at that particular angle. A graphical user interface (GUI) is created to input some operating conditions and constraints. The outputs of this program are the J1723 isentropic efficiency, volumetric efficiency, temperature and pressure profiles for one whole cycle, and the pressure profile at a single transducer location (refer to Figure 2.33 for the transducer location). More detailed information about this computation procedure will be discussed later on in this chapter.

3.1.1 Supercharger Model Algorithm

The algorithm schematic for the M-45 supercharger model is shown in Figure 3.1. As previously discussed, the program runs through two iteration processes; one is an iteration to get temperature convergence (light shaded area) and the other is an iteration to get pressure ratio convergence (dark shaded area). Following is a brief description of the algorithm steps in Figure 3.1. More detailed information on each step will be presented later in this chapter. The numbers in this step correspond to the numbers in the schematic.

1. The program obtains the initial guess for the outlet volumetric flow rate from the inputs.
2. The program obtains initial guess for the temperature and pressure for each control volume.
3. The program runs for 1 cycle, 120 degrees, to calculate new values for the temperature and pressure at every angle increment specified for each control volume that exists.
4. At the end of the temperature and pressure calculation, temperatures are checked for convergence. To be considered as converged, temperatures for each control volume at -15 degree and 105 degree have to agree within 0.01%.
   - If temperature convergence is not achieved, the program will go back to step 2 and use the new calculated temperature and pressure for each control volume to replace the initial guess for the temperature and pressure.
   - If temperature convergence is achieved, the program will proceed to step 5.
5. The new calculated pressure ratio is obtained and checked for convergence. To be considered as converged, the new calculated pressure ratio has to be between the upper and lower limits specified.
   - If the pressure ratio convergence is not achieved, and the program will go back to step 1 and use an adjusted outlet flow rate to replace the initial guess for the outlet flow rate.
   - If the pressure ratio convergence is achieved, then the solution is determined and the program ends.

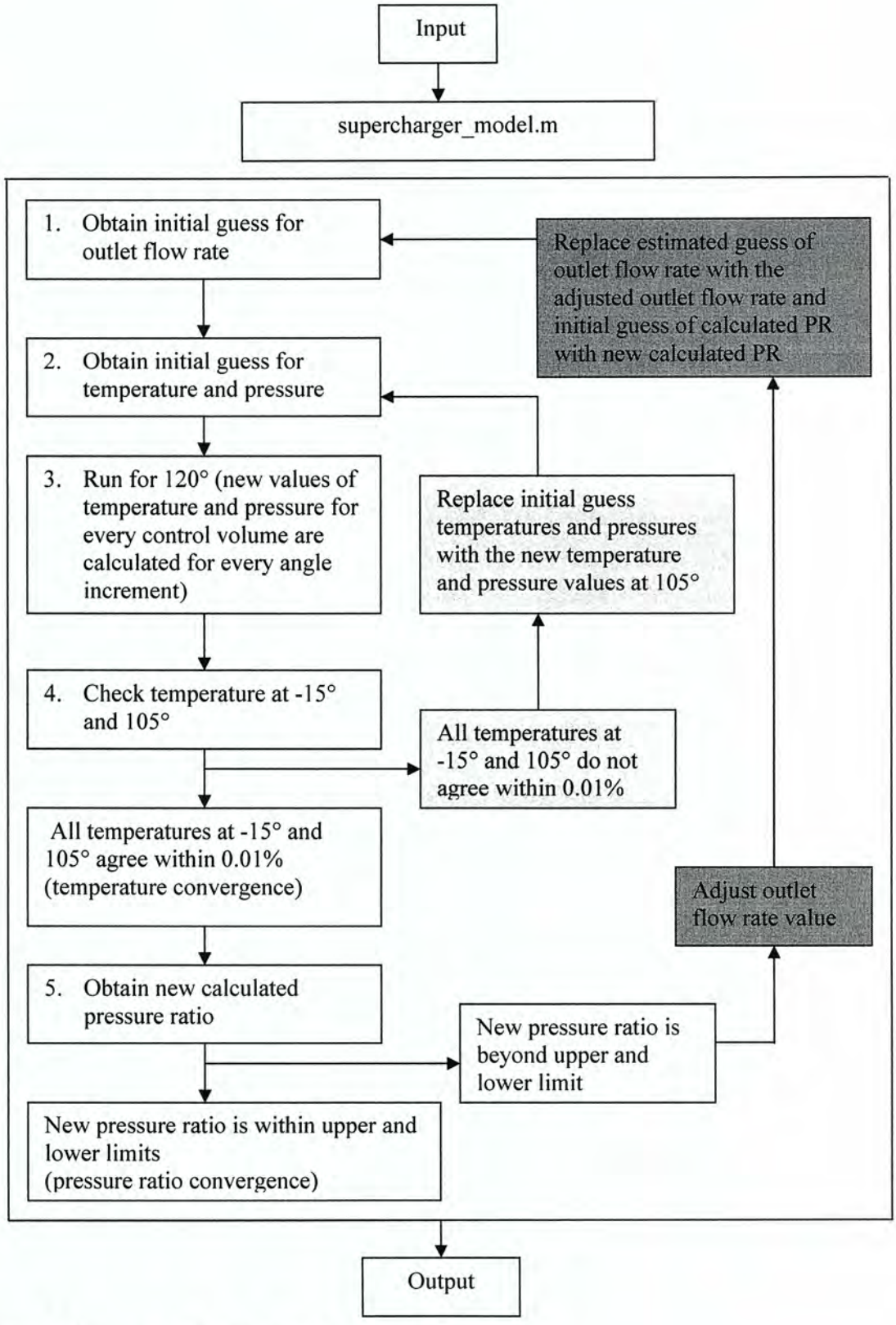

Figure 3.1 Program algorithm schematic.

3.1.2 Input

There are three types of input to the M-45 supercharger model. One is the information that defines the supercharger, the next are initial estimates of values so that the program can start. These initial estimates are updated by the program in order to achieve a converged solution. The third type of input defines the convergence criteria.

Input that defines the supercharger includes the supercharger operating conditions, the supercharger geometry for every control volume as the rotors turn, and known constant values. The operating conditions include the rotor speed (RPM) and requested pressure ratio. The rotor speeds that are used in the analysis are 4000 RPM, 8000 RPM, 12000 RPM, and 16000 RPM. The requested pressure ratios are 1.0 (min boost), 1.2, 1.4, and 1.6. These values are chosen for comparison with the measured data since these are the operating condition that Eaton Corporation ran the testing.

The geometry file consists of volumes, surface areas for all control volumes, and flow areas including the backflow slot area for a 120 degree cycle. These values can be in any angle increment. The smaller the angle increment, the more precise the result will be. The geometry file that is used for M-45 supercharger in this program is m45_geo.txt. This file contains values for each control volume at a 1degree angle increment. A more detailed description of the geometry file can be found in Appendix B.

As previously discussed in chapter 2, there are 4 different geometrical configurations for the M-45 supercharger, one of which is assigned to each angle depending on which volumes exist at that particular angle:

- Configuration 1: Outlet, T1, T2, and inlet volume exist.
- Configuration 2: R1, outlet, T1, T2, and inlet volume exist.
- Configuration 3: Outlet, T1, T2, and inlet volume exist.
- Configuration 4: R2, outlet, T1, T2, and inlet volume exist.

Configuration 1 and 3 may seem to be exactly similar; however, they are in fact not (refer to section 2.2.1). The difference amongst the two is that in configuration 1, T1 is approaching and almost open to the outlet. Whereas in configuration 3, T2 is approaching and almost open to the outlet. ("1" and "2" denote the left and right hand side of supercharger,

respectively). The difference in these two configurations leads to the differences in controlling pressures for the leakage flow and also the time when the backflow slots open.

The geometrical configuration of the four possible configurations has to be known at each angle in order to model the supercharger. Therefore, for this model the four geometrical configurations have to be manually input every 1 degree in the geometry text file so that the program knows which set of equations to be used. More detailed information on this can be found in Appendix C.

Each geometrical configuration has two thermodynamic conditions; whether or not the outlet pressure is the same as the low receiver pressure or the trapped pressure. For example: configuration 1 has two thermodynamic conditions. One is when P_{T1} is less than P_{R3} and the other is when P_{T1} is equal to P_{R3}. For configuration 2, the two thermodynamic conditions are when P_{R1} is less than P_{R3} and when P_{R1} is equal to P_{R3}. This similar pattern is true for configuration 3 and 4. Hence, there are a total of 8 different geometric and thermodynamic conditions for the M-45 supercharger.

Known constant values include the upstream temperature, flow coefficients, gas constant for air, specific heat (both constant volume and constant pressure), specific heat ratio (γ), and convection heat transfer coefficient for each control volume. The upstream temperature is assumed to be at 300K. The gas constant for air is 287 J/kg K. Since Sorenson did not specify flow coefficient values that he used, trial and error was done in order to obtain these values that could best fit the measured data. These values are dimensionless and as follows:

- Flow coefficient for low pressure receiver (Cf_{RPT}) : 0.5
- Flow coefficient for leakage to inlet (Cf) : 0.3
- Flow coefficient for leakage to trapped volume (Cf_T) : 1.5
- Flow coefficient for backflow slot (Cd) : 2

The specific heat constant volume and constant pressure values are 718 J/kg K and 1005 J/kg K, respectively. The convection heat transfer coefficient value is assumed to be 172.5 W/m^2K for all control volumes.

The second type of input, the input that is an initial estimate to start the program, consists of an estimated guess and also the guess for the initial conditions. For this supercharger model, the estimated guess is the supercharger wall temperature (K). At this time, since the M-45 supercharger is based on Sorenson's model, the wall temperature value is assumed to be 320K for all operating conditions. Later in chapter 4, it will be found that this wall temperature has to be adjusted accordingly with respect to the pressure ratio so the results match the measured data

The guess for initial conditions include the guess for the outlet volumetric flow rate (m^3/hr), calculated pressure ratio, as well as temperature and pressure values for each control volume. Unlike the estimated guess (the supercharger wall temperature), the initial guess values will be updated at every iteration process. The guess for outlet volumetric flow rate is different from the other initial condition guesses. The guess for initial outlet volumetric flow rate has to be adjusted accordingly with respect to pressure ratio and rotor speed, while the other initial guesses stay constant at all operating conditions. For the computation process to be fast, the guess for initial outlet volumetric flow rate has to be close to the converged volumetric flow rate. The following is the rule of thumb for guessing the outlet flow rate. High rotor speeds result in a large outlet flow rate and a high pressure ratio results in a low outlet flow rate.

The initial guess for calculated pressure ratio works as a dummy variable to get the program running. For this program, the initial pressure ratio is set at 0.5 for all operating conditions. The initial guess for temperature and pressure for the control volume other than the outlet are 285K and 90 kPa, respectively. The initial guess for the outlet pressure is the initial guess for the inlet pressure multiplied by the requested pressure ratio. The initial guess for the outlet temperature is assumed to be at 290K. The carryback volume is assumed to start off at the same temperature and pressure as the outlet.

The input that defines the convergence criteria (the third type of input) includes constraint values and an angle increment. Constraint values are the upper and lower limits for the calculated pressure ratio.

The angle increment is the other convergence criteria input. The angle increment that is used for this program is normally 0.5 degree or 1 degree. The smaller the angle increment,

the more accurate the results are, but the more time it takes for the program to converge to a solution. Since the geometry input is in a 1 degree increment, when the angle increment is set as 0.5 degree, a linear interpolation has to done to get those geometry values at a 0.5 degree increment.

All these inputs, except the known constants and initial guess for temperature and pressure, are input to the program through graphical user interface (GUI). Figure 3.2 shows an example of the GUI for this program. In this particular example, the program runs at a 1.6 pressure ratio and 16000 RPM rotor speed. The geometry file used is m45_geo.txt. The outlet volumetric flow rate and wall temperature are guessed to be around $260m^3/hr$ and 320K, respectively. In order to get an accurate new calculated pressure ratio result, the upper and lower limits are set to be 1.02 and 1.00, respectively. Temperature and pressure results are calculated every 0.5 degree increment for each control volume.

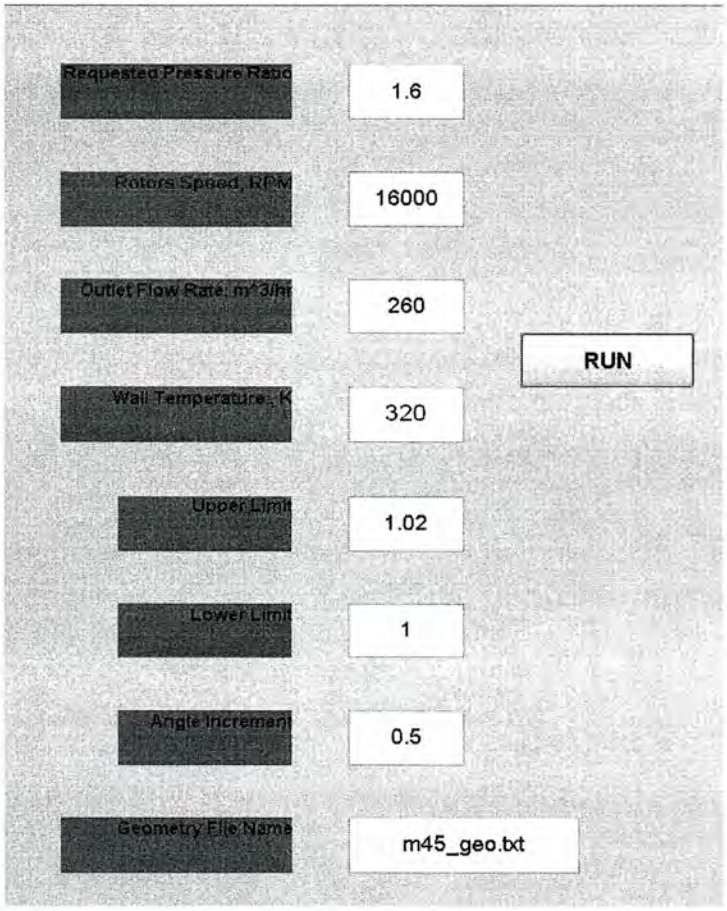

Figure 3.2 Graphical user interface for supercharger_model.m.

3.1.3 Main Program

The main program in this M-45 supercharger model, supercharger_model.m, contains 8 different subprograms (from the 8 different geometrical and thermodynamic conditions). All these subprograms are run for the whole 120 degree cycle; one subprogram for every angle increment depending on which geometric and thermodynamic conditions exist. At each angle increment, the temperature and pressure for every control volume that exists are solved for.

There is a temperature and pressure transition that has to be made to the supercharger_model.m when the subprogram switches from configuration 1 to configuration 2 and from configuration 3 to configuration 4. When switching from configuration 1 to 2, a new control volume (R1) appears; therefore, its temperature and pressure have to be assigned. The initial temperature and pressure for R1 is the temperature and pressure for T1 at the previous angle increment. The same is true when the subprograms switch from configuration 3 to 4. The initial temperature and pressure for R2 is the temperature and pressure for T2 at the previous angle increment.

From the trial and error process when developing the program, it was found that to model the supercharger correctly, the program has to go through two types of iteration; temperature iteration and pressure ratio iteration. The temperature iteration checks whether the temperature values for each control volume converge; that is whether the temperature at the beginning of the cycle (-15 degree) and the end of the cycle (105 degree) are within 0.01%. If the temperature convergence is not attained, then the calculated temperature at 105 degree will be used at the beginning of the cycle (-15 degree) to replace the initial guess for temperatures. The example of temperature iteration (at the 1^{st} iteration and at the final iteration) and how many iterations it takes to converge for one operating condition will be presented in chapter 4.

The pressure ratio convergence checks whether the calculated pressure ratio is within the upper and lower limit of the requested pressure ratio. In every cycle the program generates a new pressure ratio, called the calculated pressure ratio. Its value is then compared to the requested pressure ratio. If it is within the upper and lower control limit,

then the pressure ratio convergence is obtained. If the value is beyond the upper and lower control limit, outlet flow rate value will be adjusted accordingly and the new adjusted outlet flow rate will replace the initial guess at the beginning of the iteration process. The constraints of the upper and lower limits are required to maintain the accuracy of the calculated pressure ratio with respect to the requested pressure ratio. The values for the upper and lower limits range from 0.9 to 1.1, respectively, with 0.9 being 10% less than the requested pressure ratio and 1.1 being 10% more than the requested pressure ratio.

For example, the requested pressure ratio is 1.60 and the program obtains the calculated pressure ratio to be 1.65. If the upper and lower limits are 1.05 and 1.00, respectively, then the actual pressure ratio is within the limit and pressure ratio convergence is achieved. If the upper and lower limits are 1.01 and 1.00, respectively, then the calculated pressure ratio is beyond the limit and the outlet flow rate value needs to be adjusted and then run through the whole program again by replacing the initial guess. This adjustment in the outlet flow rate value is done until the calculated pressure ratio is within upper and lower limit of the requested pressure ratio.

The scheme to adjust the pressure ratio is as follows. If the calculated pressure ratio is higher than the upper limit times the requested pressure ratio, then the adjusted volumetric flow rate is:

$$\dot{V}_{R3\,\mathrm{adj}} = \dot{V}_{R3}\,(1 + \mathrm{constant}) \qquad \textbf{3.1}$$

however, if the calculated pressure ratio is lower than the lower limit times the requested pressure ratio, then the adjusted volumetric flow rate is:

$$\dot{V}_{R3\,\mathrm{adj}} = \dot{V}_{R3}\,(1 - \mathrm{constant}) \qquad \textbf{3.2}$$

Hence, this constant operates as a percentage increase or decrease of outlet volume flow rate depending on the calculated pressure ratio being above or below the limit.

Note that this constant determines whether the program will converge to a solution and also the time it takes to converge. Hence, its value has to be carefully chosen. In the case where the range of outlet volume flow rate is known, a small constant number like 0.005 is good, because it gives more accuracy. When the range of outlet volume flow rate is not known at all, a higher constant number like 0.05 or 0.1 is good for faster computation process. However, if the constant number is too large, the program may not converge to a solution. The examples showing the results for these cases will be presented in chapter 4. The M-45 supercharger model uses a constant of 0.005.

3.1.4 Output

When both the temperature and pressure ratio convergence are attained, the program will output the pressure as a function of angle at every control volume, the pressure plot at one transducer location (refer to Figure 2.33 for the transducer location), and the M-45 supercharger performance table. Here are some output examples. Table 3.1 shows the M-45 supercharger performance table. Figure 3.3 shows pressure profile at one transducer location

As seen in the M-45 Supercharger performance table, with the operating conditions and all other inputs given in Figure 3.2, the program runs through 12 iterations to converge on the pressure ratio. The calculated pressure ratio is 1.605, which is right on target since the requested pressure ratio is 1.6. At the requested pressure ratio, the J1723 isentropic efficiency is 87.6% and volumetric efficiency is 79.5%. Since the initial guess for the outlet volumetric flow rate is $260 m^3/hr$, which is close to the converged outlet volumetric flow rate ($247.3 m^3/hr$), the computation process only took less than 1 minute. The carryback mass flow to the inlet side ($\dot{m}_{cbl}$) at -3 degree is $6.6*10^{-8}$ kg/deg. This value will be used for the pulse model as one of the input.

Figure 3.3 shows a pressure profile at one transducer location. This is the other M-45 supercharger model output that is used as input for the pulse model. As seen, there is no pulsation in the pressure profile.

Table 3.1 The M-45 supercharger performance table.

M-45 Supercharger Performance Table		
Angle increment	0.5	deg.
Pressure ratio iteration	12	
Outlet volumetric flow rate	247.3	m^3/hr
Calculated pressure ratio	1.605	
Rotors speed	16000	RPM
Pout	153212.4	Pa
Pin	95474.4	Pa
Tout	352.3	K
Tin	302.3	K
mdot carryback	6.60E-08	kg/deg.
J1723 isentropic efficiency	87.6	%
Average inlet volumetric flow rate	562	m^3/hr
Volumetric efficiency	79.5	%
Wall temperature	320	K

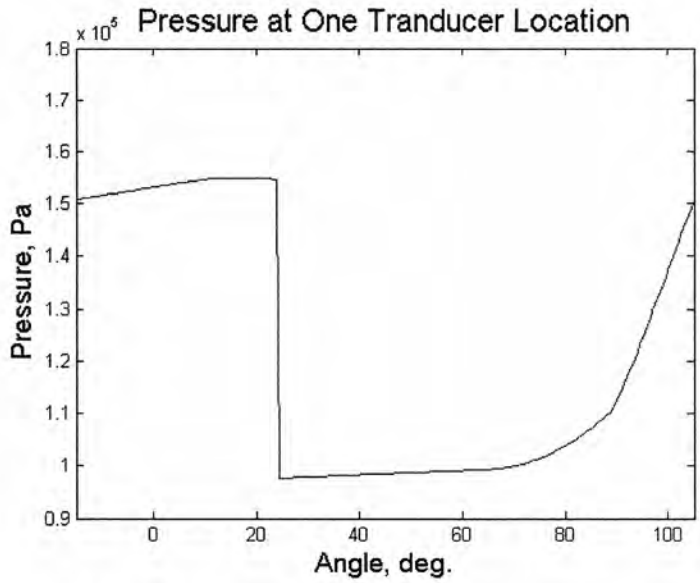

Figure 3.3 Pressure profile at one transducer location.

3.2 Pulse Model

The carryback pulsation is modeled separately. In comparison to the M-45 supercharger model, this pulse model is rather small since there is no iterative process. The program is basically a straight forward calculation process for the 120 degree cycle. The

body of this program is a time step procedure to calculate the direct path, the 1st reflection, the 2nd reflection, and the 3rd reflection pulses from both the inlet and outlet sides. In the end, the direct path, the 1st reflection, the 2nd reflection, and the 3rd reflection pulses are superimposed to the pressure profile output from the M-45 supercharger model. The output for this pulse model is a graph of the pressure at one transducer location with the pulses from the carryback slot.

3.2.1 Input

As seen in the graphical user interface, the two inputs that are output by the M-45 supercharger model are $\dot{m}_{cbl}$ and pressure profile at one transducer location. The pressure profile is input from a text file. The measured data are also input to the GUI for comparison purposes. The angle shift and offset are the parameters to adjust the predicted plot with respect to the measured plot.

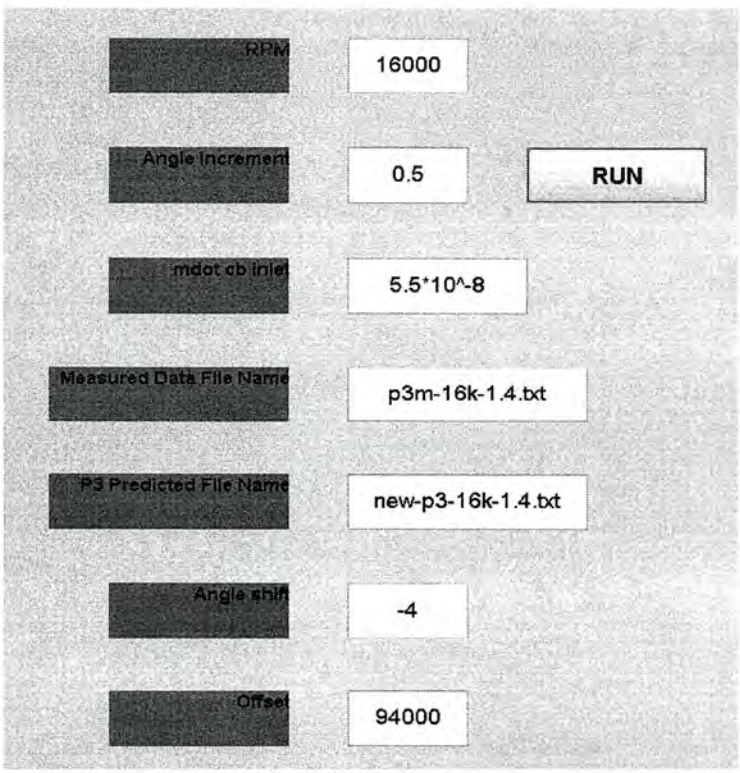

Figure 3.4 Graphical user interface for the pulse model.

3.2.2 Main Program

The main program consists of a straight forward calculation of the pressure pulse at each angle increment specified in the GUI. First the amplitude of the pulse is calculated using the siren equation, equation 2.27. The amplitude obtained is then used for calculating the pulse propagation for each path (direct, 1st reflection, 2nd reflection, and 3rd reflection) using the exponential decay equation, equation 2.28. The final pulse predicted is the pulse propagation superimposed to the input pressure profile at one location.

3.2.3 Output

Figure 3.5 shows an example of the pulse model output; it contains 3 different curves: predicted, measured, and predicted without pulse. The predicted is the pressure profile with the pulse; the measured is the pressure profile from the data provided by Eaton Corporation; and the predicted without pulse is the output from the M-45 supercharger model (before the pulse is added).

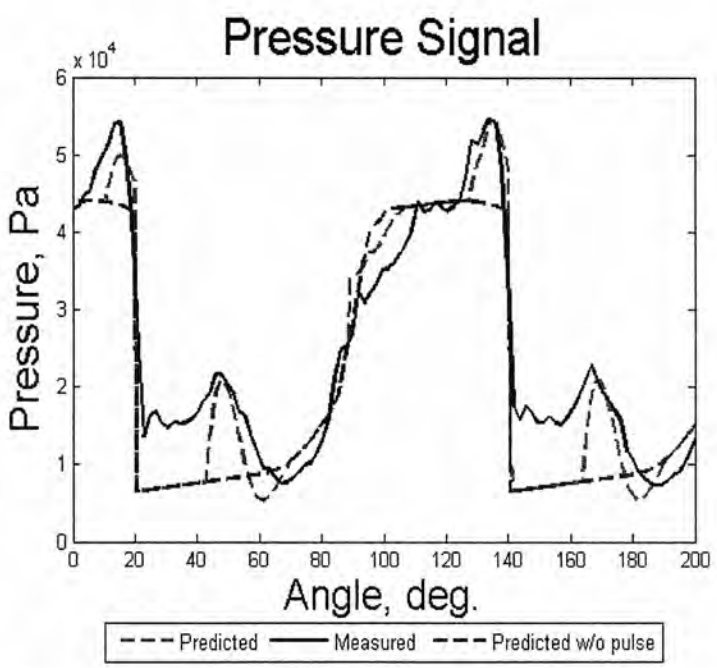

Figure 3.5 Pressure pulse output for an input condition in Figure 3.4.

Chapter 4
Results

This chapter consists of two parts; a computational process results section and a section comparing computational and experimental results. The computational process results section contains the results from different options for modeling the M-45 superchargers, including the two options of converting temperature to pressure as well as the temperature and pressure ratio convergence results.

After all these different options of modeling the supercharger are settled, the M-45 supercharger model is considered ready to be compared with the measured data. All the measured data was provided by Eaton Corporation and much of it has been documented in Meyer's and Carroll's thesis. In section 4.2 the efficiency results will be presented along with a sensitivity analysis, backflow slots addition, and the pulse generation model. It was found that for the predicted efficiency to closely match the measured efficiency, some minor adjustments need to be made to the M-45 supercharger model. The adjustment will be described.

4.1 Computational Process Results

The results that are presented in this section will determine which method will be used in the model for temperature to pressure conversion. Both temperature and pressure convergence results are also covered in this section, such as the case when the program has to go through some temperature iterations as well as the case when the program does and does not converge to the requested pressure ratio.

4.1.1 Temperature to Pressure Conversion Results

As discussed in chapter 2, there are two ways to do the temperature to pressure conversion; one is by using the ideal gas equation and the other is by using the isentropic flow equation. For a 4000 RPM rotor speed, the available data from Eaton Corporation is at

pressures ratios of 1.0, 1.2, and 1.4. For the rest of the rotor speed (8000 RPM, 12000 RPM, and 16000 RPM), the data for pressure ratio 1.0, 1.2, and 1.6 are available. Figure 4.1 shows the volumetric efficiency results comparing the two temperature to pressure conversion methods. The isentropic flow method, equation 2.19, is denoted as model 1 and the ideal gas method, equation 2.20, is denoted as model 2. Note that the scale in the graph is from 60% to 100% efficiency. As seen in Figure 4.1, the volumetric efficiency predictions using the two methods are about the same; the difference between the two is within 5 to 10 %. Hence, it can be concluded that volumetric efficiency is not significantly affected when either of the method is used.

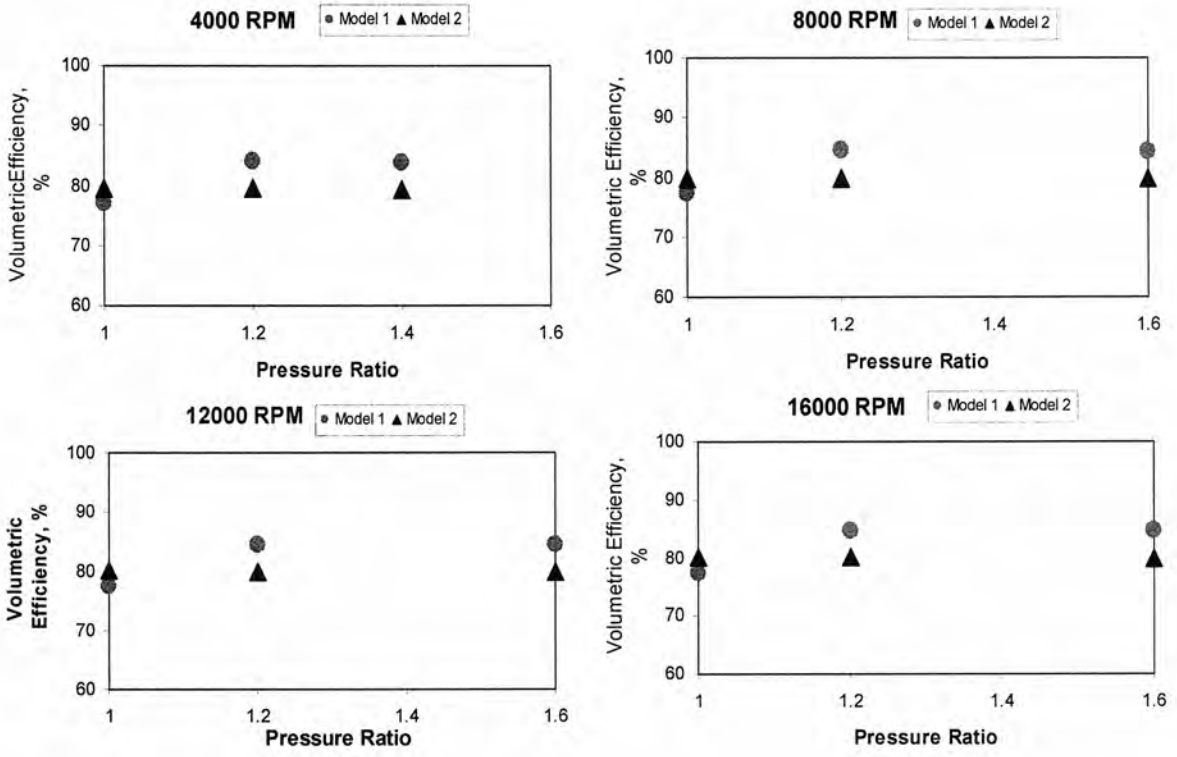

Figure 4.1 Volumetric efficiency comparison between model prediction using isentropic flow formula (model 1), and model prediction using ideal gas formula (model 2).

Figure 4.2 shows the J1723 isentropic efficiency prediction. Note that the scale here is from 0% to 125%. Figure 4.2 shows that the two prediction methods produce range of the J1723 isentropic efficiency that is much bigger than for the volumetric efficiency. Overall, the two models show similar trends; that is the J1723 efficiency is low at 1.0 pressure ratio and high at other pressure ratios for all rotors speeds. Model 1 (isentropic flow approach), however, predicts some extreme values; the efficiency is close to 0% for 1.0 pressure ratio and over 100% for other pressure ratios. On the other hand, model 2 (ideal gas approach) gives more promising results, i.e. the predicted values are more logical. Hence, the ideal gas equation approach is the method chosen to convert temperatures obtained from the energy equations to pressures.

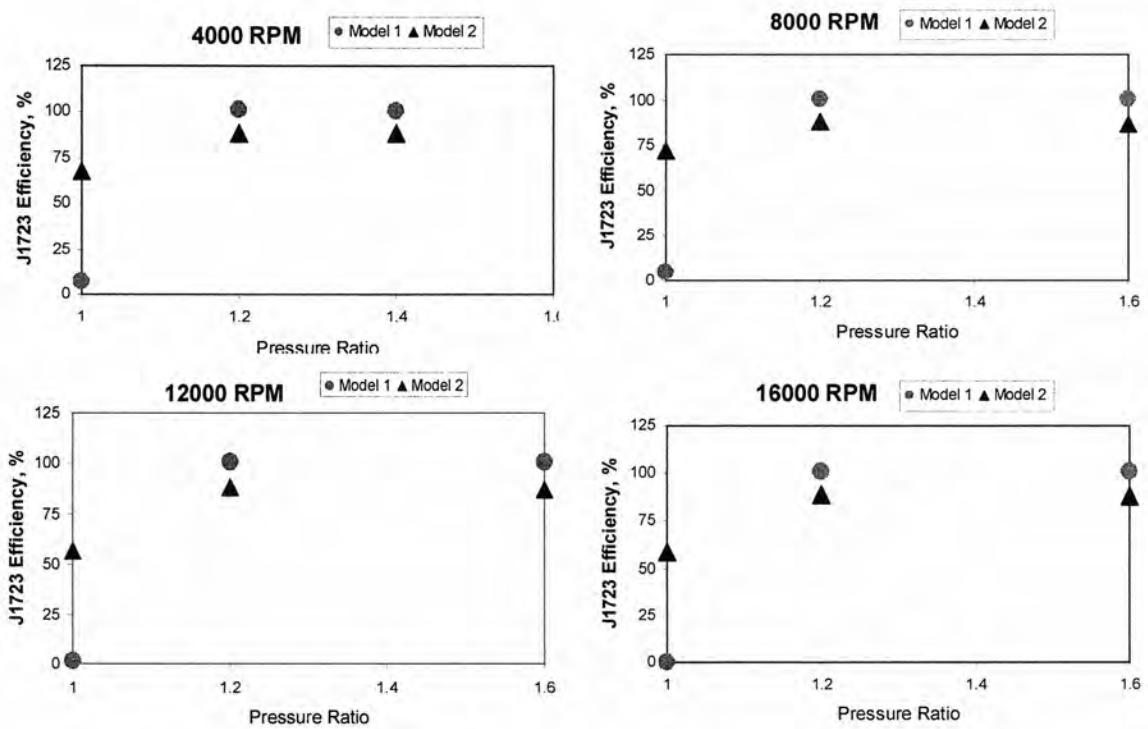

Figure 4.2 J1723 isentropic efficiency comparison between a model using the isentropic flow formula (model 1) and a model using the ideal gas formula (model 2).

4.1.2 Temperature Convergence Results

The first iteration that the M-45 supercharger model will go through is the temperature iteration. For the temperature convergence to be attained, the differences between temperature values for all control volumes at the beginning of the cycle (-15 degree) and at the end of the cycle (115 degree) have to be within 0.01%. Figure 4.3 shows the temperature profile at the first iteration. As seen, the temperatures at -15 degree (initial guess) are different from the temperatures at 105 degree; hence, the temperatures at 105 degree will be used to replace the initial guess at the beginning of cycle (-15 degree) for the next temperature iteration. This process continues until the temperature convergence is attained, Figure 4.4, where the temperature of each control volume at 105 degree is within 0.01% of the temperature values at -15 degree.

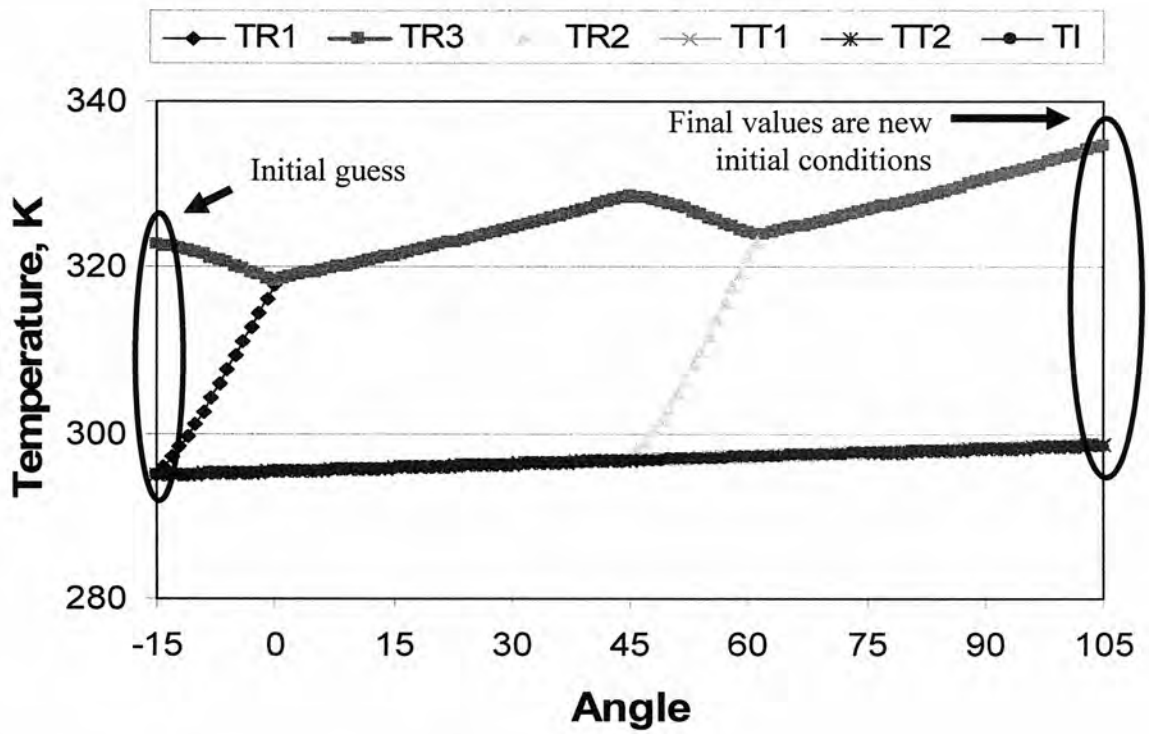

Figure 4.3 Temperature profile at the first iteration.

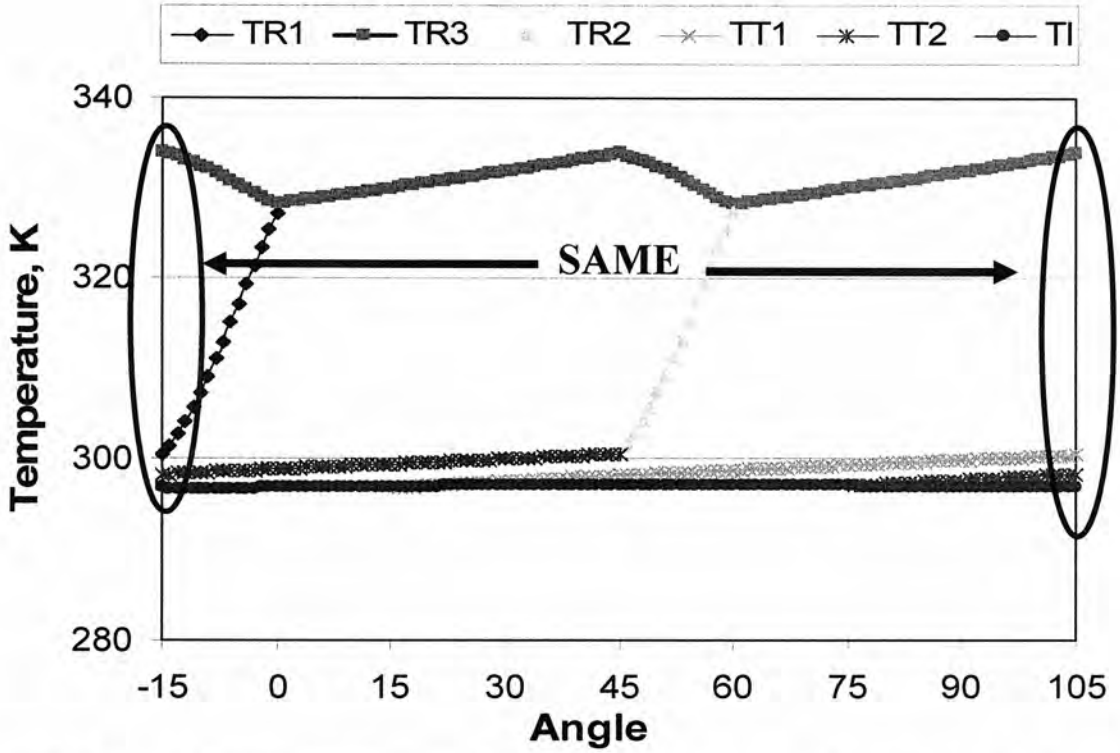

Figure 4.4 Temperature profile at final iteration. Temperature convergence is attained.

After the temperature convergence is attained, the pressure ratio is calculated and compared to the upper and lower limits specified by the user. If the calculated pressure ratio is beyond these limits, then pressure ratio convergence is not attained in which case the outlet volumetric flow rate is adjusted and used to replace the volumetric flow rate initial guess.

4.1.3 Pressure Ratio Convergence Results

After temperature convergence is attained, the program will go to the next iteration, which is the pressure ratio iteration. Figure 4.5 shows the outlet volumetric flow rate (top picture) and calculated pressure ratio (bottom picture) for each step in the process of reaching pressure ratio convergence. As seen, in this example, it takes 10 pressure ratio iterations for the program to obtain the final solution. In this case, the guessed outlet volume flow rate is smaller than the outlet volume flow rate needed for the calculated pressure ratio to converge

to the requested pressure ratio. Hence, the value of the outlet volume flow rate is raised at every increment. With a low guessed outlet volume flow rate, the program outputs a high calculated pressure ratio. Therefore, as the outlet volume flow rate is increased, the calculated pressure ratio value reduces.

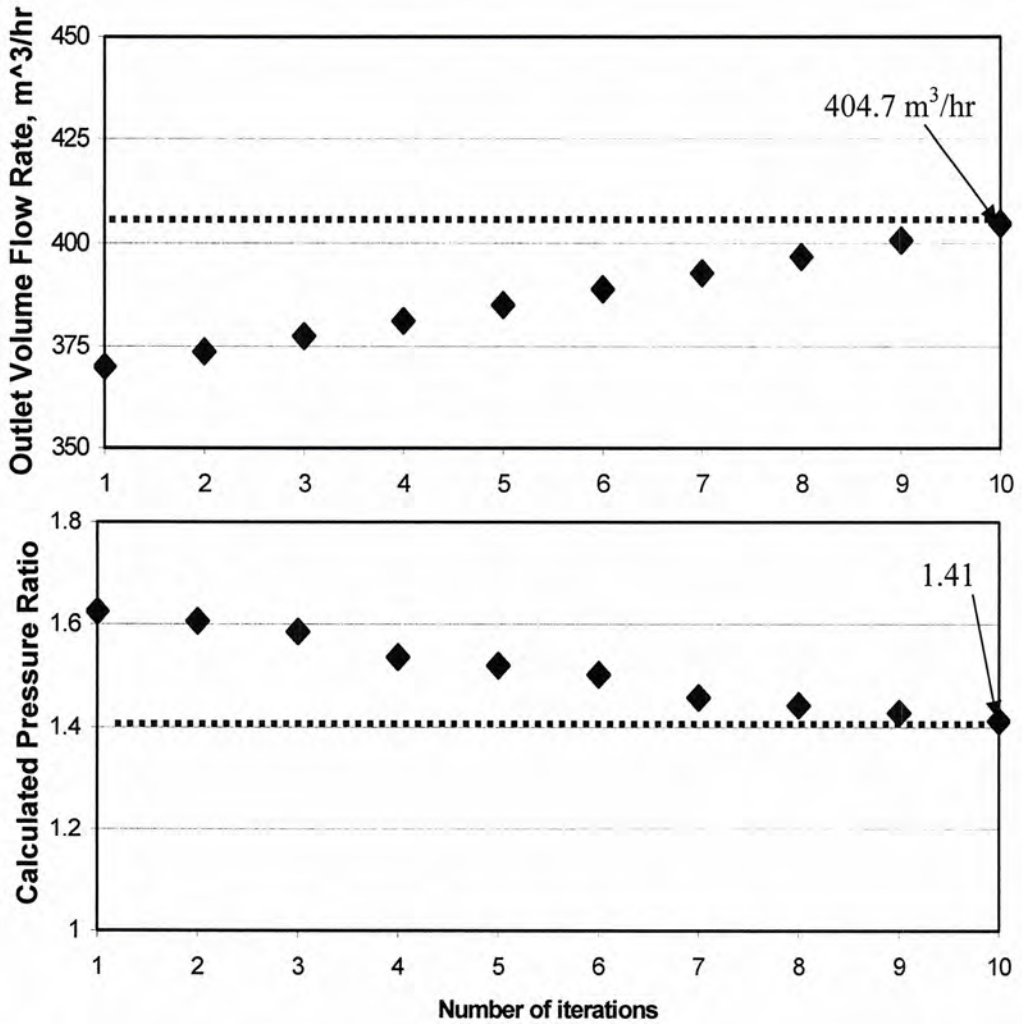

Figure 4.5 Outlet volume flow rate and calculated pressure ratio plots when pressure ratio convergence is attained.

Figure 4.6 shows the outlet volume flow rate iterations when pressure ratio convergence is not attained. This is caused either by the upper and lower limits being too narrow or by the constant for increasing or decreasing the flow rate being too large. Note

that the operating conditions for Figure 4.5 and 4.6 are the same; the only thing different is the constant value. Figures 4.5 and 4.6 have constant values of 0.005 and 0.05, respectively. As seen, both the outlet volume flow rate and calculated pressure ratio values do not converge to a solution; 404.7 m^3/hr for the outlet flow rate plot and 1.41 for the calculated pressure ratio plot. Both values are oscillating above and below the final converged solution. The percent increase or decrease of the volumetric flow rate is too large so that the pressure ratio does not converge.

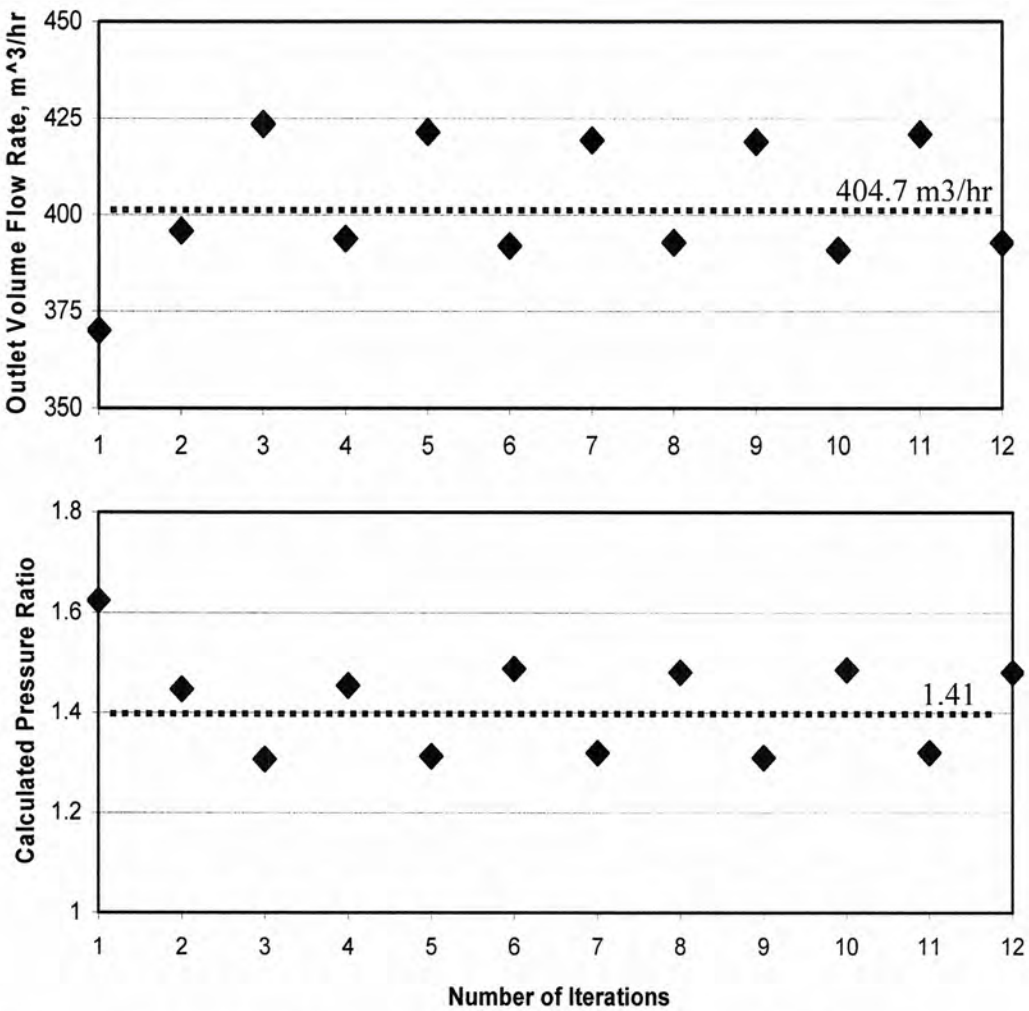

Figure 4.6 Outlet volume flow rate and calculated pressure ratio plots when pressure ratio convergence is not attained.

4.2 Model Results

With these changes made in section 4.1, the data output from M-45 supercharger model is now considered ready to be compared with the data provided by Eaton Corporation. At first, the predicted results do not match the measured results and some adjustments with the parameters and the models needed to be made. The adjustments made, however, are not major changes to the equations presented in section 2.2. The adjustments are changes in the parameters and adding some equations before or after the model without changing any part of the base equations developed in section 2.2.3. After these adjustments are completed, the prediction results were found to closely match the measured data.

In this section, a sensitivity analysis will be discussed first; followed by the results of the backflow slots feature addition and the efficiency results output by the supercharger model. Finally, the results from the pulse generation model will be presented.

4.2.1 Sensitivity Analysis

There are many parameters involved in this model; hence, a sensitivity analysis is performed to determine which parameters have significant impact on pressure values; P_{R1}, P_{R2}, P_{R3}, P_{T1}, P_{T2}, P_I. The sensitivity analysis is done by varying each parameter in the model by ±10% and ±20%. Each parameter is varied one at a time; changes in the pressure values at each control volume are then calculated to quantify sensitivity to the parameter variation. A ±5% change in pressure is considered significant. Table 4.1 shows the sensitivity analysis results.

The highlighted cells are the parameters that give at least a ±5% range of pressure variations when they are varied by ±10% and ±20%. For example, when VR3 is varied by ±10% and ±20%, PR1 varies from -5% to 13%, PR3 varies from 20% to 30%, and PR2 varies from -5%to 13% (See the highlighted cells in Table 4.1 on the volume section). The parameters that are varied in this sensitivity analysis include volumes, heat transfer areas,

flow areas, heat transfer coefficients, flow coefficients, the supercharger wall temperature, the upstream temperature, and the outlet volumetric flow rate.

As seen in the sensitivity analysis result, heat transfer areas, heat transfer coefficients, flow areas, and flow coefficients for every control volume do not have a significant impact to pressure values. When those values are varied by ±20%, pressure values only changes by at the most ±1%. The trapped and inlet pressures are not sensitive to volumes at all. The outlet pressure (P_{R3}) is sensitive to V_{R1}, V_{R2}, and V_{R3}. The pressure at R1 and R2 (P_{R1} and P_{R2}, respectively) are only sensitive to change in V_{R3}.

All pressures are found to be sensitive to both the supercharger wall temperature (T_{wall}) and the supercharger upstream temperature (T_{up}). The values of P_{R1}, P_{R3}, and P_{R2} are also sensitive to VdotR3 (outlet volumetric flow rate).

Table 4.1 Sensitivity Analysis Results.

		PR1	PR3	PR2	PT1	PT2	PI	NOTE
	V_I	±0.5%	±0.5%	±0.5%	±0.5%	±0.5%	±0.5%	
	V_{R1}	- 1% to 0.5%	- 7% to 6%	±3%	±0.5%	±0.5%	±0.15%	
Volume	V_{R2}	±3%	- 7.5% to 5.5%	- 1% to 0.5%	±0.5%	±0.5%	±0.15%	
	V_{R3}	- 5% to 13%	20 % to 30%	- 5% to 13%	±2%	±2%	- 0.5% to 0.8%	
	V_{T1}	- 0.6% to 1%	±0.6%	±0.3%	±1%	±0.1%	±0.1%	
	V_{T2}	±0.3%	±0.5%	- 0.6% to 1%	±0.1%	±1%	±0.1%	All volumes are varied by ± 10% and ± 20%
	AHT_I	±0.3%	±0.3%	±0.3%	±0.3%	±0.3%	±0.4%	
	AHT_{R1}	±0.1%	±0.1%	±0.1%	±0.1%	±0.1%	±0.1%	
Heat Transfer	AHT_{R2}	±0.1%	±0.1%	±0.1%	±0.1%	±0.1%	±0.1%	
Area	AHT_{R3}	±0.1%	±0.1%	±0.1%	±0.1%	±0.1%	±0.1%	
	AHT_{T1}	±0.3%	±0.2%	±0.1%	±0.3%	±0.1%	±0.1%	
	AHT_{T2}	±0.1%	±0.2%	±0.3%	±0.1%	±0.3%	±0.1%	All heat transfer areas are varied by ± 10% and ± 20%
	ARPT1	±2%	±0.5%	- 0.3% to 0%	±0.1%	±0.1%	±0.1%	
	ARPT2	- 0.3% to 0%	±0.5%	±2%	±0.1%	±0.1%	±0.1%	
Flow Area	AL	±0.5%	±0.1%	±0.5%	±0.5%	±0.5%	±0.1%	
	Atip	±0.1%	±0.2%	±0.1%	±0.1%	±0.1%	±0.1%	All flow areas are varied by ± 10% and ± 20%
	h_I	±0.3%	±0.3%	±0.3%	±0.3%	±0.3%	±0.3%	
	h_{R1}	±0.1%	±0.1%	±0.1%	±0.1%	±0.1%	±0.1%	
Heat Transfer	h_{R2}	±0.1%	±0.1%	±0.1%	±0.1%	±0.1%	±0.1%	
Coefficient	h_{R3}	±0.1%	±0.1%	±0.1%	±0.1%	±0.1%	±0.1%	
	h_{T1}	±0.3%	±0.2%	±0.1%	±0.3%	±0.1%	±0.1%	
	h_{T2}	±0.1%	±0.2%	±0.3%	±0.1%	±0.3%	±0.1%	All heat transfer coefficients are varied by ± 10% and ± 20%
	Cf	±0.5%	±0.2%	±0.5%	±0.5%	±0.5%	±0.1%	
Flow Coefficient	Cf_{RPT1}	±0.2%	±0.5%	- 0.3% to 0%	- 0.1% to 0%	- 0.1% to 0%	±0.1%	
	Cf_{RPT2}	- 0.3% to 0%	±0.5%	±0.2%	- 0.1% to 0%	- 0.1% to 0%	±0.1%	All flow coefficients are varied by ± 10% and ± 20%
	Twall	± 10%	± 13%	± 10%	± 10%	± 10%	± 6%	
All Other	Tup	- 25% to 35%	- 20% to 30%	- 25% to 35%	-30% to 40%	-30% to 40%	-30% to 40%	
Variables	VdotR3	- 5% to 20%	- 30% to 50%	- 5% to 20%	±3%	±3%	±1%	T_{wall} and $Vdot_{R3}$ are varied by ± 10% and ± 20%% and Tup is varied by ± 10% only

The conclusion that can be drawn from the sensitivity analysis is that geometrical values (especially volume), the supercharger upstream temperature, the supercharger wall temperature, and the outlet volumetric flow rate need to be very precisely known in order to get reliable results.

4.2.2 Backflow Slots Addition Results

This section will discuss the difference in the pressure plots between the case where backflow slots exist and the case where backflow slots do not exist. As seen in Figure 4.7 and 4.8, when the backflow slots do not exist (left side), the trapped pressure 1 and 2 plots (P_{T1} and P_{T2}) rise at a slow rate. They then suddenly rise as the trapped volume starts to open to the outlet and switch to P_{R1} and P_{R2} (low pressure receiver) at 30 degree and 90 degree, respectively.

In contrast, when the backflow slots exist (right side in Figures 4.7 and 4.8), P_{T1} and P_{T2} start to increase significantly when the leading rotor tip of the trapped volume passes the backflow slots (at 5 degree). The pressures P_{T1} and P_{T2} then switch to P_{R1} and P_{R2} when the trapped volume opens to the outlet. Once P_{T1} or P_{T2} open to the outlet, a new trapped volume is reformed from the inlet portion of the supercharger. This result can be seen graphically at angle 30 degree and 90 degree, where P_{T1} and P_{T2} plots go back down and start at the inlet pressure again. For the right side in Figure 4.7 case, the rotor speed is high enough so that there is no time for the trapped volume to reach the outlet pressure before opening to the outlet, i.e. P_{T1} and P_{T2} switch to P_{R1} and P_{R2}, respectively.

In the low rotor speed cases such as 4000 RPM, the trapped volume has enough time to reach the outlet pressure before the leading tip opens to the outlet port, Figure 4.8 (right side). The fact that the trapped pressures rise when backflow slots are added agrees with the purpose of backflow slots, which is to reduce the noise created by a sudden pressure change in the supercharger.

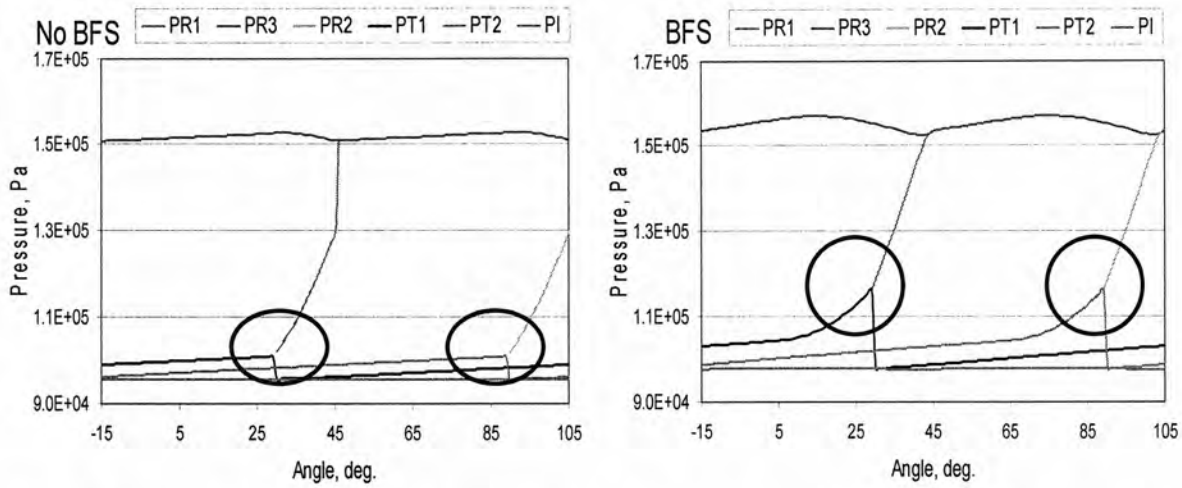

Figure 4.7 Pressure plot with and without backflow slot at 16000 RPM and 1.6 pressure ratio.

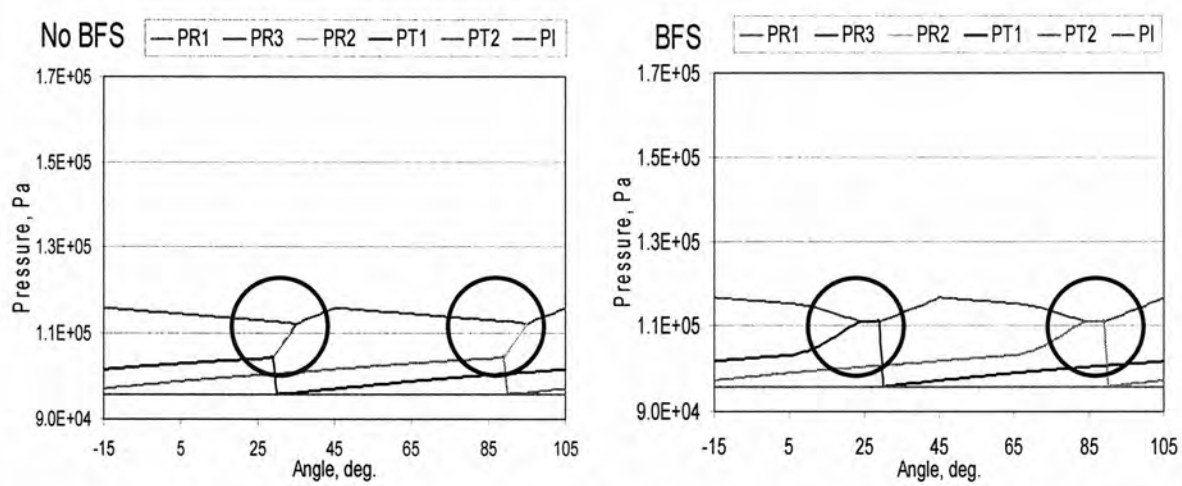

Figure 4.8 Pressure plot with and without backflow slot at 4000 RPM and 1.2 pressure ratio.

Another plot that depicts the effect of adding the backflow slot is shown in Figure 4.9. This is a plot of the pressure at one transducer location. Similar trends are found; the pressure rises smoothly when the backflow slots feature is added, although from this plot, it cannot be detected which control volume the transducer is reading the pressure from.

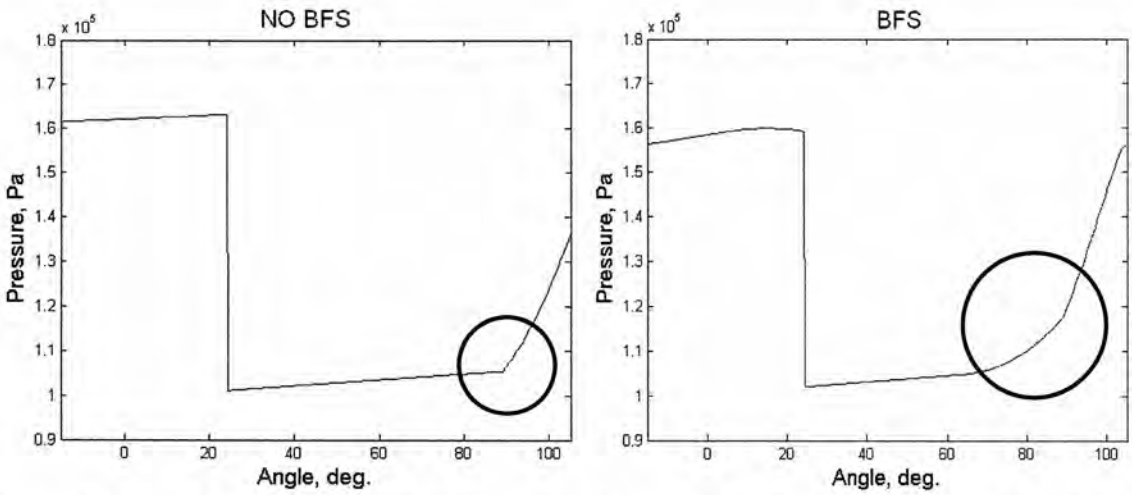

Figure 4.9 Pressure plot at 1.6 pressure ratio and 16000 RPM at one transducer location with and without backflow slot.

4.2.3 Efficiency Results

Several different approaches have been attempted in order to match the model output (volumetric efficiency and J1723 isentropic efficiency) with the measured data provided by Eaton Corporation. These outputs, volumetric efficiency and J1723 isentropic efficiency, can be seen in Figure 4.10 and 4.11, respectively. In these plots, the efficiency result from the M-45 supercharger model after all changes in section 4.1 has been made is denoted by "original". As seen, the model made some good predictions on volumetric efficiency for all cases; the predictions are within 10%. However, this is not the case for the J1723 isentropic efficiency predictions where the model always over-predicts the J1723 efficiency, and the difference increases as the rotor speed increases, Figure 4.11. Also, note that the model cannot get a pressure ratio convergence for the minimum boost pressure (pressure ratio =1.0). When the upper and lower limits are set close to 1.0, the model will not converge to a solution. Hence, the closest efficiency results that can be predicted (around 1.1 pressure ratio) are obtained.

The over-prediction of the J1723 isentropic efficiency is caused by discrepancies between the average inlet and outlet pressure and temperature from the model and the measured data. Going back to the J1723 isentropic equation in chapter 2,

$$J1723\ \text{efficiency} = \frac{T_{inlet}\left(PR^{0.286}-1\right)}{T_{outlet}-T_{inlet}} \times 100 \qquad \textbf{4.1}$$

a large J1723 efficiency can be caused by either a large numerator or a small denominator. In this case the denominator, the difference between the outlet and inlet temperature, is the source of discrepancy. As seen in the circled columns of Table 4.2, the model always under-predicts the outlet temperature at any given pressure ratio. The difference between the two gets larger as the pressure ratio and rotor speed increase. On the other hand, the difference between the calculated and measured inlet temperature is within 1 to 3 degrees Kelvin; therefore, the work to match the J1723 isentropic efficiency is focused on increasing the predicted outlet temperature (T_{R3}).

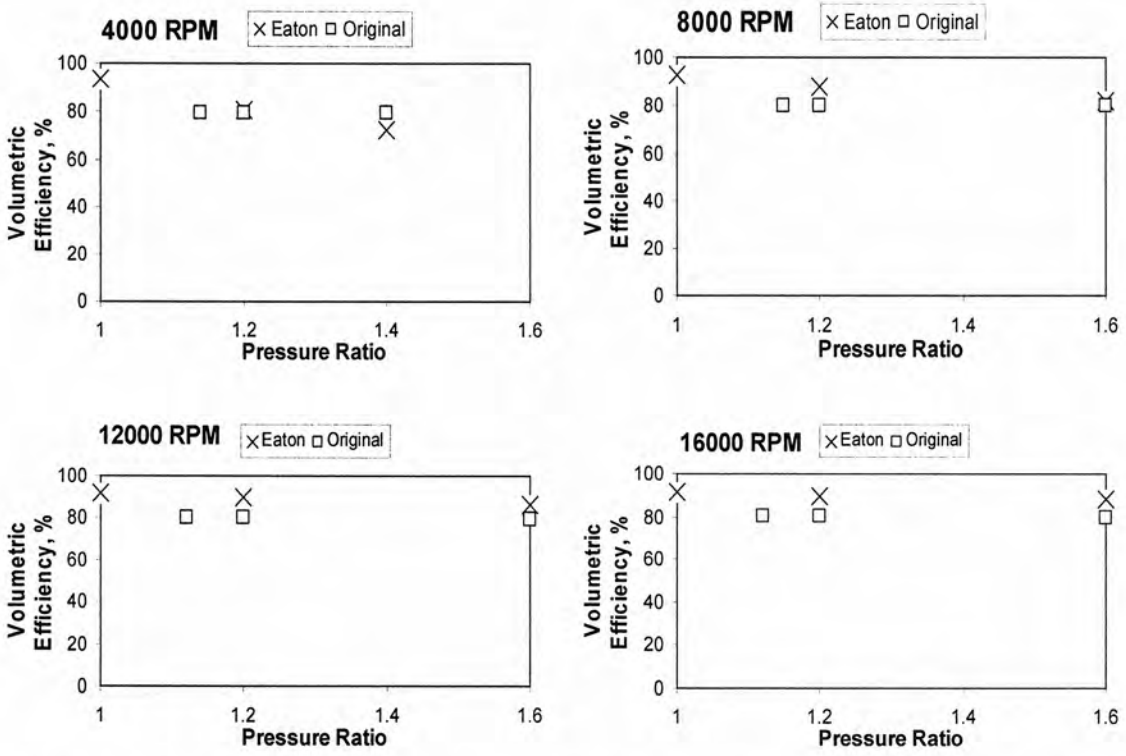

Figure 4.10 Volumetric efficiency comparison between the measured data and the model output.

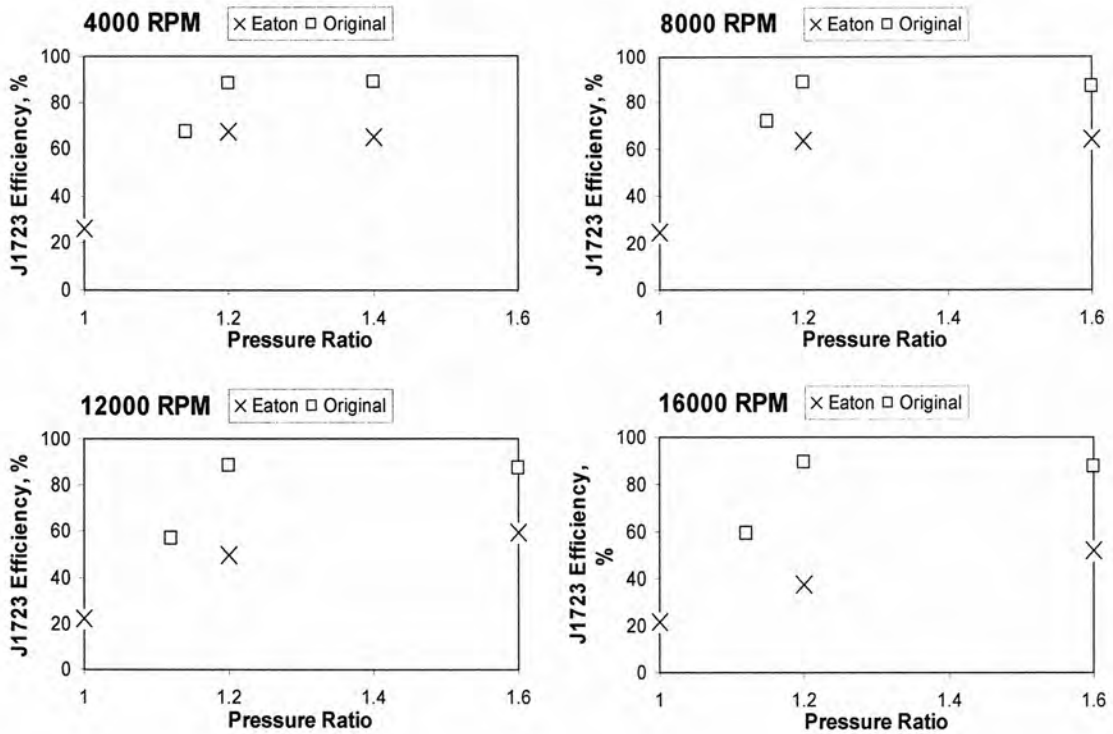

Figure 4.11 J1723 isentropic efficiency comparison between the measured data and the model output.

Table 4.2 Temperature and pressure results comparison between the measured data and the model output.

		Calculated Data (Model)				Measured Data (Eaton)			
RPM	PR	T outlet	T inlet	P outlet	P inlet	T outlet	T inlet	P outlet	P inlet
4000	1					306.1	303.9	98785	98105
4000	1.14	319.3	301.4	109160	95190				
4000	1.2	320.1	301.5	114650	95200	325.4	302.5	117040	98195
4000	1.4	336.9	301.6	134560	95250	349.6	303.2	137435	98355
8000	1					310.7	303.1	99230	97070
8000	1.15	318.8	301.4	109750	95180				
8000	1.2	319.9	301.4	114480	95180	327.6	302.2	116695	97185
8000	1.6	353.3	301.6	154500	95240	370.6	303.1	156115	97435
12000	1					319.2	302.2	99765	95420
12000	1.12	318.9	301.4	106620	95170				
12000	1.2	320.1	301.4	114710	95170	334.3	302.2	114430	95510
12000	1.6	352.1	301.5	153550	95210	375.3	302.8	153045	95810
16000	1					331.4	301.6	100570	93300
16000	1.12	318.7	301.4	106950	95170				
16000	1.2	320.2	301.4	115090	95170	344.7	302.4	111920	93480
16000	1.6	351.5	301.5	153160	95200	385.6	302.8	149830	93735

From this efficiency result analysis, the J1723 isentropic efficiency is found to be very sensitive to the inlet temperature, operating pressure ratio, and especially the outlet temperature. Some possible factors that might contribute to the discrepancies in the efficiency prediction can include the actual transducer location, the flow coefficient, and the supercharger wall temperature. These factors were analyzed one by one and implemented in the model.

In the laboratory set up the pressure transducers and temperature probes are placed at some distance upstream and downstream from the supercharger itself. However, in the model, the values are assumed to be directly at the inlet and outlet.

Figure 4.12 and 4.13 show inlet and outlet adaptors that were used for testing at Eaton Corporation. In Figure 4.12, the inlet static pressure transducer is 20 inches upstream from point A, the inlet temperature probe is 22 inches upstream from point A, and the flow meter is 40.5 inches upstream from point A. The outlet static pressure transducer and outlet temperature probe are 23.35 inches and 28.25 inches downstream from supercharger outlet flange. Figure 4.13 shows the picture of outlet adaptor.

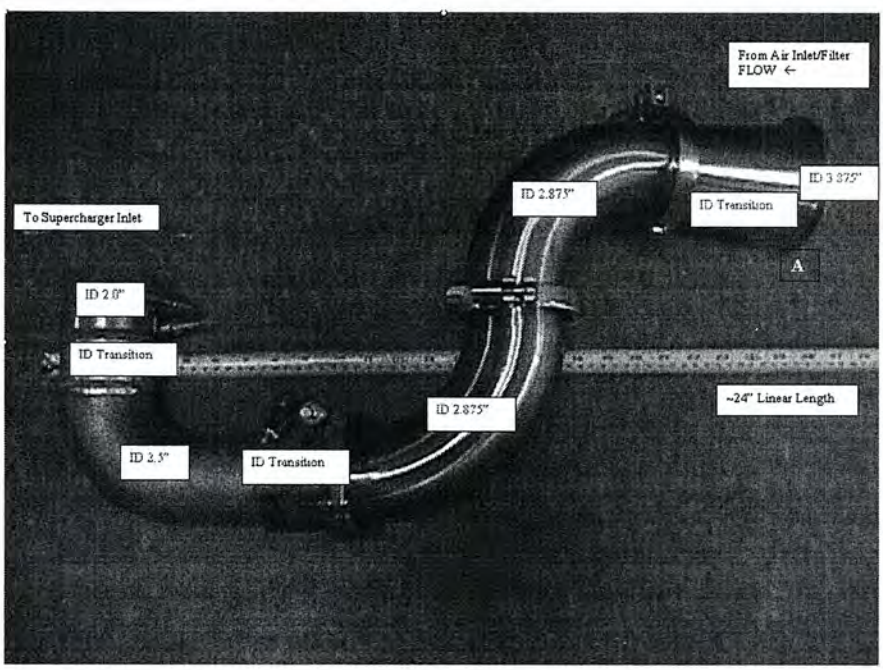

Figure 4.12 Inlet adaptor.

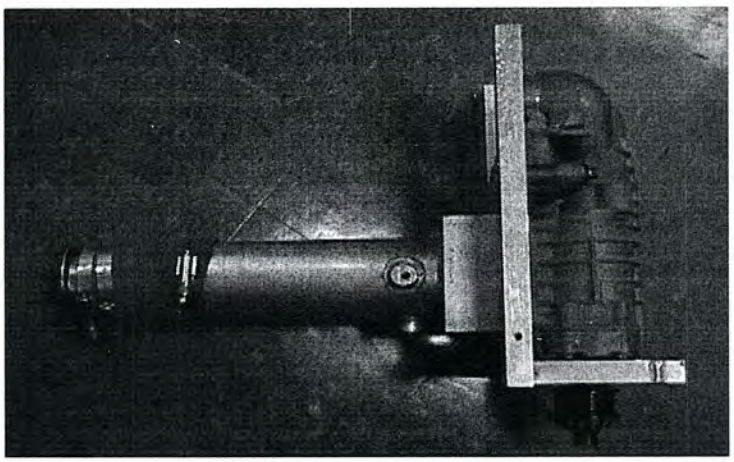

Figure 4.13 Outlet adaptor.

Since the model calculates the inlet pressure right at the inlet volume of the supercharger and outlet pressure right at the outlet volume of the supercharger, the calculation for the inlet and outlet pressure in the model need to be adjusted. This is done by calculating the pressure drop due to friction effect from the transducer location to the actual supercharger inlet and outlet. These changes are done before and after the program; hence, the main program in the M-45 supercharger model does not change at all.

A rough schematic of supercharger with transducers is shown in Figure 4.14. The actual inlet and outlet of the supercharger are labeled as points "in" and "out". The locations of the inlet and outlet transducers are at point 1 and 4, respectively.

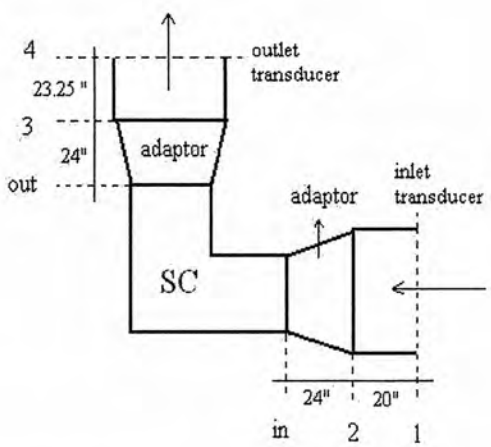

Figure 4.14 Rough supercharger schematic with pressure transducers.

It is assumed that there is pressure drop from the point 1 to the point "in" and from the point "out" to the point 4. Using Bernoulli's equation (Munson 2002, 119), these pressure drops are calculated as:

$$\frac{p_1}{\gamma}+\frac{1}{2}\cdot\rho_1\cdot v_1^2+\rho_1\cdot g\cdot z_1=\frac{p_2}{\gamma}+\frac{1}{2}\cdot\rho_2\cdot v_2^2+\rho_2\cdot g\cdot z_2 \qquad \textbf{4.2}$$

where:

p : pressure (Pa)

γ : specific gravity (N/m)

ρ : density (kg/m^3)

V : velocity (m/s)

g : acceleration due to gravity (m/s^2)

z : height (m)

Since inlet and outlet of supercharger is mounted at the same elevation, the third term in the equation, potential energy term, cancels out and equation 4.2 becomes:

$$\frac{p_1}{\gamma}+\frac{1}{2}\cdot\rho_1\cdot v_1^2=\frac{p_2}{\gamma}+\frac{1}{2}\cdot\rho_2\cdot v_2^2 \qquad \textbf{4.3}$$

The analysis above results in pressure drops of about 100 to 300 Pa due to piping friction effects, which are very small when compared to the operating pressures (between 90,000 Pa and 150,000 Pa). The fact that these pressure drop values are very small when compared to the working pressure of the supercharger leads to a conclusion that friction effect due to piping can be neglected in the comparison of calculated and measured data.

Flow coefficients were also adjusted in an attempt to match the measured data. The idea was that since the simplified model under-predicted the outlet temperature, reducing the leakage flows from the outlet control volume would maintain the outlet volume at a high temperature. That is, transferring more air through leakage flows from the outlet control

volume to the trapped and inlet volumes reduces the outlet temperatures. The result for adjusting the flow coefficients can be seen in Figure 4.15 and 4.16. The model prediction when the flow coefficients are adjusted is denoted as "Trial 1".

After attempting to adjust these flow parameters, it turns out that the changes made to the flow coefficients also did not give a sufficient increase in outlet temperature to change the J1723 isentropic efficiency significantly. Outlet temperatures increase about 1 or 2 degrees Kelvin; hence, the J1723 isentropic efficiencies reduce by about 1 to 2%. Table 4.3 shows the temperature and pressure results from trial 1. As seen, the difference between the calculated and measured outlet temperature is still very large, especially at high rotor speeds. The volumetric efficiencies also do not show any significant increase or decrease from the "original".

When the supercharger wall temperature (T_{wall}) is changed according to the pressure ratio and rotor speed, the model yields better result, i.e. efficiency values (both volumetric and J1723 isentropic efficiencies) predicted by the model were much closer to the measured data. These results can be also seen in Figure 4.15 and 4.16. The efficiency predicted by the model when the supercharger wall temperature is changed is denoted as "Trial 2".

With the adjusted wall temperature, the model can also now give a closer pressure ratio convergence; the model converges to a pressure ratio between 1.05 and 1.08 for the minimum boost (pressure ratio =1.0). Table 4.4 shows the temperature results from trial 2; as seen, the difference between the calculated and measured outlet temperature is reduced to within 1 to 3 degrees Kelvin. For future work, an analysis on this model could be done to determine why it does not converge when the pressure ratio is requested to be 1.0.

It is important to note that the wall temperature needs to be 3 to 8 degrees Kelvin hotter than the outlet air temperature for the model to predict a closer J1723 efficiency. The higher the rotor speed and pressure ratio, the higher the difference between supercharger wall and outlet temperature. This contradicts Sorenson model's assumption (in chapter 2) that the direction of the convection process can be both ways depending on whether the air inside the control volume or the supercharger wall is hotter. The fact that the wall temperature is always hotter than the outlet temperature for all operating pressure ratio and rotor speeds only allows the heat transfer to occur from the supercharger wall to the air inside the control volume.

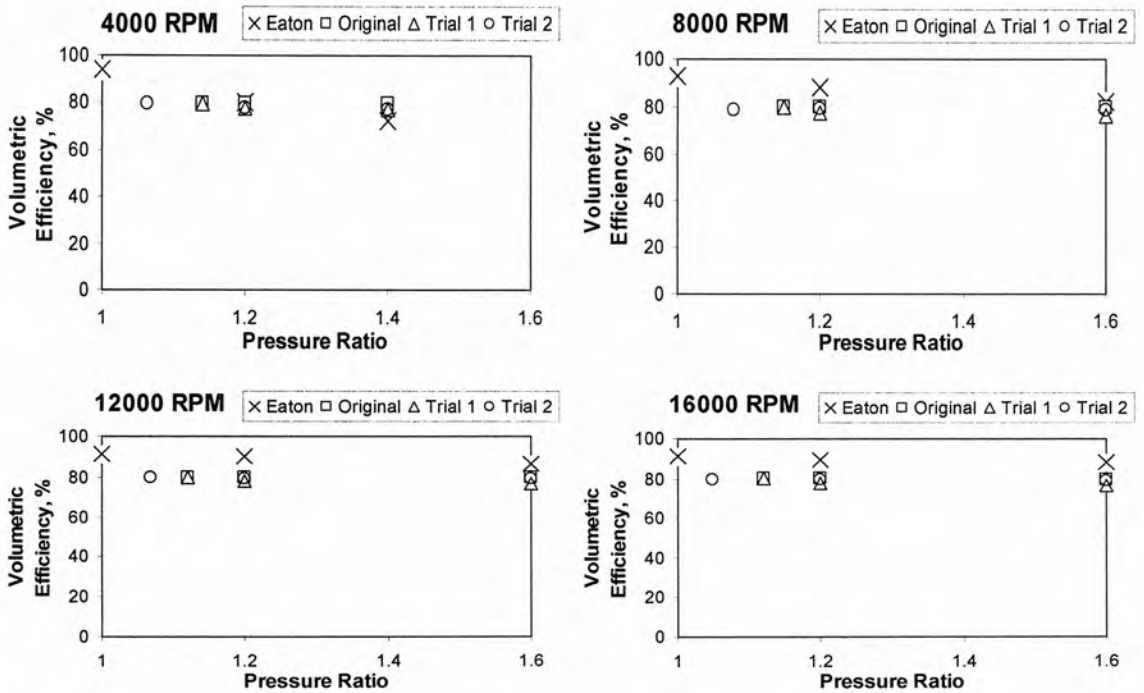

Figure 4.15 Volumetric efficiency comparison between measured data and other trials.

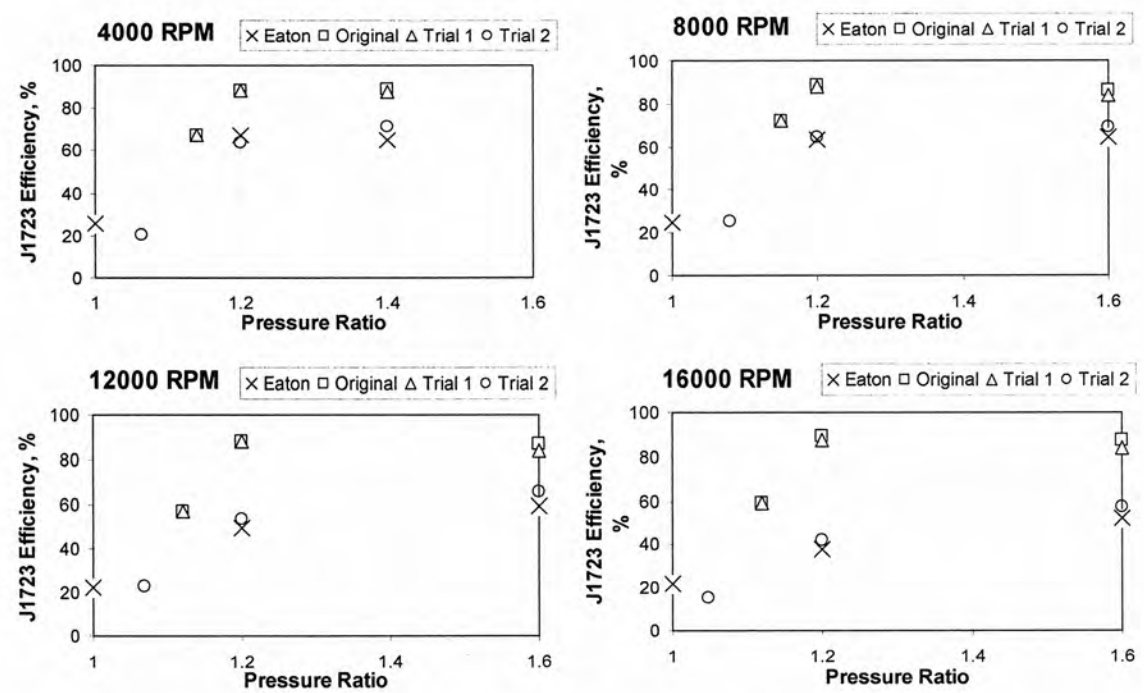

Figure 4.16 J1723 isentropic efficiency comparison between measured data and other trials.

Table 4.3 Temperature and pressure results comparison between the measured data from trial 1 and the model output.

		Calculated Data (Model, Trial 1)				Measured Data (Eaton)			
RPM	PR	T outlet	T inlet	P outlet	P inlet	T outlet	T inlet	P outlet	P inlet
4000	1					306.1	303.9	98785	98105
4000	1.128	320.6	301.7	110004.1	95264.8				
4000	1.2	322.3	301.8	117123.3	95299.6	325.4	302.5	117040	98195
4000	1.4	339.5	302.4	136739.6	95486	349.6	303.2	137435	98355
8000	1					310.7	303.1	99230	97070
8000	1.107	320.4	301.6	107972.4	95254.4				
8000	1.2	322.7	301.8	117509	95301.6	327.6	302.2	116695	97185
8000	1.6	356.6	303	155489.7	95697.6	370.6	303.1	156115	97435
12000	1					319.2	302.2	99765	95420
12000	1.093	320.3	301.6	106552.6	95246.7				
12000	1.2	322.6	301.8	117411	95299.9	334.3	302.2	114430	95510
12000	1.6	356.3	303	155083.8	95697.8	375.3	302.8	153045	95810
16000	1					331.4	301.6	100570	93300
16000	1.1	320.2	301.6	107148.4	95248.1				
16000	1.2	322.7	301.8	117367.6	95299.5	344.7	302.4	111920	93480
16000	1.6	355.8	303	154291.5	95695.8	385.6	302.8	149830	93735

Table 4.4 Temperature and pressure results comparison between the measured data from trial 2 and the model output.

		Calculated Data (Model, Trial 2)				Measured Data (Eaton)			
RPM	PR	T outlet	T inlet	P outlet	P inlet	T outlet	T inlet	P outlet	P inlet
4000	1					306.1	303.9	98785	98105
4000	1.063	329	303.1	101722.8	95725.2				
4000	1.2	328.6	302.7	115147.6	95575.2	325.4	302.5	117040	98195
4000	1.4	348.9	304.7	135614.1	96231.1	349.6	303.2	137435	98355
8000	1					310.7	303.1	99230	97070
8000	1.079	329.2	303.4	103329.4	95797				
8000	1.2	328.1	302.3	115039.5	95473.4	327.6	302.2	116695	97185
8000	1.6	371.1	306.6	155572.4	96813.3	370.6	303.1	156115	97435
12000	1					319.2	302.2	99765	95420
12000	1.069	328.6	303.1	102279.5	95707.9				
12000	1.2	333	302.6	114865.1	95555.3	334.3	302.2	114430	95510
12000	1.6	374.9	306.9	155778.1	96914.9	375.3	302.8	153045	95810
16000	1					331.4	301.6	100570	93300
16000	1.048	328.9	303	100242.3	95696.5				
16000	1.2	344.4	304	116019.6	95986	344.7	302.4	111920	93480
16000	1.6	384.8	307.4	155653.4	97086.9	385.6	302.8	149830	93735

The supercharger wall being hotter than the air inside suggests that there are other sources of energy that has not been accounted for in the analysis. This heat generation in the supercharger can be caused by mechanical loss, such as friction. Since the clearance between the rotor blade tips and supercharger wall is very small, the hypothesis is that the friction effect due to the small clearance heats up the wall and finally increases the wall temperature. As the rotors speed gets higher, the friction increases and the supercharger wall gets even hotter. There has not been any laboratory testing on the supercharger wall temperature to support this hypothesis. Therefore, a further study needs to be conducted to obtain the supercharger wall temperature and determine whether the convection heat transfer is really coming from the supercharger wall to the air inside. Further, it is also not clear if the source of energy is the heat from the wall or another energy source not currently included in the model. Future work is needed to identify additional sources of energy if the increased wall temperature is not confirmed from the experiments.

4.2.4 Pressure Results from the Carryback Pulse Model

The next improvement made to the model was including pulses from the carryback slot. The pulses are superimposing on the pressure signal from the modified Sorenson model. At the end of the model calculation, after efficiency values are predicted, the pressure signature at a transducer is obtained and combined with the pulse generated by the carryback slot. As discussed in chapter 2, the process of fitting the pulse profile is done experimentally. Even though the siren model is the base concept for creating pressure pulse, there are still many variables that can be manipulated. For instance, the reflection coefficient. From trial and error of comparing the predicted response to the measured data, a reflection coefficient of 0.5 best fit the measured data for a pressure ratio 1.4.

There were several other factors that were determined from a study of the experimental data. These factors are determined by considering the propagation path and the spin of the rotors. There are times when the transducer would read pulses until the 3rd

reflection and there are times when the transducer would not even read any reflection due to the rotors blade position. In addition, two pulses are modeled in the supercharger; one is from the inlet and one is from the outlet side of the supercharger. Further, for each pulse the reflection of the pulse was timed considering the propagation distances that the pulses would propagate. In the development of the results that are presented, it was determined that the distance needed to be reduced by the distance the rotor would rotate in the time of the propagation.

Since there are many discrepancies between the predicted and measure pulses at a pressure ratio of 1.0, Figure 4.17, the determination of parameter values in the pulse model focused on the measured data from a pressure ratio of 1.4 only. Part of the discrepancies is caused by the fact that the model cannot converge at pressure ratio 1.0.

Figure 4.18 shows the pressure signature at one transducer location at 4000, 8000, 12000, 16000 RPM and 1.4 pressure ratio. The solid line represents the measured pressure signal; the dark-dashed line represents the predicted pressure signal with carryback slot pulses; and the light-dashed line represents the predicted pressure signal without carryback slot pulses.

Stronger pulses due to the carryback slot are observed at higher rotors speeds. As seen, the model better represents the pressure pulses at high rotor speeds than it does at lower rotor speeds (especially at 4000 RPM). While there are some significant discrepancies between the measured and predicted signals, the results do indicate that the simplified model, augmented by models of an acoustics pulse propagating in the supercharger, can represent the primary features of the signals in the supercharger.

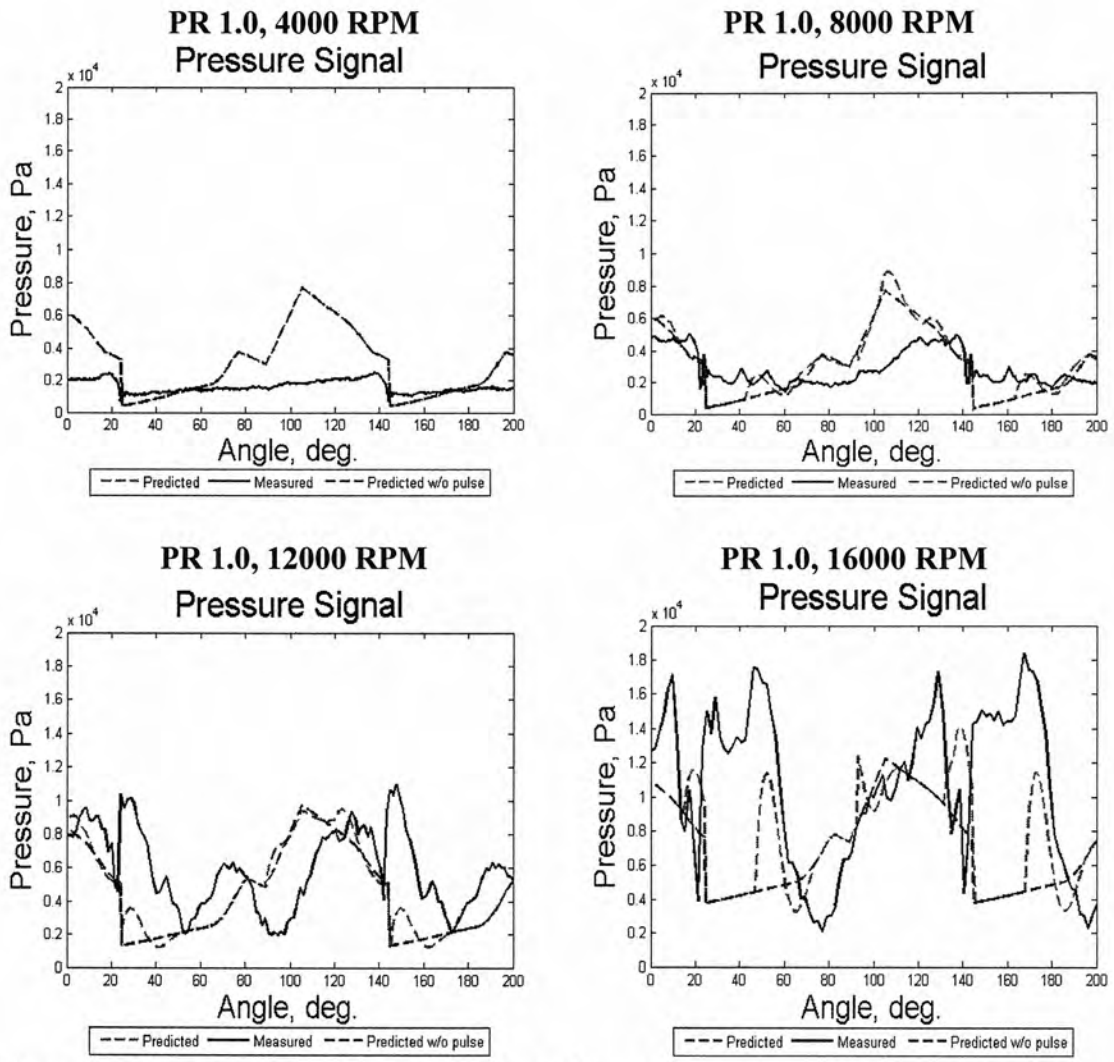

Figure 4.17 Pressure Pulse Signal for various rotors speed at 1.0 pressure ratio.

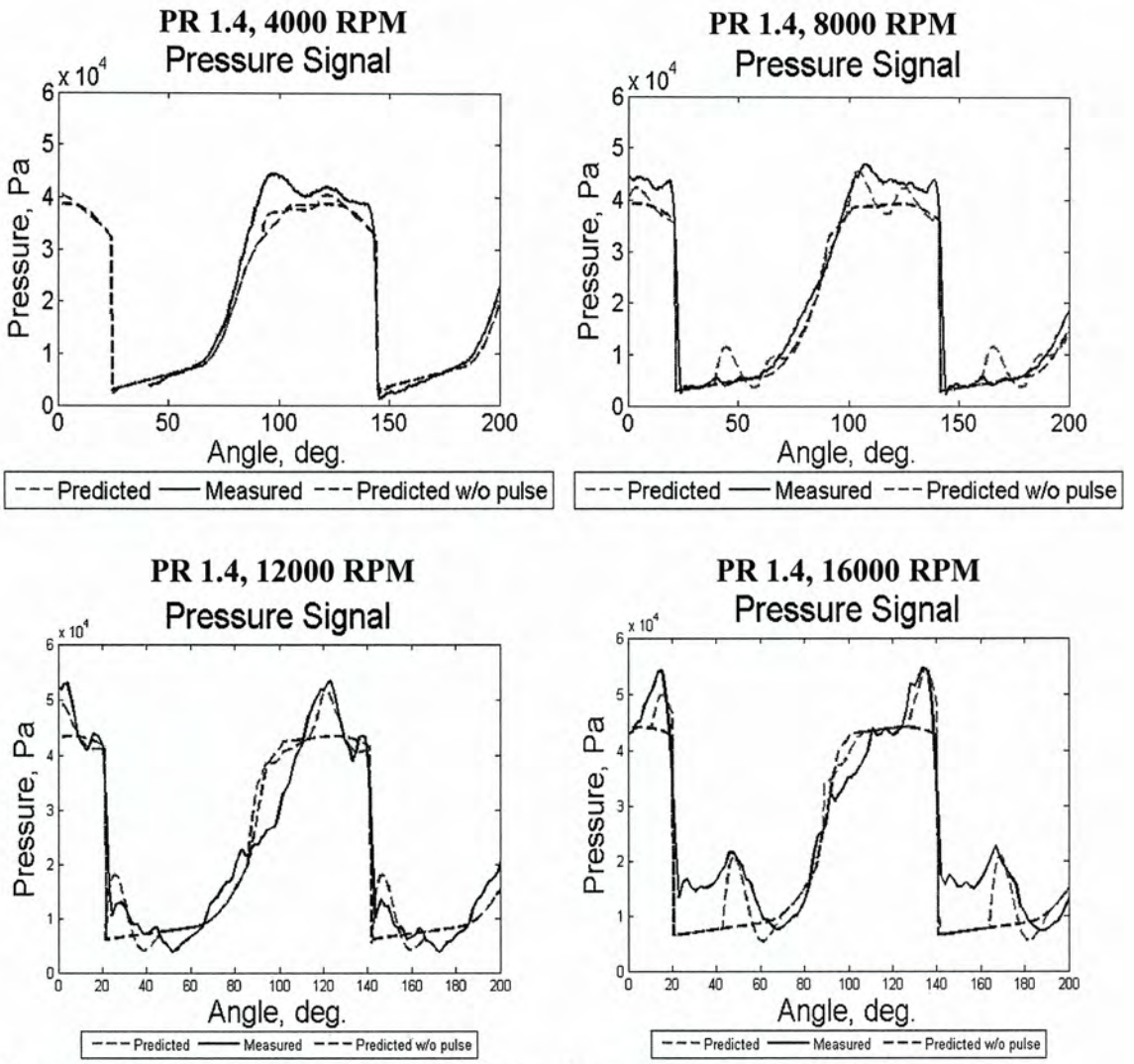

Figure 4.18 Pressure Pulse Signal for various rotors speed at 1.4 pressure ratio.

Chapter 5
Summary and Recommendation

The analysis in this thesis focuses on three areas. First, Sorenson's supercharger model was discussed to give an overview of the method for dividing a three lobe roots type supercharger into several control volumes and analyzing each control volume to finally obtain a performance prediction. Second, the improvements to Sorenson's model were presented; including all modifications to the base equations for modeling the M-45 supercharger, as well as adding the backflow slots, carryback flow features, and the carryback slot pulse generation. Finally, a comparison between the efficiency predicted by the M-45 supercharger model and the measured data provided by Eaton Corporation was presented.

5.1 Summary

S.C. Sorenson developed a methodology to analyze a three lobe roots type supercharger. He used a one dimensional model from a thermodynamic perspective to calculate the temperature and pressure inside a supercharger. The strength of his model is that it takes into account leakage flows and heat transfer effects. His model, however, does not include the backflow slots, which is one of the basic features in superchargers.

Curtis Carroll did a significant work on modeling the backflow slots in the supercharger using thermodynamic relationships. The model could generate the pressure rise profile caused by the backflow slots. As Carroll recommended in his thesis, a possible future work is to combine Sorenson's supercharger model and his backflow slot model to have a model that better represents the actual supercharger. Carroll also investigated the backflow slots to determine if they cause some of the pulse fluctuation seen in the measured data provided by Eaton Corporation. He then concluded that the backflow slots are not the source of these pulses seen in the measured data and suggested that the carryback slot be investigated as a source of pulsation.

Hence, work to develop a new supercharger model that incorporates all these effects (backflow slots, carryback slot, and the pulse fluctuations) was conducted. The supercharger that is being modeled is the M-45 supercharger provided by Eaton Corporation. It is a three lobe roots type supercharger with 60 degree twisted rotors. The basic features of this M-45 supercharger are the same as the supercharger that was modeled by Sorenson. However, some adjustments need to be made to the size and shape of the outlet to model the M-45 supercharger more accurately.

The output of Sorenson's model is the temperature inside control volumes as a function of rotor position. These signals were then converted to pressure signals. Two methods for converting temperature to pressure (isentropic flow and ideal gas approach) were studied by comparing the efficiency calculated using each approach. The isentropic flow equations turned out to give extreme efficiency values: close to 0% and over 100% for some cases. The efficiency results obtained from the ideal gas approach were more realistic and follow the same trend as measured data. Hence, the ideal gas approach was used to convert temperature to pressure with some further additional adjustments to match the efficiency values calculated from the Eaton data.

There were two ways to add the backflow slot features to the supercharger model; using Carroll's backflow slots model and using Sorenson's method by expanding some of the equations. Both methods were proved to be similar in that they both use isentropic flow equations and also adjusts to the flows being choked or not. Hence, Sorenson's method was chosen by modeling the flows through the backflow slots as leakage flows for the uniformity in the equations purpose. The results for adding the backflow slots can be seen in the pressure profiles where there is no more sudden pressure increase when the trapped volume opens to the outlet. The trapped pressure now increases smoothly as the leading rotor tip of the trapped volume passes the backflow slots.

The addition of a carryback slot for predicting the pulse generation requires some major changes to the continuity and energy equations. The equations now have to take into account a new control volume between the inlet and outlet volume, although only the mass flow rate term from the carryback to the inlet volume is needed to generate pressure pulsations. In order to generate the pressure pulses, a siren noise model was adopted. A new

separate model from the supercharger model was developed. It takes into account the pressure pulsation caused by the noise source propagating inside the supercharger as well as the travel distances of these pulses as the rotors turn. Up to three reflections were considered in this model. The results from this pulse model were compared to the measured data at 1.0 and 1.4 pressure ratios. Overall, the pulse generation results were promising, although less correlation with the measured data was found for 1.0 pressure ratio case. It is not clear at this time if the discrepancies are caused by differences in the pulse model or the supercharger performance being predicted at a pressure ratio above 1.0. The work, therefore, focused on matching the pressure pulsation profile for the 1.4 pressure ratio cases.

After all the model improvements were made, the supercharger model was considered ready to be compared with the results from the measured data provided by Eaton Corporation. Only the predicted volumetric efficiency results had a good agreement with the results from Eaton Corporation. The predicted J1723 isentropic efficiency results were off by 30 to 60%, although followed similar trends. Further adjustments to the model were needed for the calculated and measured efficiency results to match each other.

Several different factors were investigated to determine the source of error in the J1723 isentropic efficiency. The locations of the transducers being some distance away upstream and downstream of the supercharger did not have much effect on the supercharger efficiency, as was true for the flow coefficients. The supercharger wall temperature turned out to have a significant effect to the supercharger J1723 isentropic efficiency. The wall temperature value has to be adjusted accordingly with respect to the operating pressure ratio and rotors speeds. The higher the pressure ratio and the rotors speeds, the higher the wall temperature will be. Further, in order to get a good agreement with the measured data, the wall temperature also has to be hotter than the air inside the supercharger. The fact that the wall temperature needs to be hotter than the air concludes that there is another heat generation source that has not been accounted in the model, which is the mechanical loss. The clearance between the two rotors and between the rotors tip and the supercharger casing (wall) is very small so it is possible to generate that much heat. Further investigation has to be made on the supercharger wall to determine if this is really what is happening.

5.2 Future Work

After all the model adjustments were made, the supercharger model was not able to converge to a solution for 1.0 pressure ratio case. The closest was between a 1.05 and 1.08 pressure ratio. Further investigation on the supercharger model needs to be conducted to resolve this issue.

Another possible future work would be combining the supercharger model with the pulse model since the output of the supercharger model is used as input for the pulse model. Although the carryback pulse model gives some pressure pulse fluctuations on the profile generated, there are some pulses in the measured data that was not predicted by the model. Hence, further study on the other sources of pulsation needs to be conducted.

Next, a test on supercharger wall temperature needs to be done to see if it does get hotter than the air inside the supercharger and to determine if the mechanical loss is the source of the heat generation. If the results do not support the hypothesis of the hotter walls, then other sources of energy that can increase the outlet air temperature should be investigated.

Appendix A
Unit Conversion

Since the system that is analyzed is a supercharger, which is a rotating system, all the rate variables are in "per degree" unit, instead of "per second". The mass flow rates ($\dot{m}$) are in kg/degree and the heat transfer rates ($\dot{Q}$) are in J/degree. Taking an example from one mass flow formula (2.1),

$$\dot{m} = \left\{ K \cdot \left(\frac{2}{\gamma+1} \right)^{\left(\frac{\gamma+1}{2\gamma-2} \right)} \right\} \cdot \frac{1}{6 \cdot N} \qquad \textbf{A-1}$$

the first term in parenthesis has a unit of kg/s. In order to have a unit of kg/degree, the term in parenthesis has to be multiplied with $\frac{1}{6 \cdot N}$, where N is the rotors speed (RPM). The following is the breakdown:

$$\frac{kg}{s} \cdot \frac{1}{N\, rev/\min} \cdot \frac{60s}{\min} \cdot \frac{1rev}{360\deg.} = \frac{1}{6}\, kg/\deg. \qquad \textbf{A-2}$$

The same approach is applied to the heat transfer rate. The heat transfer rate formula (2.7) is:

$$\dot{Q}_i = h_i \cdot A_i \cdot \left(T_{wall} - T_i \right) \qquad \textbf{A-3}$$

where $\dot{Q}_i$ has a unit of Watts, which is J/s. In order to have a unit of J/degree, the formula above has to be multiplied by $\frac{1}{6 \cdot N}$ as well.

Appendix B

Details on the Equations and Analysis

In order to solve for temperature, the energy equation (2.6) has to be manipulated algebraically. The first section of Appendix B covers these algebraic steps. First, the energy equation looks is:

$$\dot{Q}_i - \dot{W}_i = \frac{d(m_i \cdot u_i)}{d\theta} - \sum_{in} \dot{m}_j \cdot h_j + \sum_{out} \dot{m}_j \cdot h_j \qquad \textbf{B-1}$$

Rearranging the equation B-1:

$$\frac{d(m_i \cdot u_i)}{d\theta} = \dot{Q}_i - \dot{W}_i + \sum_{in} \dot{m}_j \cdot h_j - \sum_{out} \dot{m}_j \cdot h_j \qquad \textbf{B-2}$$

Expanding the partial derivative term:

$$\frac{dm_i}{d\theta} \cdot C_v \cdot T_i + m_i \cdot C_v \cdot \frac{dT_i}{d\theta} = \dot{Q}_i - \dot{W}_i + \sum_{in} \dot{m}_j \cdot h_j - \sum_{out} \dot{m}_j \cdot h_j \qquad \textbf{B-3}$$

Since an equation is needed to relate temperature at two angles, equation B-3 is rearranged:

$$\frac{dT_i}{d\theta} = \frac{\dot{Q}_i - \dot{W}_i - \frac{dm_i}{d\theta} \cdot C_v \cdot T_i - \left(\sum_{out} \dot{m}_j \cdot h_j - \sum_{in} \dot{m}_j \cdot h_j \right)}{m_i \cdot C_v \cdot} \qquad \textbf{B-4}$$

Expanding the temperature rate of change term using 1st order finite difference:

$$\frac{T_{i(new)} - T_i}{d\theta} = \frac{\dot{Q}_i - \dot{W}_i - \frac{dm_i}{d\theta} \cdot C_v \cdot T_i - \left(\sum_{out} \dot{m}_j \cdot h_j - \sum_{in} \dot{m}_j \cdot h_j \right)}{m_i \cdot C_v \cdot} \qquad \textbf{B-5}$$

Finally, the new incremental temperature is:

$$T_{i(new)} = T_i + d\theta \cdot \left[\frac{\dot{Q}_i - \dot{W}_i - \frac{dm_i}{d\theta} \cdot C_v \cdot T_i - \left(\sum_{out} \dot{m}_j \cdot h_j - \sum_{in} \dot{m}_j \cdot h_j \right)}{m_i \cdot C_v \cdot} \right] \qquad \textbf{B-6}$$

where $d\theta$ is the angle increment.

The second section of Appendix B is the details of the analysis in section 2.1.5. Almost all flows analyzed in this supercharger model are leakage flows, which can be calculated using formula 2.1 or 2.2, depending on whether the flow is choked or not. However, when the inlet control volume is analyzed, there is one flow rate that is not a leakage flow, which is the inlet mass flow rate ($\dot{m}_{in}$). Inlet mass flow rate is calculated differently. Mass flow rate term can be split into two terms:

$$\dot{m}_{in} = \rho_{in} \cdot \frac{dV_{in}}{d\theta} \qquad \textbf{B-7}$$

The air density in the inlet volume can be calculated using the ideal gas equation. Further, the angular rate of change of the inlet volume is

$$\frac{dV_{in}}{d\theta} = \frac{V_{in(new)} - V_{in}}{d\theta} \qquad \textbf{B-8}$$

where:

$V_{in(new)}$: inlet volume at the next angle increment (m^3)

V_{in} : inlet volume at current angle increment (m^3)

$d\theta$: angle increment (degree)

The other flow rate that has to be computed differently is the outlet mass flow rate, $\dot{m}_{out}$. In this case, it was initially known from the laboratory procedure that in order to adjust

the pressure ratio, the outlet volume flow rate has to be adjusted first. Hence, the outlet volume flow rate is estimated for each pressure ratio and assumed to be constant throughout the cycle. Then the outlet mass flow rate becomes:

$$\dot{m}_{out} = \rho_{out} \cdot \dot{V}_{out} \qquad \textbf{B-9}$$

where:

$\dot{V}_{out}$: estimated outlet volumetric flow rate (m^3/s)

ρ_{out} : density of air at the outlet volume (kg/m^3)

Since the flow rate calculated has a unit of kg/s, it also needs to be multiplied with $\frac{1}{6 \cdot N}$ to have a unit of kg/degree.

Appendix C

Geometrical Consideration for the M-45 Supercharger Model

The information describing the geometry of each control volume and flow area is written in a text file. For the M-45 supercharger, the file name is m45_geo.txt. The file consists of 21 columns. The first 7 columns are volumes, which consists of V_{R1}, V_{R2}, V_{R3}, V_{T1}, V_{T2}, V_I, and V_{cb}. The next 6 columns are heat transfer areas, which are AHT_{TR1}, AHT_{TR2}, AHT_{TR3}, AH_{TT1}, A_{HTT2}, and A_{HTI}. The following 5 columns are leakage flow areas, A_{RPT1}, A_{RPT2}, A_L, A_{tip}, and A_{Lcb}. Then, the next 2 columns are back flow slot areas, A_{BFS1} and A_{BFS2}. Finally, the last column is the geometrical configurations of the supercharger.

For m45_geo.txt, the geometrical values were obtained from the first 60 degree at 3 different angle positions (-15 degree, 29 degree, and 45 degree). This is a little bit different when creating a geometry text file for the supercharger in Sorenson's model, where the geometry values were obtained at -15 degree, 0 degree, 15 degree, 30 degree, and 45 degree. Due to symmetry, the second 60 degree values can be obtained from the first 60 degree by switching the left portion to the right portion of the supercharger. In order to get better accuracy, each geometrical value in the text file is written every 1 degree increment. This is done by a linear interpolation from those 3 different angle positions.

The last column is for the geometrical configurations of the supercharger. As discussed in chapter 2, there are 4 different geometrical configurations for the M-45 supercharger. Hence, in this column the values are either 1, 2, 3, or 4 for each angle. These numbers will then tell the program which set of equations to use for that particular angle. Therefore, in order to run the supercharger model correctly, one would have to know which geometrical configurations of the supercharger for the whole 120 degree cycle.

Here is the list of the variables in the m45_geo.txt along with their explanations. They are listed in the same order as the text file.

V_{R1} : Low pressure receiver 1 volume (left hand side part)

V_{R2} : Low pressure receiver 2 volume (right hand side part)

V_{R3} : Outlet volume

V_{T1} : Trapped 1 volume (the left hand side part)

V_{T2} : Trapped 2 volume (the right hand side part)

V_I : Inlet volume

V_{cb} : Carryback volume

A_{HTTR1} : Heat transfer area for control volume R1

A_{HTTR2} : Heat transfer area for control volume R2

A_{HTTR3} : Heat transfer area for control volume R3 (outlet)

A_{HTT1} : Heat transfer area for control volume T1

A_{HTT2} : Heat transfer area for control volume T2

A_{HTI} : Heat transfer area for inlet control volume

A_{RPT1} : Flow area for between outlet and low pressure receiver 1

A_{RPT2} : Flow area between outlet and low pressure receiver 2

A_L : Leakage flow area

A_{tip} : Tip leakage flow area

A_{Lcb} : Carryback flow area

A_{BFS1} : Backflow slots 1 flow area (left hand side part)

A_{BFS2} : Backflow slots 2 flow area (right hand side part)

Condition : Configuration number of the supercharger (1, 2, 3, or 4)

References

Anderson, John D. Modern Compressible Flow with Historical Perspective Third Edition. New York: McGraw-Hill Companies, Inc. 2003.

Carroll, Curtis C. "Development and Analysis of Models of a Supercharger." Iowa State University Master's Thesis. 2004.

DeWitt, David P., Frank P. Incropera. Fundamentals of Heat and Mass Transfer Fifth Edition. New York: John Wiley and Sons, Inc. 2002.

Harris, Bill. "How Superchargers Work." HowStuffWorks, Inc. 12 May 2006 <http://auto.howstuffworks.com/supercharger.htm>.

Meyer, Nathanael A. "Developing Tools to Understand and Predict Noise Phenomena in a Supercharger." Iowa State University Master's Thesis. 2003.

Moran, Michael J., Howard N. Shapiro. Fundamentals of Engineering Thermodynamics Fourth Edition. New York: John Wiley and Sons, Inc. 2000.

Munson, Bruce R., Theodore H. Okiishi, Donald F. Young. Fundamentals of Fluids Mechanics Fourth Edition. New York: John Wiley and Sons, Inc. 2002.

Pla, Frederic G. "An Experimental and Theoretical Study of High-Intensity , High-Efficiency Sirens," Pennsylvania State University Ph.D Dissertation, 1987.

Sorenson, S.C. "Simulation of a Positive Displacement Supercharger." SAE Technical Paper # 840244: 115-129, 1984.